Environmental Control of Charge Transport through Single-Molecule Junctions

Brian Capozzi

Submitted in partial fulfillment of the
requirements for the degree
of Doctor of Philosophy
in the Graduate School of Arts and Sciences

COLUMBIA UNIVERSITY

2015

ABSTRACT

Environmental Control of Charge Transport through Single-Molecule Junctions

Brian Capozzi

Metal-molecule-metal junctions have become a widely used test-bed for the study of nanoscale electronic phenomena. Single-molecule junctions in particular have provided a deeper understanding of charge transport across interfaces, and single-molecule electronic components have been proposed as a successor for silicon technology. This thesis presents an experimental approach for controlling the electronic properties of single-molecule junctions by manipulating the environment about the junction. With this tunable functionality, we are able to demonstrate single-molecule variants of transistors and diodes.

We begin our work by probing charge transport through single-oligomers of commonly used molecules in organic electronic devices. We focus on these systems due to their narrow band gaps, giving them the potential for exhibiting high molecular conductances. Single-molecule junctions are formed using the Scanning Tunneling Microscope-based break junction (STM-BJ) technique. We first consider a family of oligothiophenes, ranging in length from 1 to 6 units. We find that this family of molecules exhibits an anomalous conductance decay with molecular length; this is mainly due to conformational effects. These conformational effects also result in very broad conductance distributions, further preventing oligothiophenes from being useful in molecular electronic devices. However, we find that thiophene dioxides are particularly well-suited for single-molecule devices, primarily due to exceptionally narrow band gaps. Oligothiophene dioxides also constitute a unique system where the dominant conductance orbital changes with molecular length. Specifically, we find that the shorter oligomers have transport dominated by the highest occupied molecular orbital (hole-type transport), but longer oligomers have transport dominated by the lowest unoccupied molecular orbital (electron-type transport).

We next demonstrate a method for gating single-molecule junctions. In order to overcome the difficulty of lithographically defining a gate electrode in close enough proximity to the molecular junction so that the gate voltage impacts the electrostatics of the junction, we turn to measurements in electrolytic solutions. Ions in these solutions form compact layers of charge at metal surfaces, and these electric double layers can be controlled by the gate electrode; such electrolytic gating results in high gating efficiencies. Using this technique, we show that we are able to continuously modulate the conductance of non-redox active molecular junctions.

Using ionic environments, we next develop a new technique for creating a single-molecule diode. Performing break junction measurements in electrolytic solutions without the presence of a gate electrode, we show that we still have control of the junction's electrostatic environment. In particular, if the source and drain electrodes are of considerably different areas, we find that we asymmetrically control this environment. Using this technique, we demonstrate single-molecule didoes created from otherwise symmetric molecular junctions. Combining this with measurements on thiophene dioxide oligomers, we show single-molecule diodes with the highest reported rectification ratios to date. This technique has the potential for application in nano-scale systems beyond single-molecule junctions. These results constitute another step toward the development of single-molecule devices with commercial applications.

Finally, the methods presented in this thesis offer further insights into the electronic structure of molecular junctions. We show that we can assess energy-level alignment at metal molecule interfaces– this alignment is a crucial parameter controlling the properties of the interface. We also demonstrate that we can probe large regions (2eV) of the transmission function which governs charge transport through the junction. By being able to control level alignment, we are also able to offer preliminary studies on single-molecule junctions in the resonant transport regime. Combined, the results presented in this thesis grant new insights into electron transport at the nanoscale and provide new routes for the development of functional single-molecule devices.

Table of Contents

List of Figures **vi**

List of Tables **vii**

1 Introduction **1**

1.1 Anatomy of a Single-Molecule Junction 2

1.2 Basic Data Collection and Analysis 4

1.3 Charge Transport through a Molecular Junction 6

1.4 The Electric Double Layer 8

1.4.1 Measurements in an Ionic Medium 11

1.5 Thesis Outline 12

2 Single-Molecule Conductance Properties of Thiophene-based Oligomers 15

2.1 Charge Transport Properties of Oligothiophenes 16

2.1.1 Abstract 16

2.1.2 Introduction 16

2.1.3 Results and Discussion 18

2.1.4 Conclusions 30

2.1.5 Supplementary Information 31

2.2 Charge Transport Properties of Oligothiophene Dioxides 37

2.2.1 Abstract 38

2.2.2 Introduction 38

2.2.3 Results and Discussion 41

2.2.4 Conclusions 48
2.2.5 Supplementary Information 48

3 Electrolyte Gating of Single-Molecule Junctions 60
3.1 Introduction 61
3.2 Results and Discussion 62
3.2.1 Break-Junction Measurements in Ionic Media 62
3.2.2 Modeling and Comparison with Theory 66
3.3 Conclusions 70
3.4 Supplementary Information 71
3.4.1 Additional Figures 71
3.4.2 Control Gating Experiment 74
3.4.3 Calculation Details 75

4 Environmentally Enabled Single-Molecule Diodes 77
4.1 Introduction 78
4.2 Results and Discussion 78
4.2.1 An Environmentally Enabled Molecular Rectifier 78
4.2.2 Mechanism for Rectification 81
4.2.3 Assessing Energy-Level Alignment 87
4.3 Conclusions 89
4.4 Supplementary Information 90
4.4.1 Experimental Methods 90
4.4.2 Additional Data and Analysis 93
4.4.3 Experimental Determination of Energy Level Alignment 98
4.4.4 Computational Details 101
4.4.5 Synthetic Details 103

5 Experimental Determination of Single-Molecule Junction Transmission Functions 104
5.1 Introduction 105

5.2 Results and Discussion 107
5.2.1 Single-Molecule Conductance Measurements 107
5.2.2 Extracting the Transmission Function 109
5.2.3 Molecular Junctions near Resonance 113
5.3 Conclusions 117
5.4 Supplementary Information 118
5.4.1 All Conductance Histograms 118

6 Conclusions and Outlook **129**
6.1 Summary 129
6.2 Future Directions 130
6.3 Complete List of Published Work 131

Bibliography **132**

List of Figures

1.1 Schematic of a single-molecule junction 3
1.2 Break junction process 4
1.3 Sample conductance data from break junction technique 5
1.4 Transport through a molecular junction 7
1.5 Electric double layers 10
1.6 Electrolyte field effect transistor 11
1.7 Procedure for insulating tips 12

2.1 Single-molecule conductance traces for the oligothiophene family. 18
2.2 Single-molecule conductance histograms and beta plot for the oligothiophene family. 20
2.3 Energy level characterization of the oligothiophene family. 22
2.4 Tightbinding model for transport through oligothiophene family. 25
2.5 Aggregation studies of the oligothiophene family. 27
2.6 The influence of conformational effects on oligothiophene conductance. . . . 29
2.7 Linear-binned conductance histograms for T1-T6. 32
2.8 Logarithmically binned conductance histograms for T1-T6. 33
2.9 T4 conductance under argon and in ambient conditions. 34
2.10 Additional oligothiophene aggregation studies: temperature data. 34
2.11 Additional oligothiophene aggregation studies: solvent data. 35
2.12 Additional oligothiophene aggregation studies: concentration data. 35
2.13 Two dimensional oligothiophene conductance histograms. 36
2.14 Oligothiophene step-length versus molecular length. 36

2.15 Influence of hexyl chains on T5 conductance. 37
2.16 Characterization of the nature of charge carriers using the scanning tunneling microscope break junction technique. 40
2.17 Energy level characterization of the TDOn family. 42
2.18 Single-molecule conductance data for the TDOn family. 44
2.19 Single-molecule thermopower data for the TDOn family. 46
2.20 Impact of thiophene oxidation on UV-vis absorption spectra. 50
2.21 Cyclic voltammetry measurements on the TDOn family. 51
2.22 Two-dimensional conductance versus displacement histograms for TDOn. . 52
2.23 Sample single-molecule thermopower measurement. 53
2.24 Thermoelectric current histograms for the TDOn series. 54
2.25 Solvent induced conductance shifts for TDO1 and TDO4. 55
2.26 Current-Voltage (IV) measurements and analysis for TDO1 and TDO4. . . 58
2.27 Two level tightbinding model for transport through TDOn junctions. 59

3.1 Single-molecule conductance measurements under electrochemical control. . 63
3.2 Gating HOMO and LUMO dominated molecular junctions. 64
3.3 Cyclic voltammograms using the break junction geometry. 68
3.4 Comparison of experimental gating data with DFT+Σ calculated transmission functions. 69
3.5 Cyclic voltammograms for gated molecules. 71
3.6 Influence of gating on molecular step-length. 72
3.7 Gating data for 4,4'-bipyridine. 73
3.8 Gating experiments with alternative sized electrodes. 75

4.1 Environmentally enabled single-molecule diodes. 80
4.2 Energy-level diagram illustrating rectification mechanism for a LUMO conducting molecular junction. 84
4.3 High rectification ratios in TDOn Junctions. 85
4.4 Rectification with Other Molecule/Solvent Systems. 86
4.5 Experimental and Computational Determination of Energy Level Alignment. 88

4.6 Sample IV measurement. 92
4.7 Bias polarity dependent conductance of TDO4 in TCB. 93
4.8 Comparison of conductance measurements taken with insulated tips in polar and non-polar solvents. 94
4.9 IV measurements on TDO4 in an electrolytic solution. 94
4.10 Cyclic voltammogram using two-electrode break junction geometry. 95
4.11 TDO conductance histograms in TCB. 95
4.12 Two-dimensional IV maps for TDO3-5. 96
4.13 Two-dimensional IV maps for additional molecules. 97
4.14 Two-dimensional IV histograms for 4,4-bipyridine (**1**) in additional polar media 98
4.15 Computed IV curves using experimentally determined parameters and a single-Lorentzian model. 100
4.16 Model rectification ratios versus applied bias using a single-Lorentzian model. 101
4.17 DFT+Σ calculated transmission functions with a dipole layer on one electrode. 103

5.1 Break junction measurements in propylene carbonate. 108
5.2 Extracting transmission for 4,4'-bipyridine and 4,4"-*p*-diaminoterphenyl. . . 112
5.3 Extracting transmission for near-resonant molecular junctions. 114
5.4 Approaching resonant transport in molecular junctions. 115
5.5 Conductance histograms for **1**. 119
5.6 Conductance histograms for **2**. 122
5.7 Conductance histograms for **3**. 125
5.8 Conductance histograms for **4**. 128

List of Tables

2.1 Orbital characterization of TDO1-4 from CV measurements 51
2.2 Single-Lorentzian model parameters for TDO1 and TDO4 56

Acknowledgments

I consider myself very fortunate to have wound up in a research group with an outstanding advisor. I am incredibly thankful to Prof. Latha Venkataraman for the mentorship she has provided during my time as a graduate student. I admire how quickly she learns, how easily she grasps a problem, and how efficiently she works toward a solution. Latha is always available to talk and is always excited to discuss any new result, no matter how minor. Beyond research, she is also genuinely concerned with the development and well-being of her students. I have learned a lot and I have grown a lot during my time in her lab– I think I have come a long way from barely being able to speak during my second year oral exam. I am confident that I have become a better person thanks to her guidance.

My time in the lab was made significantly more fulfilling and enjoyable thanks to the other students and postdocs in the group. As a new student, I found that the more senior members were happy to offer assistance and advice, making the foray into research far less overwhelming. This cooperative environment has persisted for the entire time I have been in the lab and has been comforting during all of the highs and lows that accompany experimental research. We are a close-knit group, and I am happy to have spent my time working with people who are also my friends. Miraculously, they even convinced me that I could join in their morning running club.

I am also appreciative of the collaborative environment that Latha has fostered for our group. This has enabled me to work with many talented groups in the Chemistry Department, including those of Prof. Luis Campos, Prof. Colin Nuckolls, and Prof. Xavier Roy. From countless meetings and discussions with these professors and the many talented students in their groups, I have learned a surprising amount of chemistry and new ways to think about many problems. Prof. Jeffrey Neaton and his group at LBNL have also taught me a lot, and my research has benefited from these conversations. I thank Prof.

Marissa Buzzeo of Barnard's Chemistry Department for walking me through the basics of electrochemistry, a subject which I knew absolutely nothing about. I would also like to thank Dr. Mark Hybertsen and Dr. Mike Steigerwald for many discussions, insights, and ideas.

Finally, I would like to acknowledge my friends and family; without their support and encouragement, the past five years would have been very different. They kept me grounded, provided many welcome distractions, and helped me remember that there is much more to life than research.

Despite how long the graduate school seemed at the onset, it feels like it has come to an end much more quickly than I would have expected. I greatly enjoyed my time at Columbia, and look forward to all of the new challenges that await.

Thank you all!
Brian

To my parents, Jayne and John

Chapter 1

Introduction

Creating a commercially viable single-molecule circuit is a tantalizing dream for nanoscientists. This has been largely fueled by Aviram and Ratner, who, in 1974, proposed a design scheme for realizing a molecular diode. [1] The initial draw of such an idea, of course, was the promise of electronic devices operating at an extraordinarily small scale. A molecule, a bound group of atoms, currently stands as the smallest component of matter which can be designed and synthesized with particular properties in mind. Given the exceedingly large number of small molecules which can be created, achieving such single-molecule devices would therefore provide what may well be the ultimate in functional device miniaturization. The field of molecular electronics has thus come to stand at the intersection of physics and chemistry, coupling physical understandings of charge transport processes with chemical knowledge and creative synthetic strategies for imbuing molecules with desirable functionality. Significant collaborative efforts have yielded demonstrations of single-molecule analogues of various conventional circuit elements including wires and resistors [2–6], switches [7–10], memory elements [11], diodes [12–15], and transistors [16–19]. Manipulating matter at such a small scale is truly an astonishing feat.

Yet, despite all of these advances, no single-molecule based technology has emerged as a viable alternative or successor to current silicon technology. Instead, efforts to create molecular devices have highlighted the ability of a single-molecule junction– a molecule bridging two electrodes– to serve as a remarkably versatile system for studying nanoscale physical phenomena. Indeed, metal-molecule-metal junctions have been used to investigate

quantum mechanical behavior such as tunneling and interference [20–22] along with more exotic many-body electron interactions including Coulomb blockade [23–25] and Kondo effects [23, 26–29]. Single-molecule junctions also serve as a simple system with which to investigate interfacial electronic structures. As the interface typically controls a device's properties [30], a deeper understanding of electronic and mechanical interactions at metal-molecule interfaces is critical for developing next generation technology, even if this technology is not ultimately based on single-molecules.

This thesis seeks to develop new techniques with which to create single-molecule circuit elements and to use these methods to further understand the electronic structure of metal-molecule-metal junctions. In particular, I look to manipulate the electrostatic environment surrounding a molecular junction in order to modulate charge transport through the junction. The methods established in this thesis also provide access to information regarding energy-level alignment in molecular junctions. In the remainder of this chapter, I present a brief overview of the experimental procedures used to create and measure the conductance of single-molecule junctions, and I provide a brief overview of the theory of current flow through these devices. I also describe the nature of electric double layers which arise at the interface of a metal in contact with a solution, as these provide a means by which to control the electrostatic environment of a molecular junction.

1.1 Anatomy of a Single-Molecule Junction

Conceptually, a single-molecule junction consists of a molecule of interest and electrodes which allow current to be driven through the molecule. The molecular backbone is designed such that it can impart some functionality and the electrodes are typically of some noble metal, for instance, gold. Molecules are then terminated with linker groups; these serve as chemical alligator clips which can connect the molecular backbone to the electrodes via donor-acceptor interactions [31], covalent bonds [2, 32], or less specific van der Waals interactions [9] (Fig. 1.1). Despite this apparent simplicity, successfully wiring up a nanometer-sized object to macroscopic leads is a challenge. Well developed lithographic techniques are unable to reliably define a gap on the order of a nanometer. Instead, tech-

niques relying on electromigration [16,33,34] and break-junction methods [2,27,35,36] have become the standard for creating molecular junctions.

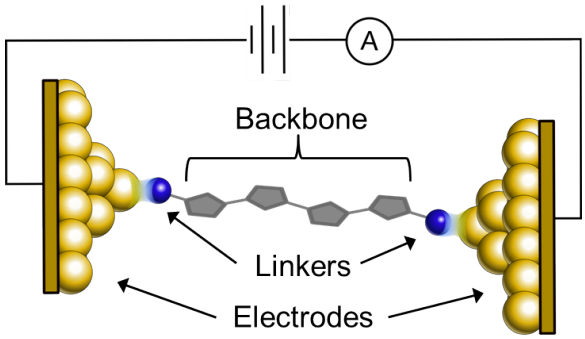

Figure 1.1: ***Schematic of a single-molecule junction.*** *Single-molecule circuit with gold electrodes, molecular backbone, and link-groups highlighted*

Break junction techniques in particular have risen to prominence in the molecular electronics community. [2,27,35–38] Here, a metal-molecule-metal junction is created by pulling apart a thin metal junction in the presence of a target molecule. As the junction is broken, a sub-nanometer gap is formed between the electrodes; this is sufficient to accommodate a small molecule. The benefits of this method are numerous. Molecular junctions can be rapidly and reproducibly formed, a crucial requirement for studying single-molecule transport due to the sensitive nature of molecular conductance on the details of junction structure. Measurements can be performed under ambient conditions, removing the complications of working under vacuum and at low temperatures. Break junction methods are also readily modified to allow the additional study of forces [39, 40], thermoelectric properties [41–43], magnetic properties [28, 44], and optical properties [45].

In this thesis, measurements presented have been acquired using the scanning tunneling microscope variant of the break junction (STM-BJ) technique with gold electrodes (Fig. 1.2). [2, 36] Here, a mechanically cut gold tip is repeatedly driven into and out of contact with a gold substrate by a piezoelectric actuator. As the tip is retracted, the gold structure which has formed is thinned down, ultimately to a point contact, where only two gold atoms are in contact with each other. Further pulling ruptures this point contact, yielding the necessary sub-nanometer gap discussed above. In order to form molecular junctions, the

process is carried out in a solution containing molecules of interest. Once the point contact ruptures, a molecule with aurophilic binding groups can bridge the gap and its conductance can be measured. The process is then repeated thousands of times in order to obtain a statistically significant amount of data to characterize the conductance properties of the molecular junction.

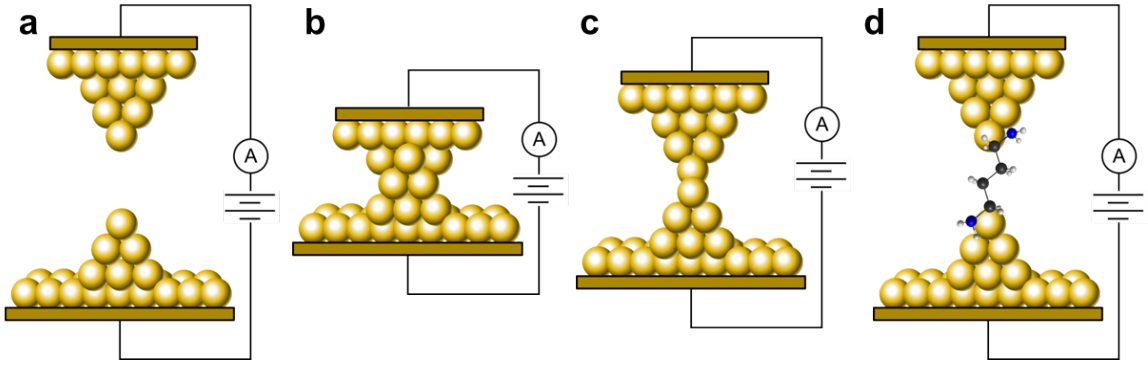

Figure 1.2: ***Break junction process.*** *Schematic representation of the break junction process. An atomically sharp gold tip (**a**) is driven into contact with a gold substrate (**b**). The tip is retracted, thinning the junction down to a point contact (**c**). Upon subsequent pulling, the point contact is ruptured and a molecule can bridge the gap (**d**)*

1.2 Basic Data Collection and Analysis

With the STM-BJ method, current (I) through and voltage (V) across the junction are measured as a function of time while the electrodes are pulled apart at a constant speed. Conductance ($G = I/V$) can then be plotted as a function of pulling distance (Fig. 1.3a). The conductance versus displacement traces show a step-wise decrease in conductance, with conductance plateaus occurring at roughly integer multiples of the quantum of conductance, $G_0 = 2e^2/h$ (77.5μS). [46] Typically, the last of these conductance plateaus occurs at $1G_0$, corresponding to the formation of a gold single-atom contact. Once this point contact is ruptured, the measured conductance drops either to instrumental noise or to through-space tunneling current between the two electrodes. The data is then analyzed by compiling thousands of conductance vs displacement traces into a one-dimensional histogram. This histogram can be created either by linearly binning (all bins have a constant size) or by

logarithmically binning (number of bins between each order of magnitude is constant) the conductance axis. Frequently observed steps in the conductance traces manifest as peaks in the conductance histogram; for clean gold without the presence of a molecule, peaks are observed at approximately 1, 2 and $3G_0$ [47–49], and a tunneling background is observed at lower conductance (see Figs 1.3b,c for linearly- and log-binned conductance histograms, respectively).

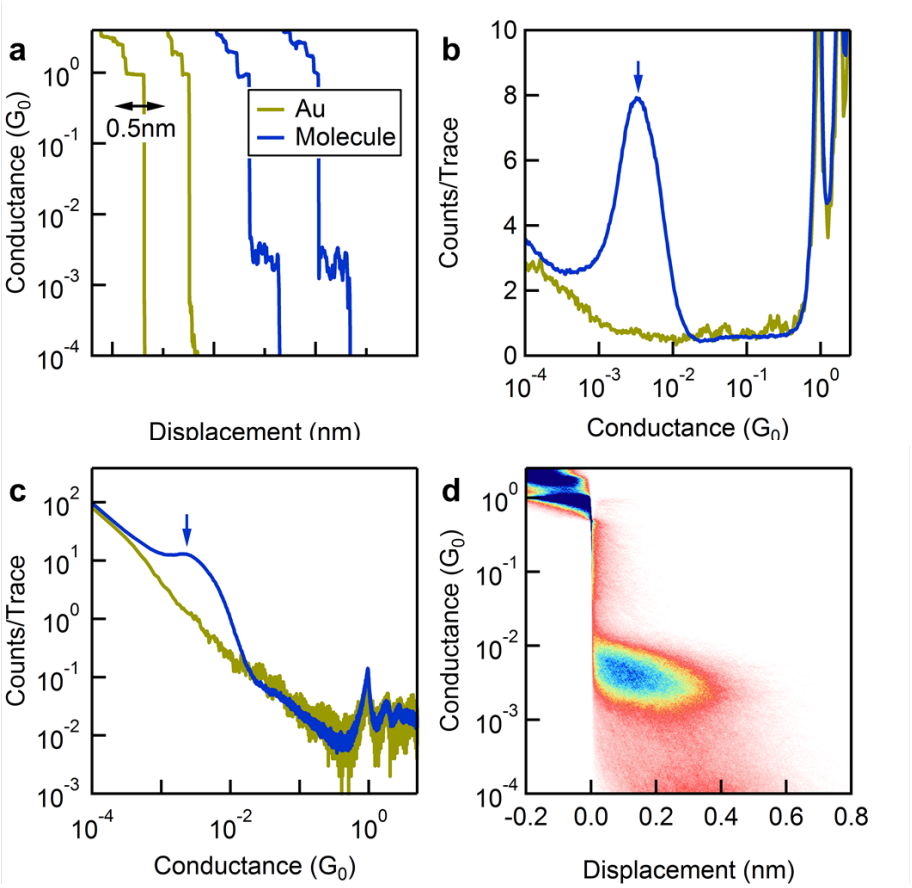

Figure 1.3: ***Sample conductance data from break junction technique.*** *(**a**) Sample conductance versus displacement traces for clean gold (gold colored traces) and for measurements in the presence of a molecule (blue traces). (**b**) Logarithmically binned conductance histograms for clean gold data (gold colored curve) and data taken in the presence of a molecule (blue curve). The arrow indicates the peak position, and therefore the most probably measured molecular conductance. (**c**) Same data as in (**b**), but now compiled into linearly binned conductance histograms. (**d**) Two-dimensional conductance versus displacement histogram, showing a molecular feature extending to roughly 0.4nm.*

After a molecular solution has been added, conductance versus displacement traces now contain additional features above the noise floor once the point contact has been ruptured (Fig 1.3a, blue traces). When histograms are now constructed, there is an additional peak visible that is associated with the formation of metal-molecule-metal junctions (blue curves, Figs 1.3b,c). These conductance peaks are generally well fit by a Lorentzian (in the case of linearly binned histograms) [36] or by a Gaussian (in the case of logarithmically binned histograms) [50]. The peak position of the fit is then taken as the most probably measured conductance of the molecular junction. The width of the fit (and therefore, of the conductance histogram) stems from various factors, such as sampling different molecular conformations [36,51,52], changes in the metal-molecule binding geometry [53], and exploring locally different environmental factors on a junction to junction basis [54].

Two-dimensional conductance versus displacement histograms can also be created in order to preserve information associated with the elongation of the molecular junction. This process is done by aligning all traces at a common reference point. In Fig. 1.3d, traces are aligned just after the rupture of the gold point contact by defining the point at which the conductance traces reaches $0.5G_0$ as the zero of displacement. After alignment, the conductance and displacement axes are binned, and all traces are simply overlaid. The resulting two-dimensional (2D) histogram has a molecular conductance plateau, and the length of this feature, the "step-length", is related to the length of the molecule being measured.

1.3 Charge Transport through a Molecular Junction

In bulk systems, current flow proceeds via diffusive transport where resistance arises due to electron scattering events. [55] At the single-molecule level, however, we must consider the wave nature of electrons. The leads, which are metals, have electrons occupying energy levels up to the Fermi level, E_F. The molecule, in isolation, has discrete molecular orbitals that arise from hybridization of its constituent atomic orbitals. For the purposes of this discussion, we shall only consider the highest occupied molecular orbital (HOMO) and the lowest unoccupied molecular orbital (LUMO), as these are generally the orbitals most

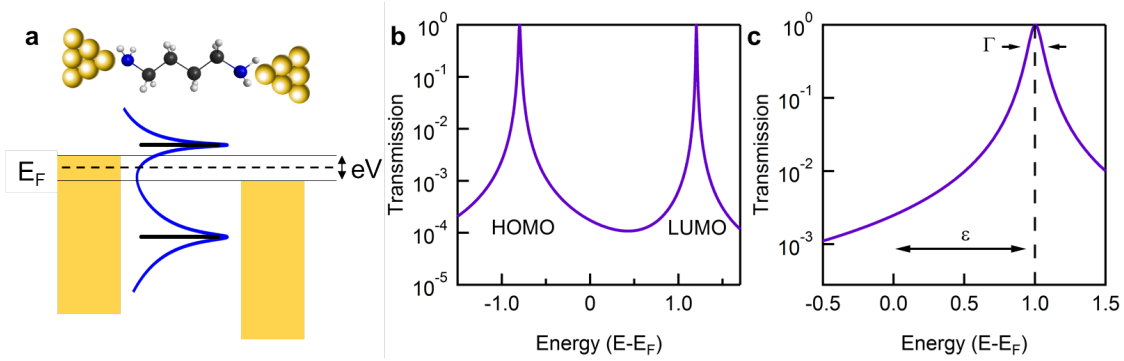

Figure 1.4: ***Transport through a molecular junction.*** *(**a**) Schematic of a molecular junction with a corresponding energy level diagram under bias.(**b**) Toy transmission function showing a broadened HOMO and LUMO. (**c**) Single-Lorentzian transmission function, showing a molecular resonance at a position ϵ from E_F with a broadening* Γ

relevant for charge transport (Fig. 1.4). Once the molecule is bound in the junction, its molecular orbitals hybridize further and broaden upon interacting with the leads. This broadening results in a molecular density of states at E_F, and under bias, current flow will proceed as electrons are incident on the molecular junction.

Due to the mismatch in energies of the incident electrons and the molecular orbitals, some fraction of the incident electrons, r, will be reflected, while the complementary fraction, $1-r$ will be transmitted. The electrons that are transmitted constitute the measured current. This process can be understood using a formalism developed Rolf Landauer in which conduction through a low dimensional system is treated as the above described transmission problem. [56] It can be shown that the current, I, transmitted through a molecular junction is given by: [55, 57, 58]

$$I = \frac{2e^2}{h}\int_{-eV/2}^{eV/2}(f(E,\mu_L) - f(E,\mu_R))T(E)dE$$

Here, e is the charge on an electron, h is Planck's constant, V is the applied voltage, $f(E,\mu_{L,R})$ is the Fermi-Dirac distribution for the left(right) lead, and $T(E)$ is the energy dependent transmission function for the molecular junction. A transmission function (Fig. 1.4b) details the probability that an incident electron, of a given energy E, is transmitted through the molecular junction. If the electron energy is equivalent to one of the molecular orbitals, the electron is resonantly transmitted through the junction (i.e. with probabil-

ity one). Otherwise, the transmission probability is substantially less. The transmission function can be calculated using a non-equilibrium Greens function formalism, [55] where transmission is then defined as:

$$T(E) = Tr(\Gamma_L \mathcal{G}^\dagger(E) \Gamma_R \mathcal{G}(E))$$

Here, $\Gamma_{L,R}$ are coupling matrices which couple the molecular "device" to the leads, and $\mathcal{G}$ and $\mathcal{G}^\dagger$ are the retarded and advanced Green's functions for the molecular "device".

While transmission functions can be calculated using state-of-the-art ab-initio methods (i.e. DFT + Σ) [59, 60], a single-Lorentzian is often a reasonable approximation for transmission through a system which has conductance dominated by only a single molecular orbital:

$$T(E) = \frac{\Gamma^2/4}{(E-\epsilon)^2 + \Gamma^2/4}$$

where ϵ is the position of the molecular orbital relative to the electrode Fermi level, E_F, and Γ is the coupling of that orbital to the electrode (Fig. 1.4c). A slightly more involved method for modeling transmission via a tight-binding formalism can be found in Section 2.2.5.

1.4 The Electric Double Layer

Typically, single-molecule measurements using the STM-BJ are carried out in non-polar solvents. We now turn to measurements carried out in polar media capable of supporting ionic species. To understand how this will impact the charge transport through a molecular junction, we shall first consider what happens when a metal surface is placed in contact with an ion-containing solution. In solid state physics, it is well known that when two solids are placed in contact, be they metals or insulators, charge transfer occurs between the two materials until their electrochemical potentials are equilibrated. [61] This charge transfer yields a large electric field at the interface, which opposes the transfer of any additional charge. This same process occurs when a solid is placed in contact with a solution, except a redox couple in the liquid contact will serve as the acceptor or donator of charge. [62] Again, the difference in electrochemical potentials of the two phases will dictate the direction and

quantity of charge transfer. Ions in solution will now be the carrier of charge in the liquid medium, while electrons in the solid act as the charge carriers. This charge separation at the interface occurs over a very small distance, on the order of a nanometer, and therefore very large electric fields can develop in this region.

When a charged metal electrode is placed in contact with an ion-containing solution, a compact layer of charge is formed at the interface as ions of like charge are repelled away and ions of similar charge are attracted to the surface. This interfacial charge layer is known as an electric double layer, and its detailed composition is generally quite complicated (Fig. 1.5a). [63] The metal side of the interface contains excess charge on the surface. The charge layer on the solution side of the interface can be thought of as having two components. The first is a strongly associated layer of ions (known as the Helmholtz layer) which behaves very much as one plate of a parallel plate capacitor and is on the order of only nanometer in width. This layer is not sufficient to fully screen out the electric field due to charges on the metal, primarily due to the large size of ions and their associated solvation shells relative to the electron size. Therefore a second, more loosely associated layer of ions, known as the diffuse layer, develops beyond the Helmholtz layer and extends further out into solution. Together, these two layers screen the electric field due to the charges present on the metal, and bulk solution essentially sees no electric field.

The immense electric fields developed in electric double layers can cause electrochemical reactions to take place. By applying a voltage to the electrode of interest (the working electrode), the Fermi level of the electrode is shifted relative to the molecular orbitals of the redox couple; in this fashion, when a molecular orbital is brought into (or close) to resonance with the electrode Fermi level, charge transfer can occur (Fig. 1.5b). These charge transfer reactions, known as Faradaic processes, include oxidation, where an electron from an occupied molecular orbital is given up to the electrode, or reduction, where an electron from the electrode is taken up by an unoccupied molecular orbital. Voltammetric methods, such as cyclic voltammetry [64], are common electrochemical techniques used to measure such oxidation and/or reduction potentials. These quantities can then be related to the vacuum level, thereby giving an experimental means for determining the energies of molecular orbitals. [65, 66]

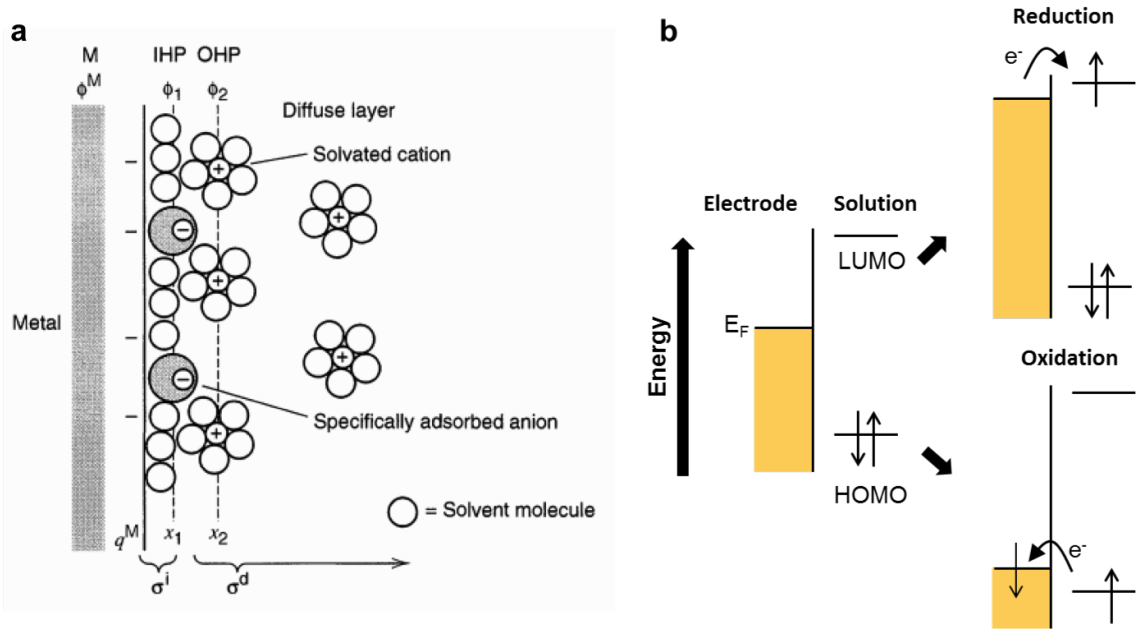

Figure 1.5: ***Electric double layers.*** *(**a**) Adapted from reference [64] Schematic of an electric double layer, depicting the Helmholtz and diffuse layers. Here, an excess of negative charge resides on the surface, and some anions have become specifically adsorbed. The layer of adsorbed ions and solvent molecules is known as the inner Helmholtz plane (IHP), and is at a potential ϕ_1. The outer Helmholtz plane (OHP) is a rigid layer of ions with solvation shells, at a potential ϕ_2. Beyond this is the less strongly associated diffuse layer. σ^i and σ^d represent the charge densities in the Helmholtz and diffuse layers, respectively (**b**) Energy level diagrams for electrochemical charge transfer reactions. During reduction, the LUMO of the redox acceptor comes into resonance with the electrode Fermi level and an electron from the electrode can transfer to the acceptor. During oxidation, the HOMO of the redox donator comes into resonance with the electrode Fermi level and an electron from the HOMO can transfer to the electrode.*

Electric double layers have been used in solid-state devices to create electrolyte field effect transistors (Fig. 1.6a). [67–69] In these devices, traditional gate dielectrics such as silicon dioxide are replaced by an ionic medium (examples of which include electrolytic solutions, ionic liquids, and polymer electrolytes). This is an appealing strategy because electric double layers typically have extremely high capacitances, dramatically increasing the coupling between semiconductor (organic or inorganic) and gate electrode. This yields devices with very high gate efficiencies since almost all of the applied gate voltage is dropped

at the electric double layer, and therefore it directly impacts the semiconductor (Fig. 1.6b). The main drawback of electrolyte gated field effect transistors is their slower response time to an electric field, due to the large ion size relative to that of an electron.

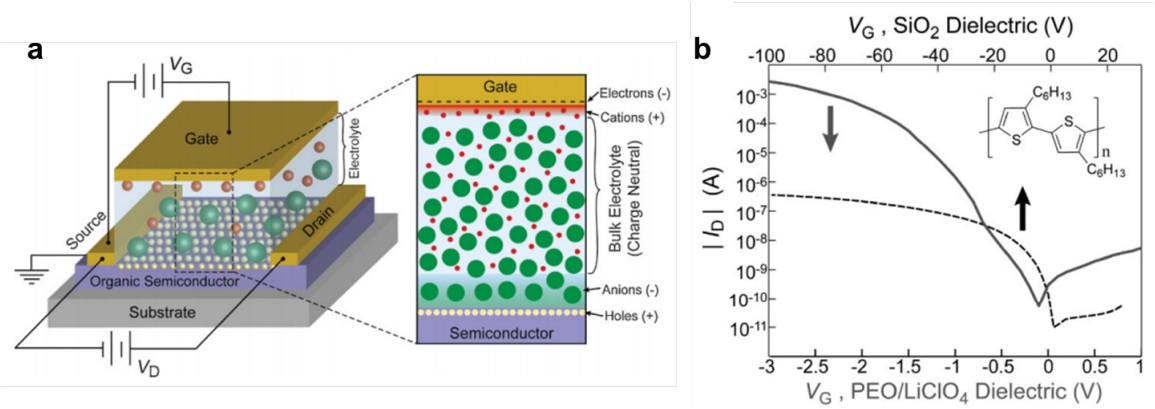

Figure 1.6: ***Electrolyte field effect transistor.*** *Adapted from reference [67] (**a**) Schematic of an electrolyte field effect transistor showing how the electric double layer is used to gate a semiconductor. (**b**) Adapted from reference [67] A comparison of a transistor made using a traditional oxide dielectric versus an electrolyte dielectric. The current versus gate potential for the electrolyte gated device shows significantly higher currents, and these currents arise at voltages that are two orders of magnitude lower than the operating voltages of the oxide gated device.*

1.4.1 Measurements in an Ionic Medium

The large electric fields developed in electric double layers can be used to impact charge transport through a molecular junction. However, current flow due to both faradaic and non-faradaic processes (capacitive processes as the double layer is charged/discharged with bias) can often be greater than the current flowing through the molecular junction. Therefore, performing break junction measurements in ionic media poses an additional challenge.

Fortunately, both components of the electrochemical contributions to the current are proportional to electrode area. Therefore, drastically reducing the area of one of the electrodes exposed to solution can substantially reduce the background currents and enable these measurements. We choose to reduce the area of the tip electrode by insulating it using a chemically inert material: Apiezon wax. Tip insulation is fairly straightforward. A copper plate with a slit is heated, and Apiezon wax is melted over the slit (see Fig. 1.7). [70]

A mechanically cut gold tip is then driven through the slit. Surface tension causes a small portion of the tip to remain exposed; this allows us to still carry out break junction measurements with the insulated probe. We find that the insulation procedure typically yields a tip with approximately $1\mu m^2$ of gold exposed. This small area reduces the background electrochemical currents and enables break junction measurements in polar and ionic media.

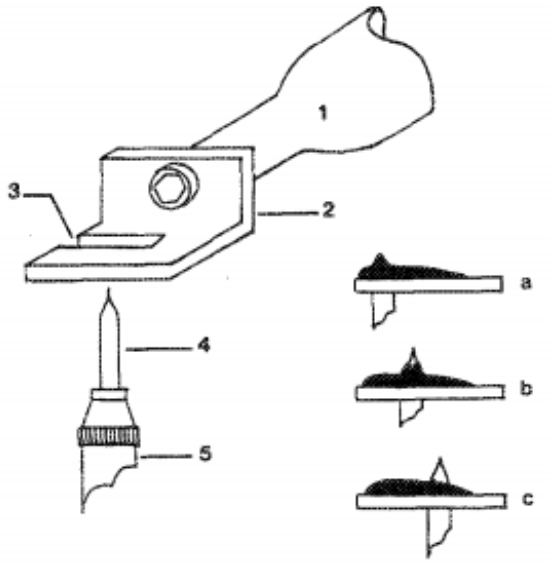

Figure 1.7: ***Procedure for insulating tips.*** *Adapted from reference [70] A mechanically cut gold tip is driven through a slit on a heated copper plate. Apiezon wax is melted over the slit. If the wax is too cool, no gold is exposed, as in a. If the wax is too warm, too much gold is exposed, as in c.*

1.5 Thesis Outline

The focus of the remainder of this thesis will be on controlling charge transport through a single-molecule junction by taking advantage of the environment about junction. We will accomplish this by leveraging the interfacial electric double layers which form about the molecular junction when measurements are performed in an ionic solution. The large electric fields generated by these double layers will be used to modulate charge transport properties. With this, we show that we are able to create single-molecule analogues of transistors and diodes, and we show that with these techniques we can quantitatively assess

energy-level alignment at metal-molecule interfaces. An outline of the work presented in the remainder of this thesis follows:

Chapter 2 presents work characterizing the charge transport properties of two families of single-molecule junctions containing thiophenes and thiophene derivatives. In contrasting measurements of oligothiophenes and oligothiophene dioxides, we find that the latter are better suited for single-molecule devices due to increased planarity (and therefore, increased conjugation) and favorable energy level alignment. Due to their ubiquity throughout the organic electronics community, a better understanding of the electronic structure of thiophene-containing molecules at the single-molecule level may help lead toward better devices. We further find, using thermopower measurements, that the thiophene dioxide family is a unique system in which transport changes from being dominated by the highest occupied molecular orbital (HOMO) to being dominated by the lowest unoccupied molecular orbital (LUMO) as the length of the molecule is increased.

Chapter 3 describes our work using electrolyte gating to control charge transport through single-molecule junctions. By performing transport measurements in an ionic medium and incorporating a third gate electrode, we find that we are able to continuously modulate the conductance of molecular junctions containing non-redox active molecules. This finding demonstrates a single-molecule analogue of a conventional three-terminal device, a transistor, and enables us to investigate energy level alignment at the metal-molecule interface.

Chapter 4 details our efforts in creating a single-molecule diode which has its functionality imparted largely by its environment. This is again accomplished by taking advantage of transport measurements in an ionic medium, and the method enables us to create a diode usings a symmetric molecule. Combining this technique with the thiophene dioxides characterized in Chapter 2, we demonstrate single-molecule diodes with very low operating voltages and having the highest reported on/off current ratios.

Chapter 5 uses the method presented in Chapter 4 as a means by which to probe the electronic characteristics of a single-molecule junction. Current flow through small molecule

junctions typically proceeds via non-resonant, coherent tunneling, and by performing measurements in an ionic medium, we find that we are able to map the probability that an electron is transmitted through the junction as a function of energy. This again serves as a simple method for assessing energy-level alignment at the metal-molecule interface. Using this, we further examine molecular junctions as we near the resonant transport regime.

Chapter 6 provides a summary of the presented work and offers an outlook on future studies that can build upon the conclusions reached in this thesis.

Chapter 2

Single-Molecule Conductance Properties of Thiophene-based Oligomers

In this chapter, we characterize the single-molecule conductance properties of two families of thiophene derivatives: oligothiophenes and oligothiophene dioxides. Despite their prevalence in organic electronic devices, surprisingly few studies existed on their conductance properties at the single-molecule level. We find that, due to conformational effects, oligothiophenes are poor candidates for single-molecule devices. The aromatic properties and 5-fold symmetry of the thiophene unit leads to broad conductance distributions, which would make it difficult to create a reliable molecular device from this family. Oxidized thiophenes, on the other hand, are very good candidates. Oxidation of the thiophene unit breaks aromaticity, resulting in increased conjugation and rigidity of the oligomer backbone. This oxidation imparts the oligothiophene dioxide series with very advantageous electronic properties: a low decay constant, narrow conductance distributions, and favorable energy level alignment. The thiophene dioxide unit also has such a powerful impact on the LUMO that we find that the dominant conductance orbital for this family changes from the HOMO to the LUMO with increasing oligomer length.

2.1 Charge Transport Properties of Oligothiophenes

This section is based on the manuscript entitled *Length-Dependent Conductance of Oligothiophenes* by Brian Capozzi[†], Emma J. Dell[†], Timothy C. Berkelbach, David R. Reichman, Latha Venkataraman, and Luis M. Campos ([†] indicates equal contributions). Synthetic procedures and material characterizations were carried out by Emma J. Dell of Prof. Luis M. Campos' group. Modeling of experimental data was carried out by Timothy C. Berkelbach of Prof. David R. Reichman's group. I performed break junction experiments and data analysis.

2.1.1 Abstract

We have measured the single-molecule conductance of a family of oligothiophenes comprising one to six thiophene moieties terminated with methyl-sulfide linkers using the scanning tunneling microscope based break-junction technique. We find an anomalous behavior: the peak of the conductance histogram distribution does not follow a clear exponential decay with increasing number of thiophene units in the chain. The electronic properties of the materials were characterized by optical spectroscopy and electrochemistry to gain an understanding of the factors affecting the conductance of these molecules. We postulate that different conformers in the junction are a contributing factor to the anomalous trend in the observed conductance as a function of molecule length.

2.1.2 Introduction

Poly- and oligothiophenes are ubiquitous throughout organic electronic devices including photovoltaics and thin-film transistors. [71–76] This prevalence stems from their favorable chemical stability and synthetic versatility, together with outstanding optoelectronic properties. [71] However, understanding the structural and electronic building blocks from oligomers to polymers that specifically contribute to their overall performance remains a challenge. There is a need to enlarge the set of characterization tools in order to enable the detailed understanding of the structure-property relationship of organic semiconductors. [77] Recently, Briseño and co-workers demonstrated the effect of conjugation on

bulk conduction properties, [78] while Smith and co-workers studied solid-state thermal properties. [79] Oligothiophenes (OTs) have received little attention in the realm of single-molecule studies. [80–82] While a small number of research groups have demonstrated that oligothiophenes are conducting, [80–82] a thorough investigation of the relationship between molecular structure and conductance is lacking in these systems, and the idea of using single-molecule studies as a tool for characterizing the building blocks that constitute macromolecules remains in its infancy. Here, we probe the electronic characteristics of a series of bare OTs, which contain gold-binding linkers directly on the thiophene moieties, by measuring their conductance in metal-molecule-metal junctions. In this work, we uncover an unusual length-dependent conductance for the oligothiophenes, and we focus on understanding the unexpectedly high conductance of quaterthiophene. [80] We demonstrate how these single-molecule measurements can reveal unexpected electronic structure features of the molecules that are not observed in bulk measurements and we describe our efforts to probe the origin of this unusual conductance trend.

To our knowledge, the most fundamental and needed study of the single molecule conductance length dependence of OTs has not been carried out. In particular, previous studies of OTs contained gold-binding linkers separated by aliphatic units [80, 82] or functional groups along the backbone, [81, 83, 84] which can affect conformation and electronic properties. Tada and coworkers have probed the conductance of long oligothiophene molecular wires, surrounded by alkylsilyl groups, [81, 84] starting at five repeat units, and have recently synthesized wires completely encapsulated by fluorine units. [83] Tao and coworkers compared the conductance properties of ter- and quaterthiophene analogs. [80] They demonstrated, as we also observe, that the latter shows a higher conductance, and they attribute this to its highest occupied molecular orbital (HOMO) level being better aligned with the Fermi level of gold. Motivated by this result, and keeping in mind that the reduced symmetry of thiophenes leads to a broad distribution in conductance histograms, [52] we have carried out a thorough evaluation of the family of OTs to shed light on this anomalous behavior.

2.1.3 Results and Discussion

2.1.3.1 Conductance Measurements

In order to probe charge transport through oligothiophenes and understand how transport scales with length, we synthesized a family of compounds containing one to six thiophene units with gold-binding methyl sulfide end groups the most fundamental family in its class to be studied in single molecule junctions (Figure 2.1a). The molecules were synthesized by palladium catalyzed cross-coupling chemistries [85, 86] and fully characterized by standard techniques.

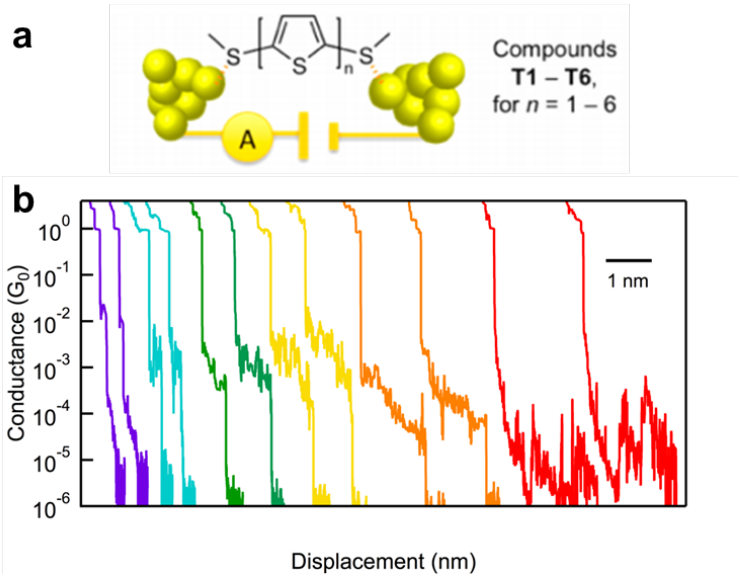

Figure 2.1: ***Single-molecule conductance traces for the oligothiophene family*** *(**a**) Schematic of the scanning tunneling microscope break-junction (STM-BJ) technique used to measure the conductance of oligothiophenes. (**b**) Sample STM-BJ conductance traces for T1 - T6 carried out under a bias voltage of 90 mV for T2, 220 mV for T3-T5, and 500 mV for T6. Note: T5 and T6 have hexyl chains for solubility, which are omitted here for clarity.*

The scanning tunneling microscope break-junction (STM-BJ) technique was used to measure the conductance of T1-T6. [2, 36] Single-molecule junctions are formed by repeatedly driving a gold tip into and out of contact with a gold-coated mica substrate; as the tip is retracted, an atomic point contact is formed and subsequently broken, creating a gap small enough to accommodate a gold-binding molecule. The measurements are carried

out in solution of 1,2,4-trichlorobenzene (TCB, 10 μM 1 mM concentration), at ambient conditions. Additionally, other solvents were used to study and confirm that the conductance traces correspond to individual molecules, and the results will be described below. We collected thousands of traces (conductance vs. displacement) that exhibit plateaus at integer multiples of the quantum of conductance, G_0 ($2e^2/h$), in addition to a plateau-like feature at below 1 G_0 that is attributed to the conductance of the molecule that bridges the ruptured gold point-contacts (Figure 2.1b). In general, the plateau length correlates with the length of the molecules present in solution. [53]

Compiling the thousands of single molecule conductance traces into logarithmically binned one-dimensional histograms yields a distribution of conductance values peaked at the most frequently measured conductance (Figure 2.2a). [50] We note that linear-binned histograms show broad features where the peak value of conductance is not easily determined (Supplementary Information section, SI Figure 2.7). The width of the peaks indicates that conductance varies significantly from junction to junction and as a function of elongation. The breadth of the plots in Figure 2.2a can generally be attributed to the reduced symmetry of thiophenes as compared with oligophenyls, which has been previously observed in bithiophene. [52] The conductance peak for each oligomer was fit with a Gaussian to determine the most probable conductance value, as indicated by the arrows in Figure 2.2a and SI Figure 2.8. These values are plotted against the distance, L, between the S atoms of the methyl sulfide groups on each of the fully elongated oligothiophenes (Figure 2.2b).

Our results show an unusual conductance trend in Figure 2.2b: we do not see a clear exponential decrease of conductance with oligomer length, as would be expected for coherent tunneling. The shorter (T1-T3 and T5) fall on an exponential (i.e., $G\ e^{-\beta L}$) with a decay constant of 0.3 per Å, a value that is close to that of other conjugated systems. [87–89] However, T4 appears to have a higher conductance than T3, and T6 has a conductance that is lower than would be expected from a simple exponential decay. This result is in contrast to measurements of alkanes [31,90–94] or oligoenes, [3,89,95] where the conductance of oligomers can be fit with a single exponential. Thus, understanding the nature of such unprecedented behavior could shed light on the factors that affect oligothiophene-based molecular junctions and can also explain the conjugation length observed in polymeric

versions of this molecule.

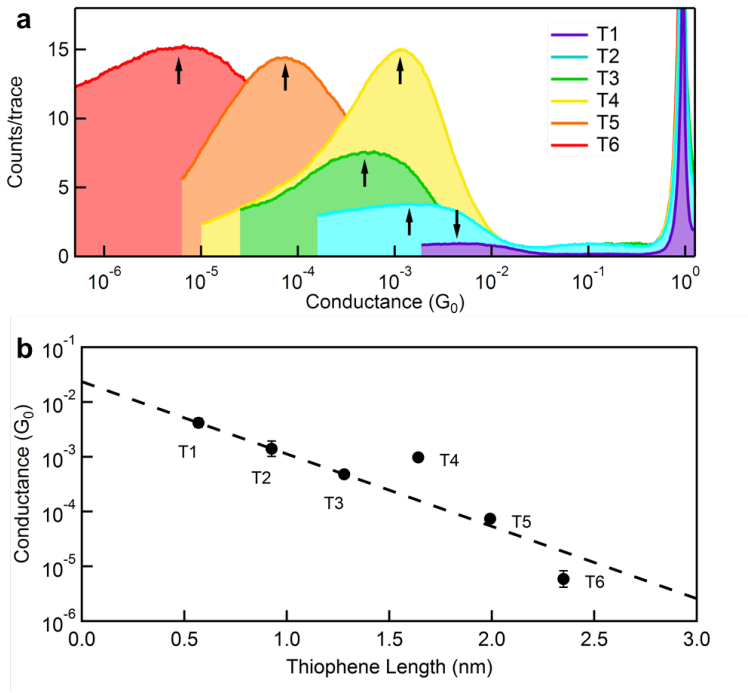

Figure 2.2: ***Single-molecule conductance histograms and beta plot for the oligothiophene family.*** *(**a**) Log-binned conductance histograms of the oligothiophenes T1-T6 (100 bins/decade). (**b**) Plot of conductance as a function of the length of the molecules T1-T6. Conductance for T1-T3, T5 have a decay constant β = 0.29 per Åand T4 and T6 are clearly off this line. Error bars indicate variation in conductance peak position determined from successive measurements.*

2.1.3.2 Origin of Anomalous Decay Constant

As discussed, a higher conductance for T4 as compared to T3 has also been observed before. [80] Since this behavior was attributed to the HOMO of quaterthiophene being closer to the gold Fermi level than that of terthiophene, we have performed cyclic voltammetry (CV) and UV-vis absorption measurements on T2-T6 in order to determine the frontier energy levels of the oligomers (Figure 2.3). The HOMO was determined from the oxidation potential (E_{ox}) by CV, and the lowest unoccupied molecular orbital (LUMO) was deduced from E_{ox} and the optical energy gap at the wavelength absorption onset from the UV-vis spectrum. We observe that the changes in the HOMO level as the number of thiophenes

increases are fairly small, indicating that the anomalously high conductance may not solely be due to changes in the energy level alignment of T4. In fact, T5 and T6 show almost the same oxidation potential as T4, which suggests that the HOMO does not get significantly closer to the Fermi level as the molecule length is increased. Had this been the trend that explains the anomaly, we would expect T5 and T6 to display conductance values similar to (or larger than) that of T4, contrary to what is seen experimentally.

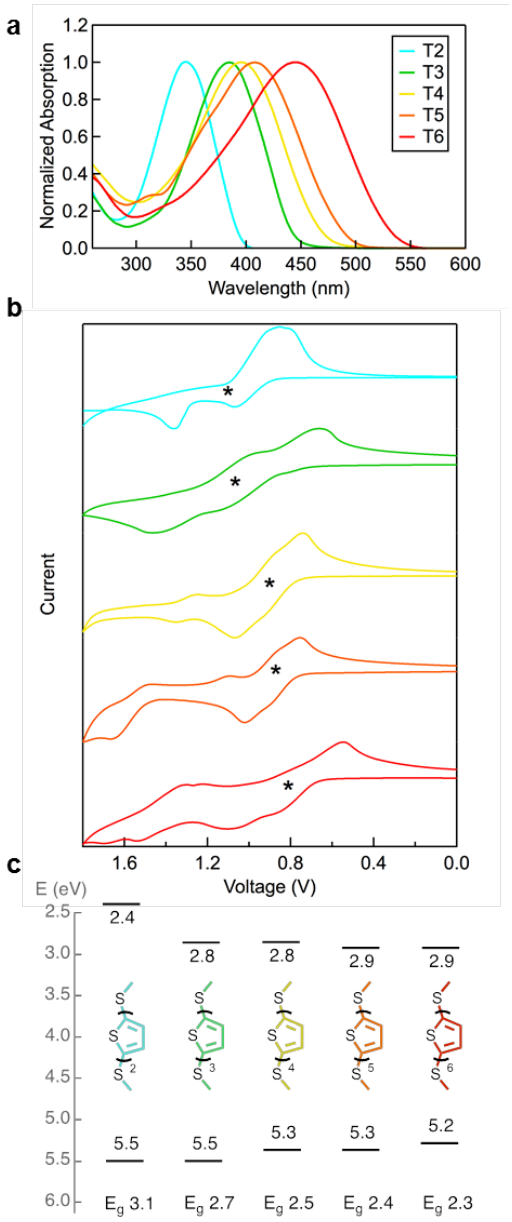

Figure 2.3: ***Energy level characterization of the oligothiophene family.*** *(**a**) Solution UV-vis absorption spectra of T2-T6 dissolved in DCM. (**b**) Cyclic voltammograms performed in dichloromethane (DCM) with Ag/AgCl reference electrode, 0.1M tetrabutyl ammonium hexafluorophosphate as the electrolyte and a scan rate of 50 mV/s for T2 to T6. Asterisks denote the position of the first oxidation potential for each molecule. (**c**) Optical gaps determined from UV-vis spectra placed relative to the HOMO obtained from the cyclic voltammetry following standard published methods. [66]*

Further insight into this hypothesis can be obtained from a coherent tunneling model. Since these molecules conduct through the HOMO, we construct a simplified Hamiltonian describing an oligomeric molecule (M) with N bridge sites, each representing the HOMO of a single thiophene unit (N = 1-6 for T1-T6) to elucidate the effect of increasing molecular length on the transmission characteristics (the linker gateway state is neglected for simplicity). The Hamiltonian also includes the coupling to the left (L) and right (R) gold electrodes. Specifically, we use $H = H_L + H_R + H_M + H_{ML} + H_{MR}$, with:

$$H_M = \sum_{n=1}^{N} \epsilon_H |n\rangle \langle n| + \sum_{n=1}^{N-1} t_H(|n\rangle \langle n+1|) + HC$$

$$H_L + H_R = \epsilon_s(|L\rangle \langle L| + |R\rangle \langle R|)$$

$$H_{ML} + H_{MR} = t_s(|L\rangle \langle 1| + |N\rangle \langle R|) + HC$$

where HC denotes the Hermitian conjugate of preceding terms. In the above equation, ϵ_s is the gold s-orbital energy, t_s is the coupling between the molecule and the gold, ϵ_H is the single-site HOMO energy, and t_H is the inter-site HOMO coupling. The model system is shown schematically in Figure 2.4a. The transmission coefficient, $T(E)$, can be evaluated by standard Greens function techniques (see section 2.1.5 for details), accounting for hybridization with the electrodes via an imaginary constant self-energy, $\Sigma = -i\Gamma/2(|L\rangle \langle L| + |R\rangle \langle R|)$.

Using reasonable approximations for the HOMO electronic coupling and the electrode hybridization (see Methods), we considered the effect of varying the offset between the HOMO site energies and the electrode Fermi energy. Through this procedure, we are simply seeking to identify a regime where we can observe an increased conductance for T4 compared to T3. When far from resonance, the transmission coefficient displays purely exponential behavior with the number of bridge sites, as typically observed. [32, 89] By raising the HOMO site energy, one can realize a situation whereby the transmission decays for T1-T3, but increases for T4, as observed experimentally (Figure 2.4b). The parameters required for this behavior also qualitatively reproduce the gating dependence observed by Tao and co-workers for T3 and T4 (Figure 2.4c). However, this resonance effect persists for

T5 and even more so for T6, predicting a continued increase in the conductance, contrary to what is seen experimentally. This behavior can be understood by tracking the molecules HOMO energy E_H (not to be confused with ϵ_H) as a function of length, which demonstrates the increased resonance for T5 and T6 (Figure 2.4d). The evolution of the molecular HOMO energy is seen to be in good agreement with the CV results (Figure 2.3c). However, the lack of agreement between the measured and predicted conductance trends for T3-T6 indicate that in a molecular junction, the HOMO is not getting significantly closer to E_F. Thus transport in these systems is due to a far off-resonance tunneling mechanism. In this regime, small changes in the location of E_H relative to E_F have a negligible impact on the trend in conductance as a function of molecular length. The simple model presented here fails to explain the data, confirming our proposition that the experimental behavior is not due to enhanced resonance effects

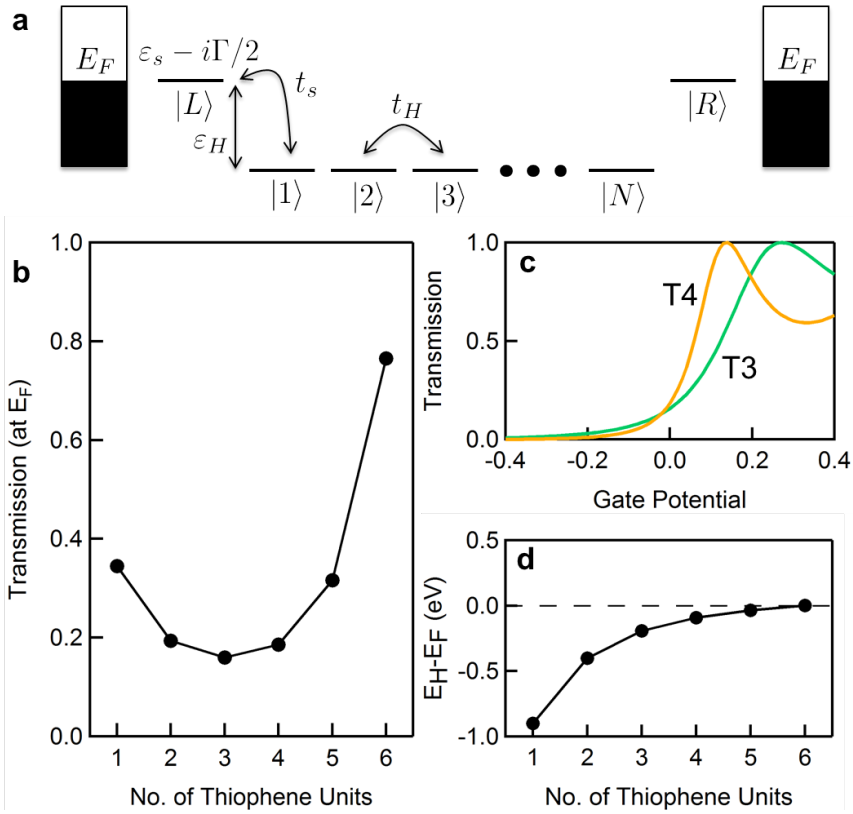

Figure 2.4: ***Tightbinding model for transport through oligothiophene family.*** *(**a**) Schematic of the tunneling model employed for transport calculations. (**b**) Calculated low-bias transmission, showing qualitatively correct behavior for T1-T4, but not T5 and T6. (**c**) Calculated gating dependence of the transmission for T3 and T4. (**d**) Difference in energy between the molecular HOMO and the Fermi energy of the gold electrodes.*

A second possible explanation for the non-exponential decay in conductance seen here could be due to a water gating effect. Recent studies show that water solvation shells around the backbone of a molecule can change transport resonances and therefore increase conductance; this effect was found to be particularly strong for long molecules. [82] To investigate whether the high conductance observed for T4 is a result of such a gating effect, we measure the conductance of T4 in an argon environment. We find that the conductance of T4 in argon is slightly higher than that in air (SI Figure 2.9), but within the width of the histograms. Therefore, water gating cannot explain the higher conductance of T4 compared to T3 that we observe in our measurements.

It has been postulated that oligothiophenes may form pi-aggregates in solution, and Tada and co-workers have synthesized oligomers bearing groups that can hinder such aggregation. [83] However, OTs are known to pack in a herringbone structure in the solid-state, and such a packing would not enhance the conductance of molecular junctions. [96–98] Nonetheless, we investigated whether the molecules formed aggregates in solution by studying the temperature, concentration, and solvent dependence on their UV-vis absorption spectra. Solutions of the oligothiophenes in TCB (the solvent used for the conductance measurements) were cooled from 55°Cto 17°C(Figure 2.5a and SI Figure 2.10). During cooling, we saw no change (bathochromic or hypsochromic) in the onset of absorption of the oligothiophenes. Solutions of aggregates typically show reductions in their extinction coefficients and blue shifts on the order of 50 nm upon cooling. [99–102] Thus our spectra are indicative of free molecules in solution. Changes in concentration should also affect the spectra of aggregates. We varied the concentration of oligothiophene in TCB and again saw no change in the positions of the onset of absorption or λ_{max} (Figure 2.5b). Molecules prone to aggregation display different behavior in good and poor solvents. When the solvent is varied, we note only a slight change in the onset of absorption and λ_{max} from the non-polar tetradecane (C14) to the slightly polar DCB (Figure 2.5c). However these changes, on the order of 5-10 nm, are minor compared to those of 50-70 nm reported as evidence of oligothiophene aggregates in solution.**[20a]** Furthermore, there is no change in the shape of the absorption curve, even across a wide range of solvents (SI Figure 2.11), and these curves are typical for fully dissolved oligothiophenes. We also measured the conductance of T4 in various solvents and at various concentrations and saw no difference in the width of the histograms (Figure 2.5d and SI Figure 2.12). Thus, we can rule out the possibility that pi-stacked aggregates are formed in the junction, and we cannot attribute the unusual decay trend to the sampling of multiple molecules or aggregates in the junction.

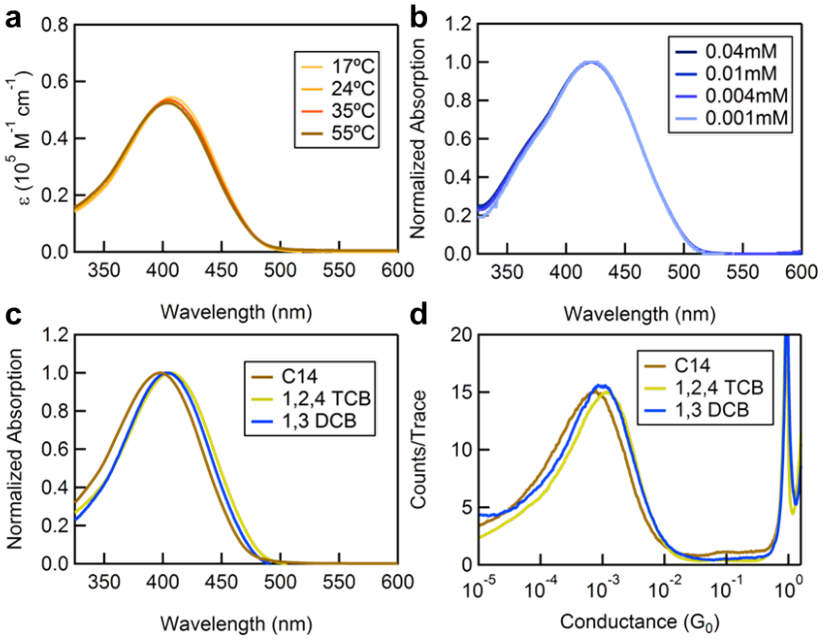

Figure 2.5: ***Aggregation studies of the oligothiophene family.*** *(**a**) UV-vis absorption data taken in 1,2,4-trichlorobenzene (TCB) for T4 at temperatures from 17°C to 55°C. (**b**) UV-vis absorption data taken in TCB for T5 at different concentrations, normalized to allow comparison of the onset of absorption. (**c**) UV-vis absorption data of T4 taken in different solvents. (**d**) Conductance histograms for T4 in three solvents: tetradecane (C14), 1,2,4-trichlorobenzene (TCB), and 1,2-dichlorobenzene (DCB).*

Having ruled out HOMO-Fermi level resonance, water gating, and aggregation as explanations for the high conductance of T4, we further analyzed two-dimensional (2D) conductance histograms to extract information on the length dependent behavior, which can correlate to conformational changes, on the conductance of the oligothiophene family. Since the length of the thiophene in the junction can depend on the orientation of the thiophene units relative to each other, we constructed 2D conductance-displacement histograms, without data selection to understand how the molecular conductance evolves with junction elongation.[**11**] Figure 6a shows these 2D histograms for T3, T4 and T5 (others are shown in SI Figure 2.13). In these plots, we see a conductance feature that extends to longer displacements with increasing number of thiophene units (SI Figure 2.14). This indicates that the conductance plateau length in individual traces scales with the molecular length

of the backbone, as has been found in other STM-BJ experiments. [53, 103] These results thus provide additional conclusive evidence that stable molecular junctions are formed with these oligothiophenes. Furthermore, a detailed comparison of the 2D histograms for T3 and T4 (Fig 2.6a) indicate that the conductance of T4 is high for small displacements (relative to the point where the Au contact breaks). It is possible that for T4, the π-system couples directly to the gold electrodes at small electrode separation, [89] enhancing conductance, though it is not clear why T5 does not show a similar effect. The 2D histograms also show that the conductance of a fully elongated T4 junction is comparable to that of a T3 junction.

To isolate and analyze the data of fully extended junctions, we determined the conductance from a subset of the two-dimensional histograms within a 0.5 nm window demarcated by the dashed lines in Figure 6a. We integrated all counts within this window to generate a conductance profile [104] (shown in the last panel of Figure 6a) and fit a Gaussian to determine a peak conductance value. These values are plotted against molecular length in Figure 2.6b, which is fit to a single decay with $\beta = 0.4$ per Å. However, we again see that T4 lies above the line and T6 below. Furthermore, β has diminished, indicating that fully extended junctions have a larger decay constants. This difference indicates strongly that the larger number of conformations that can be sampled in a fully elongated junction decreases the overall conjugation length in these oligothiophenes. Note that the decay constants determined here for T1-T3 are also different from that found by Yamada et al. (0.1 per Å), [81] however, their measurements were for alkylsilylamino-substituted oligomers of 8 or more units where conductance could be through a hopping mechanism. [81,84] Therefore, we see that this conductance trend is not entirely due to trapping molecular conformations that have shorter overall lengths.

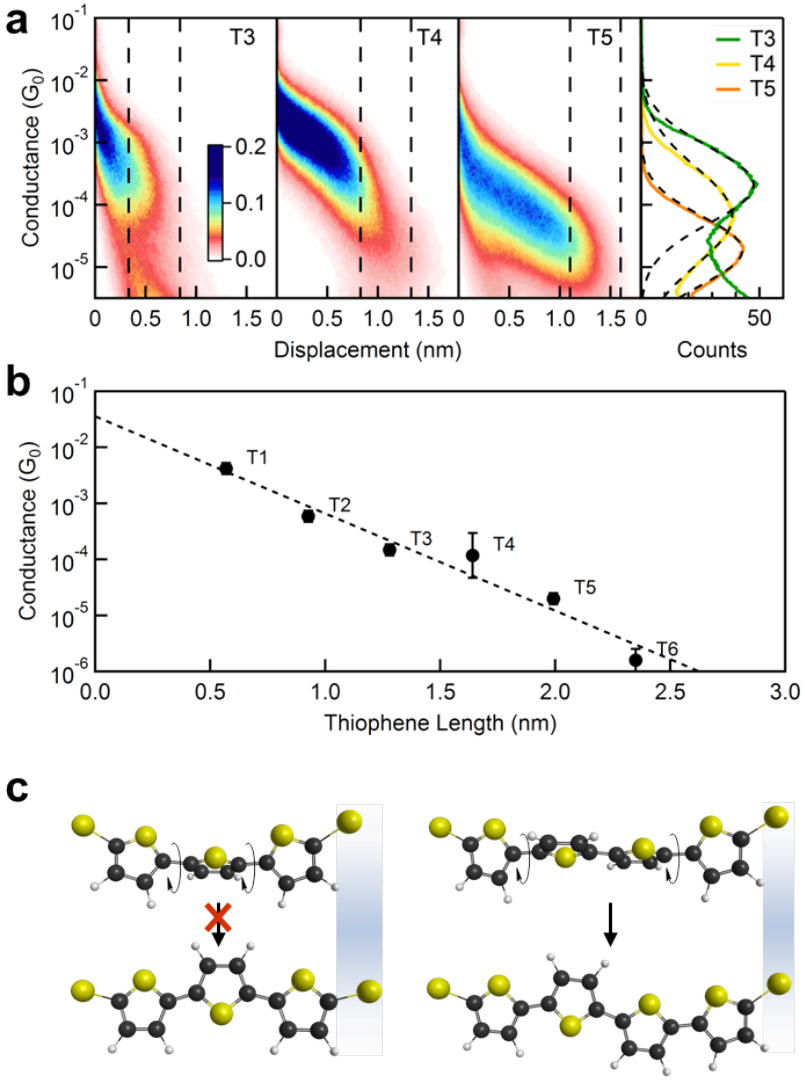

Figure 2.6: ***The influence of conformational effects on oligothiophene conductance.*** *(**a**) Two-dimensional (2D) conductance histograms of T3, T4 and T5, along with the respective conductance profiles (last panel) generated from the indicated 0.5nm windows. (**b**) Plot of the conductance obtained from the 2D plot for a fully elongated junction (demarcated by the dashed lines in Figure (**a**) as a function of the length of the molecules T1T6. A line fit through the entire data set gives a decay constant $\beta = 0.4$ per Å. (**c**) Illustration of the hindered T3 rotation in a junction and the length increase (left) compared to the lower energy rotation and length conservation in T4 (right).*

We now turn to discuss the conformational effects in these molecular junctions, which have been previously shown to play an important role when comparing bithiophene to biphenylene conductance trends focusing on the difference between T3 and T4. [52] When chains of five-membered rings are bound in a junction their rotational freedom is restricted; this effect is more pronounced for T3 than T4. If a T3 molecule enters the junction in a twisted conformation, it is unable to rotate to a more conjugated, planar form, both due to the high degree of rotational strain and the increase in overall molecular length which would result in the junction rupturing, as illustrated in Figure 2.6c. In contrast, if a T4 molecule enters the junction in a twisted conformation, rotation to the more planar form is possible. A simultaneous rotation of the middle two rings does not change the end-end length significantly, avoiding junction rupturing, thus leading to planar conjugated structures more feasibly than when compared with T3 (Figure 2.6c). Such a difference could explain the higher conductance observed for T4 when compared to T3 as well as the narrower conductance histogram (Figure 2.2a). Extending this argument to T5 and T6, one might expect an even narrower distribution in conductance than for T4. However, the extra thiophene units now yield multiple rotational degrees of freedom which add extra disorder to the system, and thus the conductance distribution becomes quite broad again. Furthermore, the two hexyl groups on the T6 might also hinder a planar conformation in a junction, yielding a lower conductance than would be predicted by a simple exponential relation.

2.1.4 Conclusions

In summary, we have carried out single molecule conductance measurements on a family of methyl sulfide-terminated oligothiophenes using the scanning tunneling microscope based break-junction technique. We find that the peak of the conductance histogram distribution does not follow a clear exponential decay with increasing number of thiophene units in the chain. We attribute this trend to different conformers formed in single-molecule junctions, which is supported by the narrow conductance distribution peak of T4 relative to all other oligothiophenes. We point out that although we have shown that a simple coherent tunneling model fails to explain the experimental data, [105] this picture precludes more

complex effects, such as Coulomb interactions on the molecule, hopping transport, and strong electron-phonon coupling. All of these effects are to be expected in conjugated polymers, especially with increasing length. A more microscopic investigation of these effects is beyond the scope of the current work, but an interesting topic for future investigation.

2.1.5 Supplementary Information

2.1.5.1 Synthetic Details

Details of the procedures used to synthesize the molecules studied in this section can be found in the manuscript *Length-Dependent Conductance of Oligothiophenes*

2.1.5.2 Model Details

Transmission functions are calculated using standard Greens function techniques, yielding $T(E) = \Gamma^2|G_{L,R}(E)|^2$, where $G_{L,R}(E) = L|(E - H - \Sigma)^{-1}|R$ and all quantities have been defined previously. The energy-dependent transmission coefficient is evaluated at the Fermi energy, which assumes low bias transport. The specific parameters used in the generation of Figure 4 are (in eV) ϵ_H=-0.9, t_H=0.5, ϵ_s=E_F=0, t_s=0.7, and Γ=3.0.

2.1.5.3 Additional Figures

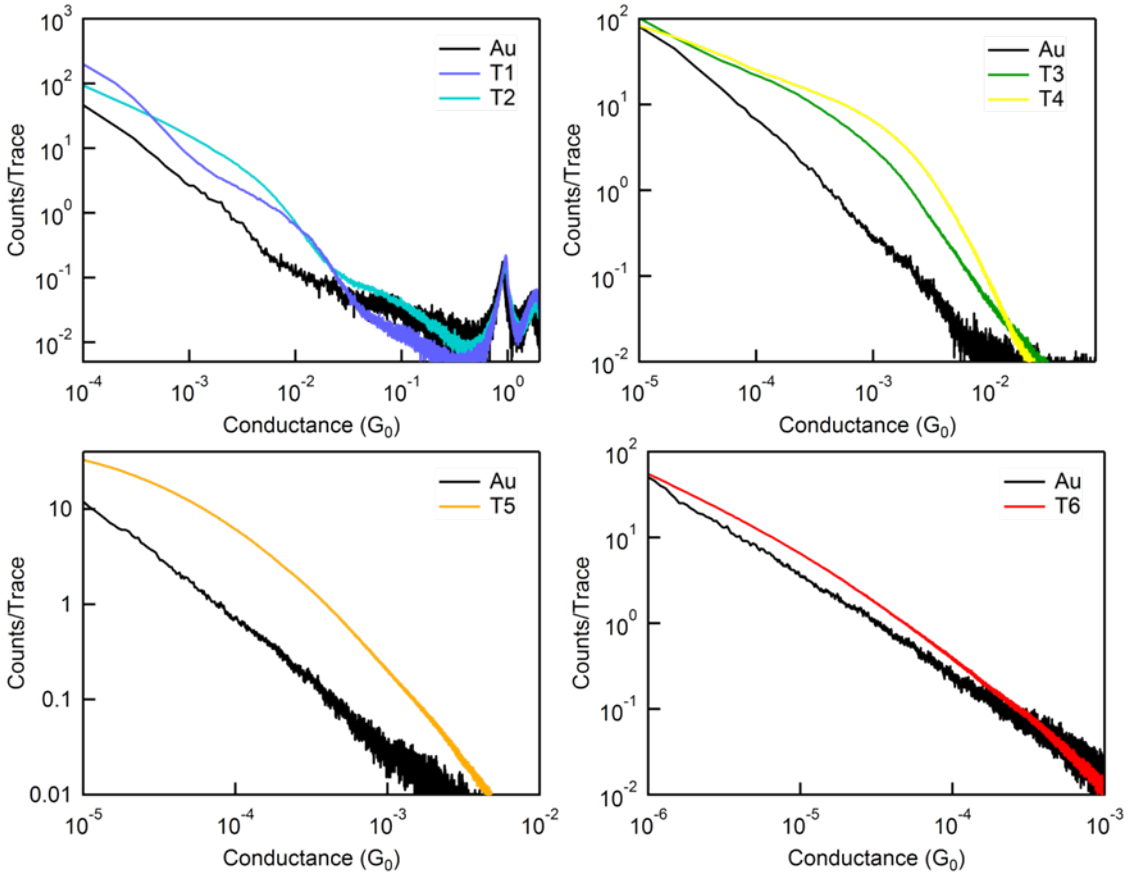

Figure 2.7: *Linear-binned conductance histograms for T1-T6.*

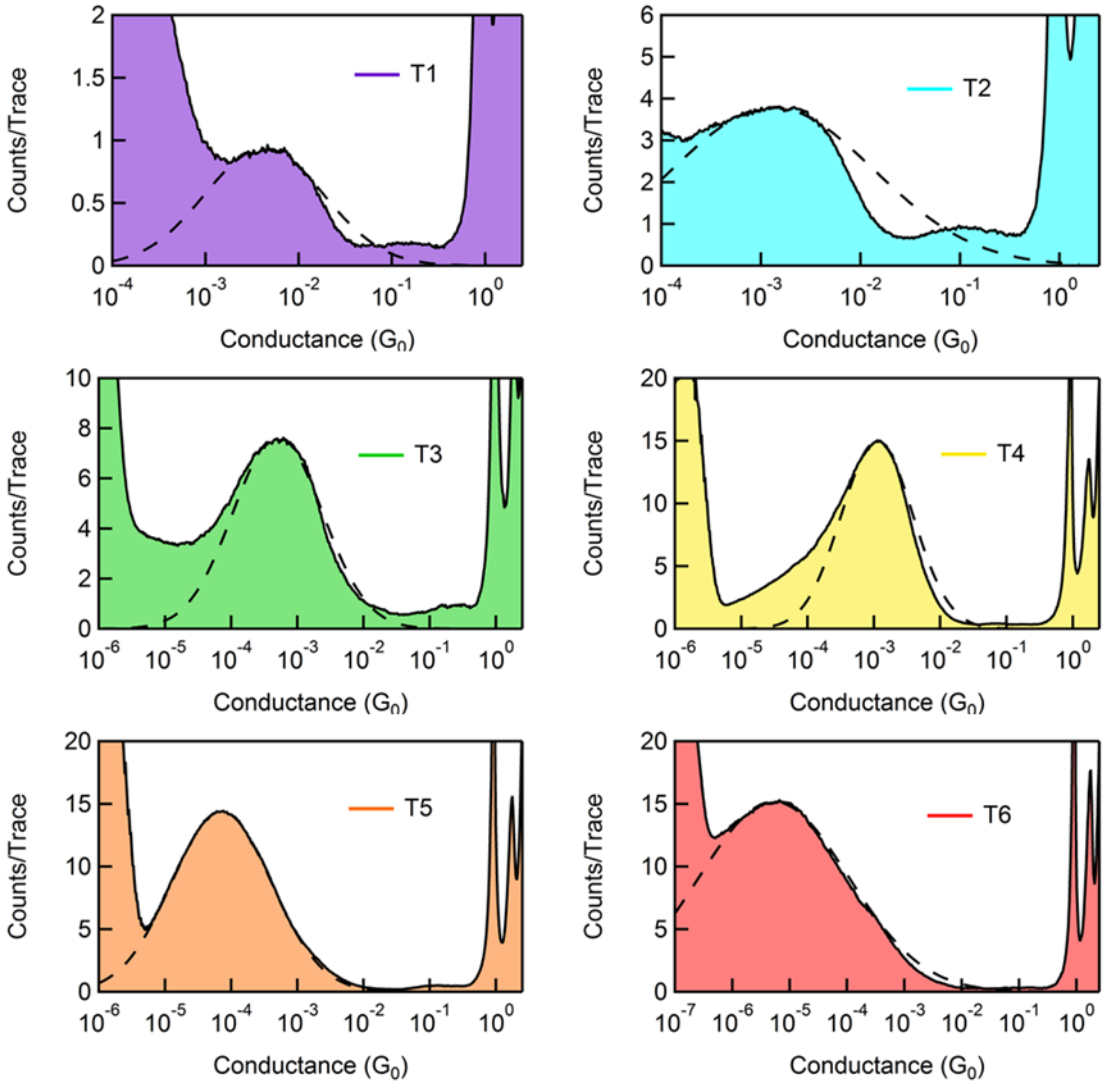

Figure 2.8: ***Logarithmically binned conductance histograms for T1-T6.*** *Black dashed curves are Gaussian fits to the conductance peak.*

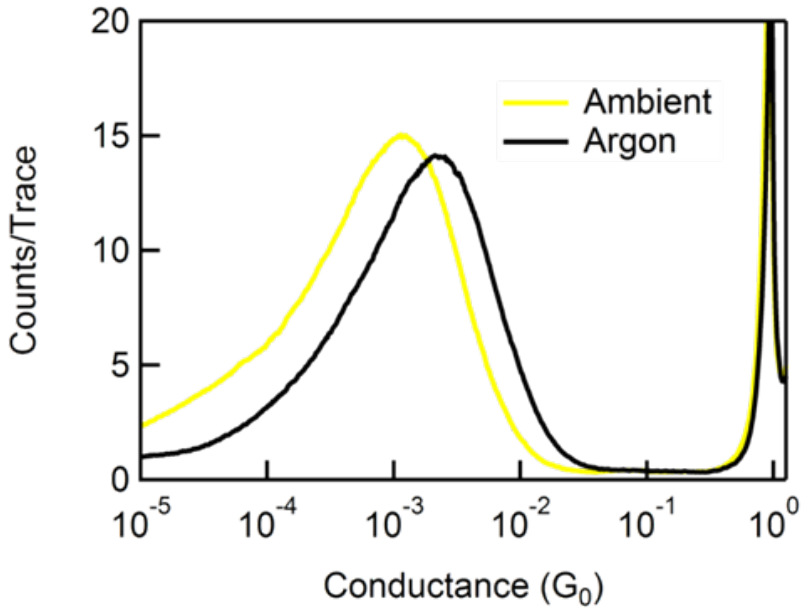

Figure 2.9: ***T4 conductance under argon and in ambient conditions.***

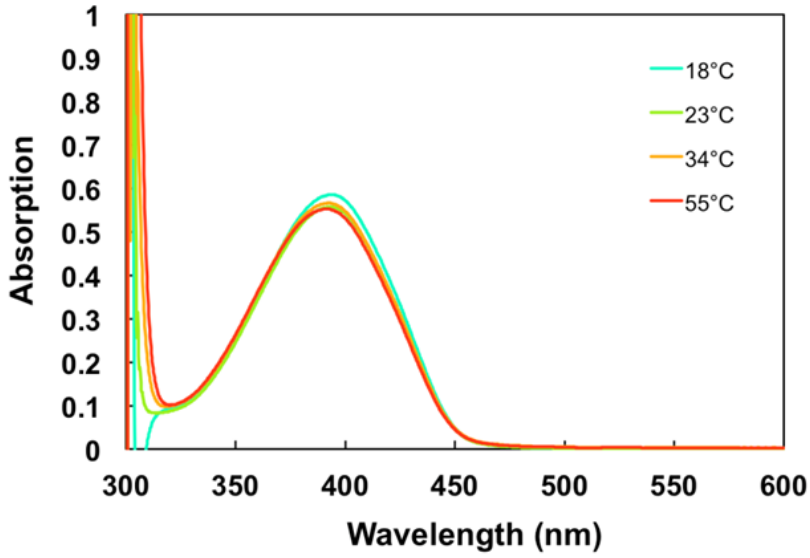

Figure 2.10: ***Additional oligothiophene aggregation studies: temperature data.*** *UV-vis absorption data taken in 1,2,4 trichlorobenzene for T3 at temperatures from 18° C to 55° C.*

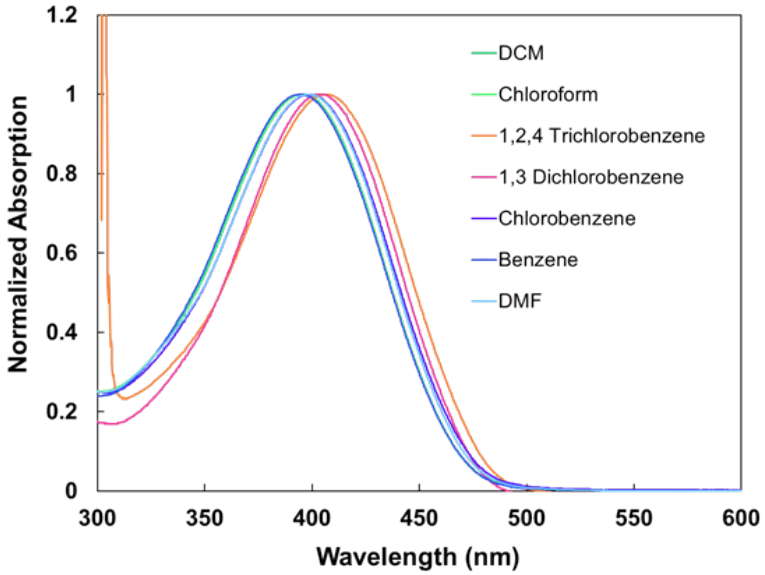

Figure 2.11: ***Additional oligothiophene aggregation studies: solvent data.*** *UV-vis absorption data taken in various solvents for T4.*

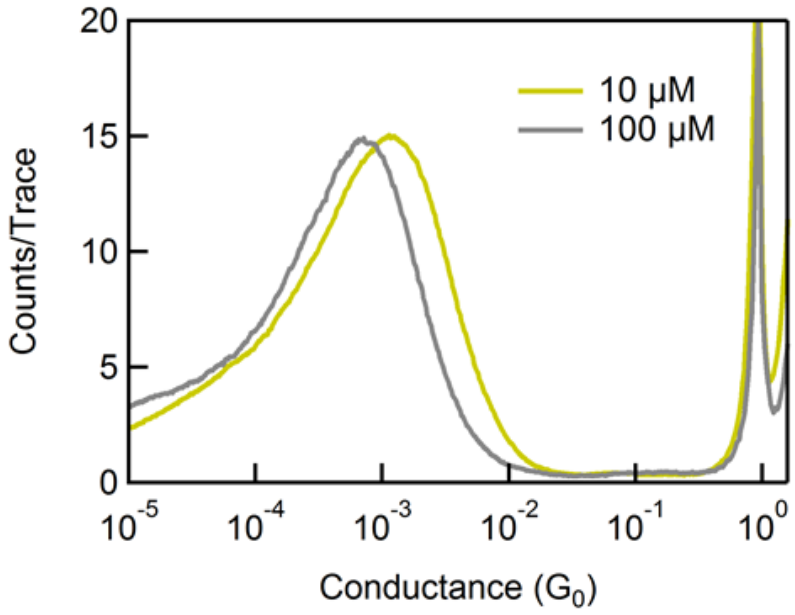

Figure 2.12: ***Additional oligothiophene aggregation studies: concentration data.*** *Logarithmically binned conductance histograms for T4 in 1,2,4-trichlorobenzne at two concentrations.*

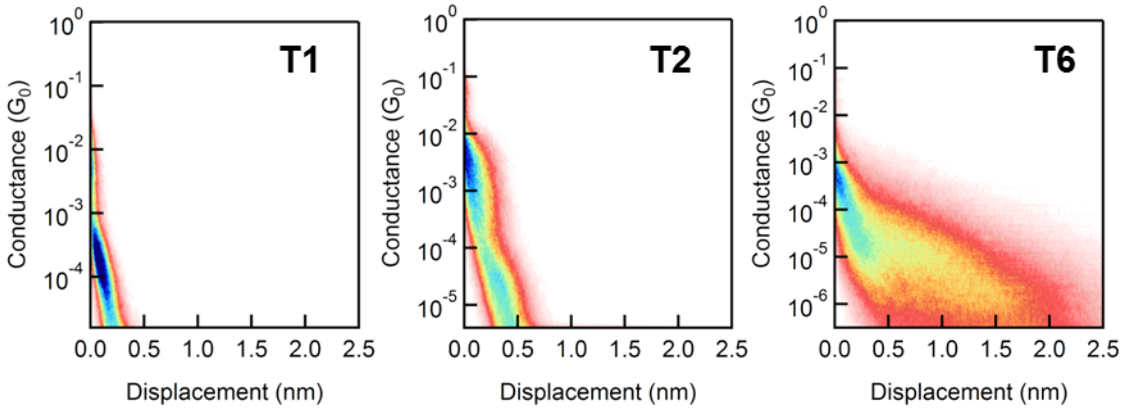

Figure 2.13: ***Two dimensional oligothiophene conductance histograms.*** *Two dimensional conductance histograms for T1, T2 and T6.*

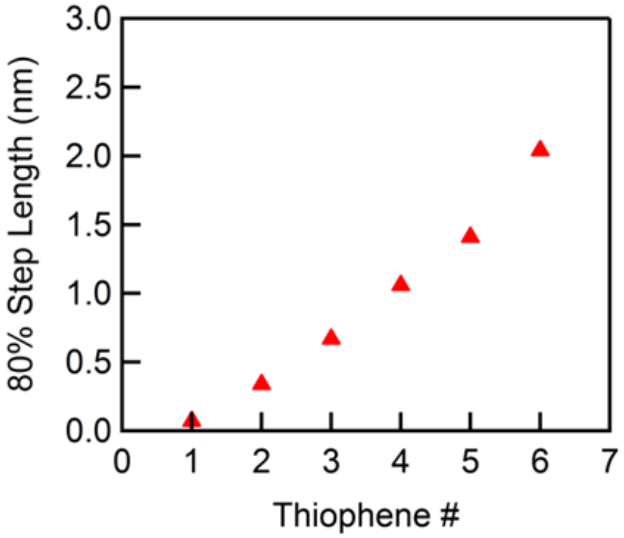

Figure 2.14: ***Oligothiophene step-length versus molecular length.*** *The relationship between the number of thiophene units and the observed step length. Step length is determined following the procedure detailed in reference [106]*

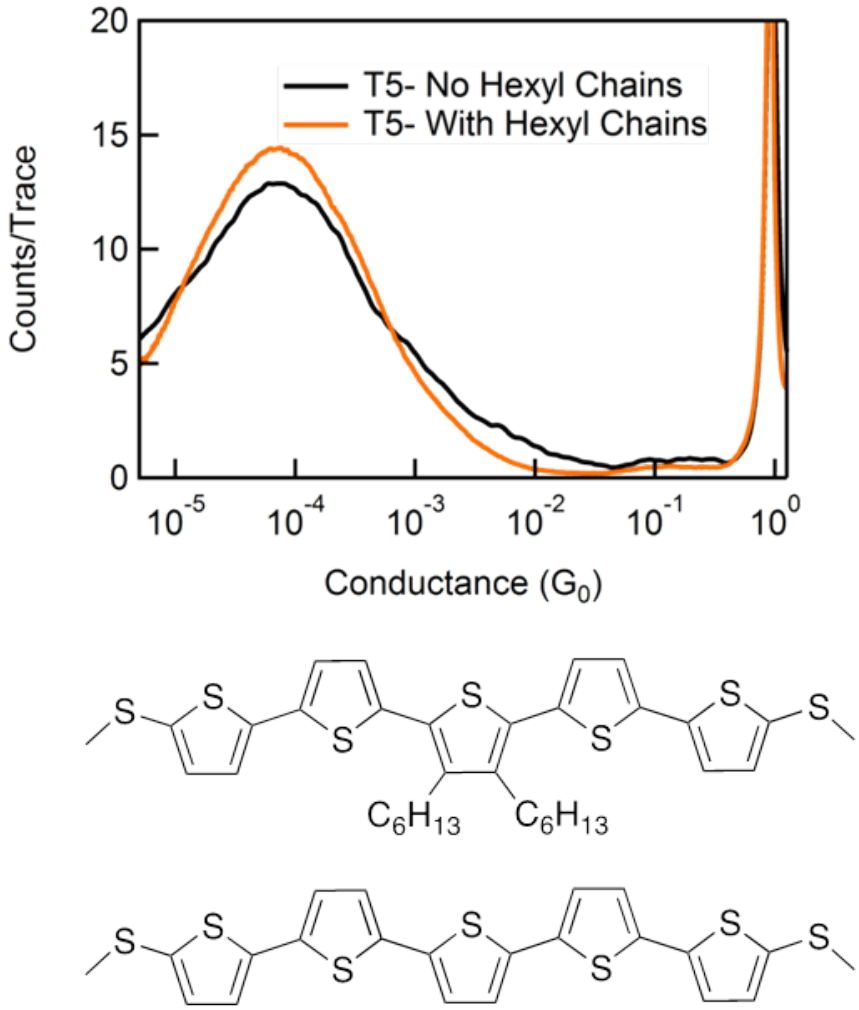

Figure 2.15: ***Influence of hexyl chains on T5 conductance.*** *Logarithmically binned conductance histograms for a T5 molecule with and without hexyl chains. Molecule structures are shown beneath the plot.*

2.2 Charge Transport Properties of Oligothiophene Dioxides

This section is based on the manuscript entitled *Molecular Length Dictates the Nature of Charge Carriers in Single-Molecule Junctions of Oxidized Oligothiophenes* by Emma J. Dell†, Brian Capozzi†, Jianlong Xia, Latha Venkataraman, and Luis M. Campos († indicates equal contributions). Synthetic procedures and material characterizations were carried out by Emma J. Dell and Jianlong Xia of Prof. Luis M. Campos' group. I performed the

experimental work and data analysis.

2.2.1 Abstract

In order to develop advanced materials for devices, it is of utmost importance to design organic building blocks with tuneable functionality and study their properties at the molecular level. For organic electronics and photovoltaics applications, the ability to vary the nature of charge carriers, creating either electron donors or acceptors, is critical. Here, we demonstrate that charge carriers in single-molecule junctions can be tuned within a family of molecules containing an electron-deficient thiophene-1,1-dioxide (TDO) building blocks. Oligomers of TDO were designed in order to increase electron affinity, maintain delocalized frontier orbitals, while significantly decreasing the transport gap. Through thermopower measurements we show that the dominant charge carriers change from holes to electrons as the number of TDO units is increased. This results in a unique system in which the charge carrier depends on backbone length, providing a new means to tune p- and n-type transport in organic materials.

2.2.2 Introduction

Organic electronic materials have impacted the development of semiconducting, [107] photovoltaic [77] and thermoelectric devices. [41, 108] The precise control afforded over molecular design by organic synthesis allows for device properties to be readily tuned. For example, the ability to design and synthesize hole-/electron-transporting (p- and n- type, respectively) and ambipolar semiconductors, from principles of electronic structure, has led to significant advancements in organic electronics. [109–112] While design principles to create stable n-type organic materials are evolving, isolating the intrinsic fundamental electronic structure contributions of the building blocks to bulk transport can be challenging. Strategies to increase electron affinity, such as incorporating electronegative functional groups onto conjugated molecules, have been developed to enable electron transport. [113–115] Although there is a wealth of organic electron-deficient building blocks that may be used to synthesize conjugated molecules, [77, 107] it is challenging predict charge carrier type prior to making the materials. For example, thiophene-1,1-dioxide (TDO, Fig. 2.16a), an oxidized

counterpart of thiophene, is unique in that it imparts vastly different electronic properties, arising from the break in aromaticity when the sulphur lone pairs are engaged in bonding. [116] This leads to electron-deficient building blocks with strong dipole moments and oligoene-like backbones (Fig. 1b). Interestingly, compounds containing TDO moieties have been found to have low-lying lowest unoccupied molecular orbitals (LUMOs) and n-type characteristics. [115, 117–121] However, the point at which these materials exhibit n-type behavior as a function of conjugation length is unknown. Since families of n-type materials are underdeveloped in comparison to their p-type counterparts, determining this crossover point is an important fundamental development that can lead to advanced materials design for applications in organic electronics. [113, 115]

Characterizing electron transport properties in these materials can be challenging since bulk transport depends on both intramolecular and intermolecular orbital coupling, the latter being a difficult parameter to control. [115] However, the scanning tunneling microscope based break junction (STM-BJ) technique provides a means of probing the fundamental electronic properties at the single-molecule level, rather than in bulk materials (Fig. 2.16a). [2, 4] In this technique, a molecule is bridged between two nanoscale gold electrodes and its conductance is measured. The conductance depends on a number of factors including the energetic alignment of the molecular frontier orbitals with the Fermi level of the gold electrodes. Whether the molecule conducts through the highest occupied molecular orbital (HOMO) or LUMO depends on which of the two frontier orbitals is better aligned with the Fermi level and better coupled to the metal. Generally, the dominant factor in this alignment has been the nature of the linker groups that bind to gold. For example, amine linker groups usually display HOMO conducting behavior while pyridine linkers display LUMO conducting behavior. [42, 122] At the molecular level, the nature of the charge carriers in single-molecule junctions can be evaluated by measuring the Seebeck coefficient (thermopower, S). [41, 42] The value of S relates to the derivative of transmission function at the electrode Fermi energy [57] and hence its sign relates to the nature of the charge carriers (Fig. 2.16c). [41, 57]

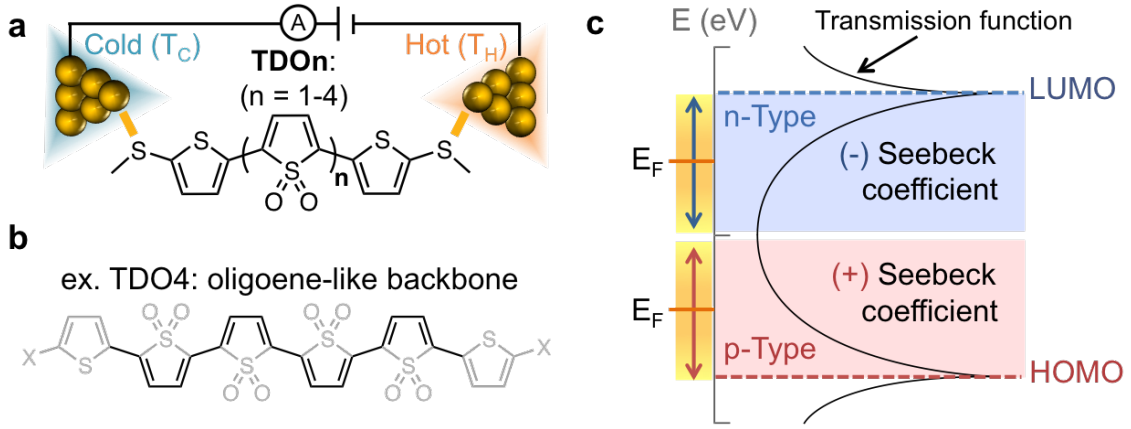

Figure 2.16: ***Characterization of the nature of charge carriers using the scanning tunneling microscope break junction technique.*** *(**a**) Schematic representation of the STM-BJ setup to measure the Seebeck coefficient of a family of molecules, TDOn (n = 1-4, TDO4 is shown in the lower panel). The STM-BJ gold substrate is heated while the gold tip is maintained at room temperature. (**b**) Diagrammatic representation of the oligoene-like backbone in TDO4 resulting from the reduction in aromaticity of the thiophene ring upon oxidation and therefore increased conjugation along the backbone (**c**) Example transmission function which determines the probability that an electron of a given energy will tunnel through the molecular junction. Sections are highlighted where the Fermi level of a gold electrode (E_F) aligns closer to the HOMO or LUMO of the molecule. The Seebeck coefficient is proportional to the slope*

Here, we study the charge transport characteristics of a family of molecules that are composed of electron-deficient oligo-TDO building blocks coupled to unoxidized thiophenes on both sides (Fig. 2.16b). This particular electron-rich/electron-poor combination yields a drastic reduction in the transport gap of these molecules (as compared to their all thiophene counterparts). We show two interesting results that impact molecular conductance. First, the conductances exhibit a very shallow decay with molecular length (similar to that of oligoenes). This is a manifestation of their small energy gaps and very well conjugated backbones, with contributions from the quinoidal character of these systems. Second, through thermopower measurements with the two electrodes at different temperatures, we find that the dominant charge carriers switch from holes to electrons when the number of TDO monomers in the molecular backbone is increased, while the linker groups remain constant. This is the first time that changing the number of repeat units in an oligomer

has been shown to change the conducting orbital, i.e. the charge carriers. This work, therefore, provides an additional handle with which to tune conductance in single molecule measurements, as well as underscoring the promise of thiophene-1,1-dioxide as a powerful electron-deficient motif with a low-lying LUMO to tune electronic properties in bulk materials.

2.2.3 Results and Discussion

2.2.3.1 Orbital Characterization

We first show that our molecule design, that couples a central electron-deficient TDOn oligomer to two electron-rich thiophenes on either end does indeed achieve a fully conjugated system with a small HOMO-LUMO gap. [123] To this end, we compare the UV-vis absorption spectra of three different trimers: (1) a fully unoxidized (ter-thiophene) trimer (2) a fully oxidized trimer and (3) a single oxidized unit flanked by two gold-binding methylsulfide [31] bearing thiophenes as shown in the supplementary information (SI, section 2.2.5) Fig. 2.20. The fully unoxidized trimer has the shortest onset of absorption wavelength (λ_{onset} = 425 nm) and thus has the largest optical energy gap (see SI Fig. 2.20). The fully oxidized non-aromatic trimer shows a significant red-shift (ca. 100 nm) at the onset of absorption. This is due to better electron delocalization along the molecular backbone, stabilization of the LUMO, and increased planarity, which is inferred from the pronounced vibronic structure of its absorption spectrum. [124] The third trimer, TDO1, displays the longest λ_{onset} (575 nm), even though only a single unit has been oxidized. This reduction in optical gap of TDO1 compared to the unoxidized trimer demonstrates the powerful donor-acceptor hybridization in these systems. [125, 126]

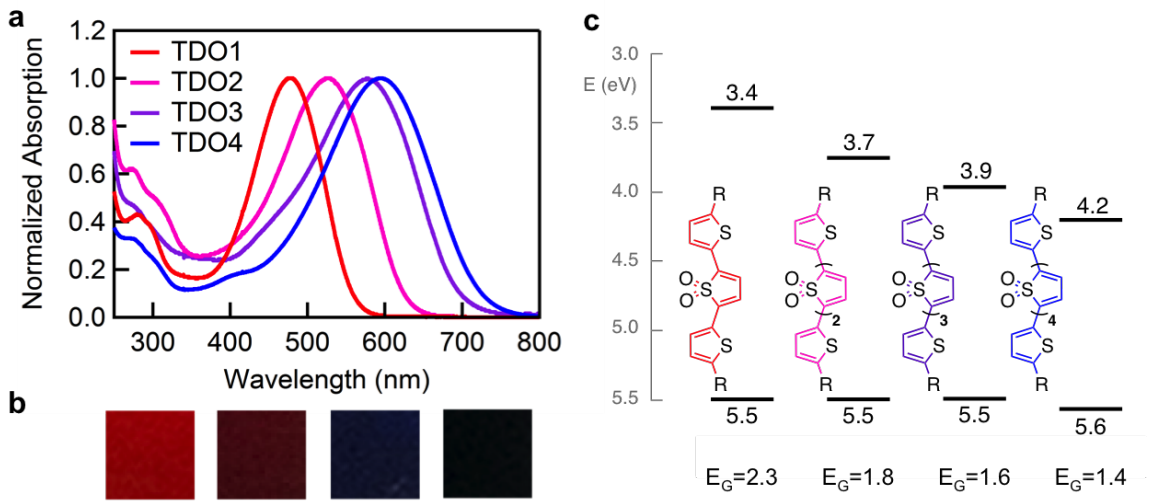

Figure 2.17: ***Energy level characterization of the TDOn family.*** *(a) Normalized UV-vis absorption spectra for the TDOn family measured in dichloromethane. (b) Color images of the 0.2 M concentration TDOn dichloromethane solutions. (c) Cyclic voltammetry-derived HOMO and LUMO levels in eV for the TDOn (R=SMe) family. These are determined by first measuring the oxidation and reduction potentials ($E_{ox1/2}$ and $E_{red1/2}$) through cyclic voltammetry carried out in dichloromethane solutions using a Pt working electrode and an Ag/AgCl reference electrode (Fig. S2 and Table S1). The HOMO and LUMO levels for TDOn are then obtained using a HOMO level for Ferrocene of -4.8 eV and $E_{ox1/2}$ 0.4 V. [31, 127] The specific relationships used are: $E_{HOMO} = e[E_{ox1/2} + 4.4]$ and $ELUMO = e[E_{red1/2} + 4.4]$.*

We now turn to UV-vis spectroscopy and cyclic voltammetry (CV) measurements to determine the trends in the frontier energy levels for the family of TDOn oligomers (with n = 1 to 4). Fig. 2.17a shows the absorption spectra where we see a clear reduction in the optical gap with increasing n, accompanied by a deepening of the colors of the molecules in solution from red to dark blue as shown in Fig. 2.17b. To understand why the gaps are decreasing, we look at CV measurements of the TDOn oligomers (SI Fig. 2.21) which show both oxidation and reduction peaks in contrast to the analogous series of all-unoxidized rings, where only oxidation peaks are seen in this electrochemical window of the solvent. [128] The oxidation peaks for the TDOn family are around +1.1V, indicating that the energy of the HOMO does not change significantly as additional TDO units are added. The reduction peaks, however, show a shift from -1 V for TDO1 to -0.3 V for TDO4,

showing that the LUMO energy decreases as TDO units are added. In Fig. 2.17c, we show the HOMO and LUMO levels derived from the CV data (see SI, section 2.2.5). We see that as the number of TDO repeat units increases, the LUMO of the molecules drops from 3.4 eV in TDO1, to 4.1 eV in TDO4 (Fig. 2.17c). The reduction potential for TDO4 is similar to that of substituted fullerenes, which could imply n-type behavior, [115, 129] starkly contrasting the unoxidized oligothiophenes which all demonstrate p-type characteristics. [74] We note here that although these CV-derived values do not determine the exact alignment of the orbitals relative to a metal electrode, [130] the trends should be discernible in transport measurements.

2.2.3.2 Conductance Measurements

Next, we perform single-molecule conductance and thermopower measurements on the TDOn family to probe how their increased conjugation, smaller optical gaps and low-lying LUMOs impact charge transport through molecular junctions. For each molecule in the series, 20,000 conductance versus displacement traces are collected using the STM-BJ technique (Fig. 2.18a, see SI, section 2.2.5 for details). [2, 4] All measured conductance traces are collected and compiled into one-dimensional, logarithmically-binned conductance histograms [50] (100 bins per decade) without data selection and are shown in Fig. 2.18b. These 1D histograms display a clear peak yielding a most probable molecular conductance value that decreases systematically with increasing number of TDO monomers (n) (Fig. 2.18b). The relatively narrow breath of the conductance histogram peaks is indicative of a rather rigid backbone in this class of molecules. [52, 128] A two-dimensional histogram, which retains displacement information, created from the same data is shown in Fig. 2.18c for TDO3 showing that these junctions sustain a 1 nm elongation. Comparing 2D histograms across the series (SI Fig. 2.22) we see a clear increase in molecular plateau length with increasing backbone length. This indicates that we probe similar junction structures for all molecules in this series. [53] The inset of Fig. 2.18b shows the peak conductance values on a semi-logarithmic scale plotted against n showing that conductance decreases exponentially with increasing n ($G\ e^{n\beta}$) with a decay constant, $\beta = 1.04/n$. Since these TDO units are non-aromatic, the conduction path follows that of a chain of alternating

double and single bonds across the backbone as shown in Fig. 2.16b. We therefore use a through-bond distance of 5.4 Å/n as opposed to a through-space distance of 3.8 Å/n to convert the measured β to a decay constant of 0.2/Å. Interestingly, this value compares well with the β determined for oligoene systems, [89, 131] and shows that transport across TDO oligomers is similar to that across alkene oligomers.

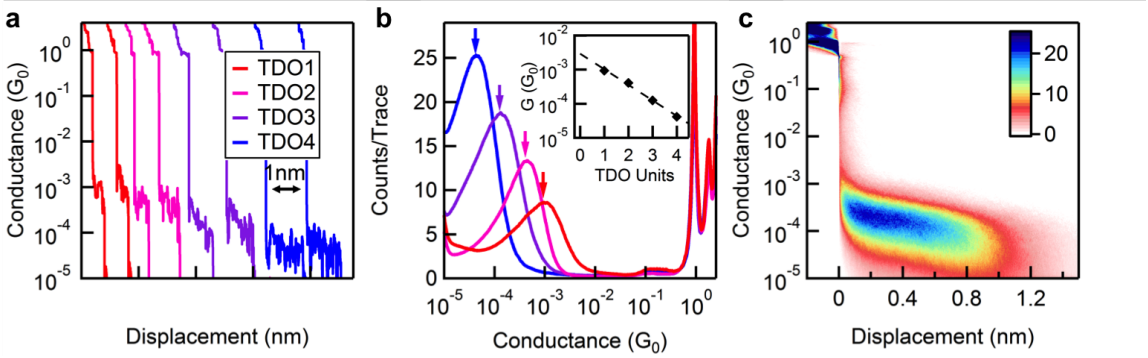

Figure 2.18: ***Single-molecule conductance data for the TDOn family.*** *(**a**) Sample conductance versus displacement traces, laterally offset, for the TDOn series. These traces display molecule-specific conductance features, which persist for longer displacements as the molecular length increases. (**b**) One-dimensional log-binned conductance histograms, each composed of 20000 traces, for TDO1-TDO4 measured at a 10 mV bias in 1-octylbenzene. Arrows indicate peak conductance positions. Inset: Plot of conductance as a function of the number of oxidized thiophene monomer units (n) in TDO1-TDO4. Using $G\, e^{\beta n}$, we obtain a decay constant of* 1.04/n. *(**c**) Two-dimensional conductance-displacement histogram for TDO3 created by aligning all traces at the point where conductance crosses 0.5 G_0, and then overlaying them. The color bar indicates number of counts per 1000 traces. For other 2D histograms see SI Fig. 2.22.*

2.2.3.3 Thermopower Measurements

While the narrow HOMO-LUMO gap of the isolated molecules is reflected in the relatively high conductances and shallow decay of the TDOn series, small bias conductance measurements alone do not provide any information on the nature of the orbital that dominates charge transport. In order to probe how such orbital alignment is impacted by the dramatic lowering of the LUMO with increasing number of oxidized thiophene units, we measure the Seebeck coefficient of these molecular junctions. The Seebeck coefficient for

a single-molecule junction is determined by heating the substrate while keeping the STM tip at room temperature and measuring the thermoelectric current while applying no external bias voltage (Fig. 2.16a, see SI, section 2.2.5 for details). [42] With the molecular conductance (G), thermoelectric current (I), and temperature difference (ΔT) known for each junction measured, S is given by $S = I/(G\Delta T)$. We compile the Seebeck coefficients from 100's of junctions for each molecule into the histograms shown in Fig. 2.19a; these are then fit with a Gaussian function to determine the most frequently measured Seebeck coefficient for each molecule.

We plot in Fig. 2.19b the Seebeck coefficient versus the molecular length. For TDO1-TDO3, this value is positive and decreases non-linearly with length, while for TDO4 it is negative and relatively large in magnitude. This trend is contrary to what has been observed in amine-, thiol-, and trimethyltin-linked oligophenyl series, where the Seebeck coefficient maintains the same sign (positive) and increases in magnitude with molecular length. [41, 122, 132] Such measurements have demonstrated that the oligophenyls conduct via hole transport through the HOMO. The increase in magnitude of S with increasing length in these oligophenyls was attributed to HOMO moving closer to E_F while simultaneously narrowing as the conducting orbital delocalizes over a longer molecule, resulting in a larger slope in the transmission function at E_F. Based on our measurements on the TDOn series, we infer that transport in TDO1 is dominated by HOMO, indicating hole-type transport. Using the conductance and Seebeck coefficient determined for TDO1 and assuming a single-Lorentzian transmission line shape, we find that the conducting orbital is -2 eV from E_F, in agreement with results from IV measurements for TDO1 (SI Fig. 2.26, and discussion in the SI, section 2.2.5).

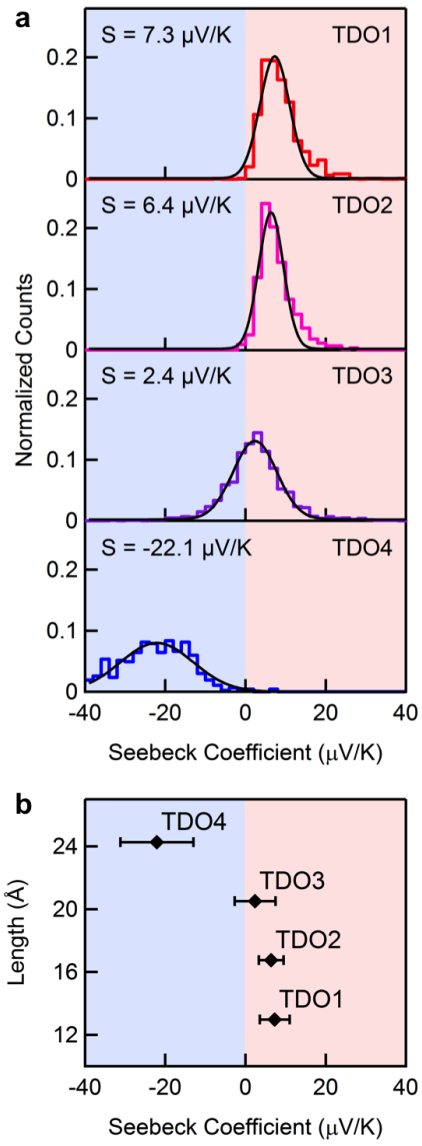

Figure 2.19: ***Single-molecule thermopower data for TDOn family.*** *(**a**) STM-BJ measurements taken with a temperature difference of 16 K between the gold tip and the substrate. While the molecule bridges the gap between the electrodes, the applied bias voltage is dropped to zero and the thermoelectric current is measured. Seebeck coefficients for each junction are then calculated using this current as detailed in the text and section 2.2.5 (SI) and compiled into the 1D histograms shown. The black curves are Gaussian fits to the Seebeck coefficient distributions. (**b**) Plot of Seebeck coefficient as a function of molecular length for the TDOn family with error bars reflecting the error in the Gaussian fits. A shift from positive to negative Seebeck values is seen with increasing length, indicating a change in the charge carriers from holes to electrons.*

The large, negative Seebeck coefficient measured for TDO4 indicates electron-transport dominated by the LUMO. In fact, the magnitude of this value is comparable to that of C_{60}, which is among the highest values of organic compounds. [133] Again, assuming a single-Lorentzian transmission for this system, we infer that the LUMO is 0.7 eV from E_F, consistent with results from IV measurements (Fig. S7). The Seebeck coefficient for TDO2 is smaller in magnitude than TDO1; if transport in TDO2 was dominated by the HOMO, we would expect a larger Seebeck coefficient when compared to TDO1. We thus conclude that transport in TDO2 is not dominated by a single orbital. Finally, the slightly positive but small magnitude Seebeck coefficient measured for TDO3 suggests that the E_F lies in relatively flat region of the transmission function, possibly in the middle of the HOMO-LUMO gap with both orbitals contributing to charge transport. This would imply that the transmission functions for both TDO2 and TDO3 do not follow a Lorentzian shape and thus, a direct determination of the level alignment for these two systems is not possible. Taken together, these measurements show that contributions from LUMO to charge transport become increasingly more important as the number of oxidized thiophene units in the molecular backbone is increased. We show additional evidence of a change in conducting orbital by carrying out solvent dependent measurements [54] on TDO1 and TDO4 (see SI Fig. 2.25 for details). This trend is in accord with the previously discussed UV-vis and CV measurements, where a decreasing optical gap and a lowering of the reduction potential are observed with increasing molecular length (Fig. 2.17).

Interestingly, despite changing conducting orbital, we still find an exponential dependence of conductance on molecular length with a well defined decay constant. To understand how we could observe this, we turn to an n-site tight-binding model, where each site is assigned an occupied and an unoccupied orbital (SI Fig. 2.27). This model is described in detail in section 2.2.5, the SI. In general, we find that the conductance decays exponentially, as long as the Fermi energy is not close to any resonance, even with a change in the dominant transport channel with increasing length. However, for longer chain lengths, we could see a deviation from this exponential dependence, if an orbital gets closer to E_F.

2.2.4 Conclusions

We have used STM-BJ conductance and Seebeck coefficient measurements to illustrate the transport characteristics of molecules containing thiophene-1,1-dioxide, a poorly studied building block which has tremendous impact on electronic properties in both polymers and small molecules. Our findings demonstrate that these molecules constitute a unique system where the charge carrier in gold-molecule-gold junctions switches from holes to electrons with increasing number of monomers. While previous studies have shown that the dominant conducting orbital is generally dictated by the gold-binding linker units, [42] control through backbone length is unprecedented. Moreover, TDO4 is shown to have a relatively high Seebeck coefficient [42, 133]suggesting that these systems may be potential candidates for thermoelectric devices. The conductance data also show that the transport properties of oligoTDOs are similar to those of oligoalkenes, reinforcing the fully-conjugated and non-aromatic nature of their backbones. These studies demonstrate that small changes in molecular structure can have a major impact on charge transport characteristics; strategic molecular design provides a method for engineering carrier type in molecular devices. Additionally, since the oxidized thiophene units have a dramatic impact on the LUMO, these studies reveal a potential new family of n-type materials.

2.2.5 Supplementary Information

2.2.5.1 Methods

Synthetic Details Details of the procedures used to synthesize the molecules studied in this section can be found in the manuscript *Molecular Length Dictates the Nature of Charge Carriers in Single-Molecule Junctions of Oxidized Oligothiophenes* [134]

Conductance Data Conductance measurements are performed using the scanning tunneling microscope-based break-junction (STM-BJ) technique, using a home-built modified STM that has been described in detail previously. [4] Conductance data is collected by driving a mechanically cut gold tip into and out of contact with a gold-on-mica substrate (100 nm 99.995% Au, thermally evaporated). As the tip is retracted at a speed of 16 nm/s, the resulting gold junction is thinned down to a gold single-atom contact, which ruptures

upon further elongation. After rupture, a molecule may bridge the gap and, as we simultaneously measure current and voltage, we can determine the molecular junction conductance ($G = I/V$). For these measurements, TDOn molecules are introduced in a 1-octylbenzene solution (10 μM - 1 mM concentrations). For each molecule, 20,000 conductance verses displacement traces are collected at an applied bias of 10mV; these traces are then used (without selection) to construct conductance histograms.

Thermopower Measurements We determine the Seebeck coefficient of single-molecules by performing break-junction measurements with an applied temperature gradient and zero applied bias voltage. [42] Instead of simply retracting the STM tip after it is driven into the substrate, we now incorporate a 150ms hold into the piezo ramp after the tip has been pulled a distance of 2.2nm. As before, we apply a 10mV bias during the pullout and during the first and last 25ms of the hold, but we now apply a 0mV bias during the middle 100ms of the hold. We collect thousands of such traces with a 0K temperature difference between the tip and the substrate and with a 16K temperature difference between the tip and the substrate. The data collected at 0K is to ensure that that we have no thermoelectric current flowing when there is no temperature gradient (and no bias voltage) applied (SI Fig. 2.24).

In order to analyze this data, we only consider traces where a molecule is present in the junction during the hold. In order to select out these traces, the conductance at the start and end of the hold (where the 10mV bias is applied) is averaged; traces where this conductance falls within the molecular conductance range (as determined from conductance histograms in Figure 2.18b) are kept. For such traces, the thermoelectric current measured during the middle portion of the hold is averaged. Thermocurrent histograms are provided in Figure S6, where the thermocurrent at ΔT=0K and ΔT=16K are provided for all four molecules. For ΔT=0K, there is a narrow distribution peaked about 0pA for all TDO molecules. As the ΔT is increased, this thermocurrent distribution broadens and shifts to negative values for TDO1 and TDO2, while it shifts to a positive value for TDO4; this is indicative of a change in the sign of the dominant charge carrier.

The thermocurrent values are then used in conjunction with the average molecular conductance before and after the hold to compute the average Seebeck coefficient of the

given molecular junction. These Seebeck coefficients are then compiled into the histograms shown in Figure 2.19a.

2.2.5.2 Additional Figures

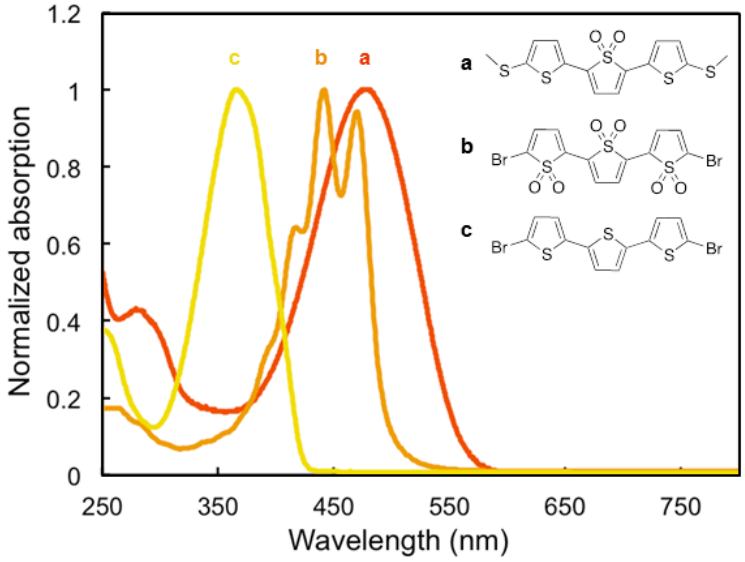

Figure 2.20: ***Impact of thiophene oxidation on UV-vis absorption spectra.*** *Normalized UV-vis absorption spectra measured in dichloromethane for T3 derivatives with varying degrees of oxidation.*

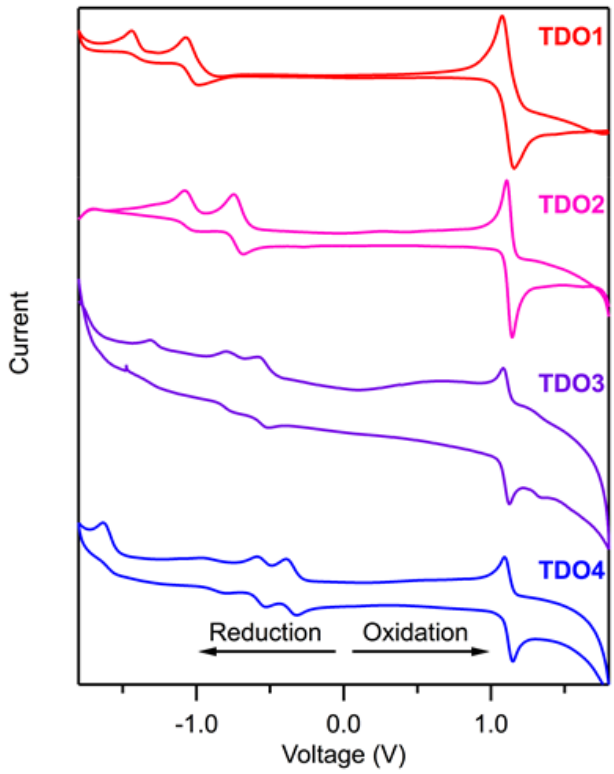

Figure 2.21: ***Cyclic voltammetry measurements on the TDOn family.*** *Cyclic voltammograms for TDOn performed in dichloromethane with Ag/AgCl reference electrode, 0.1M tetrabutyl ammonium hexafluorophosphate as the electrolyte and a scan rate of 50 mV/s.*

	$E_{ox1/2}$(V)	$E_{red1/2}$(V)	E_{HOMO}(eV)	E_{LUMO}(eV)
TDO1	1.12	-1.03	5.5	3.4
TDO2	1.13	-0.72	5.5	3.7
TDO3	1.12	-0.51	5.5	3.9
TDO4	1.12	-0.34	5.5	4,1

Table 2.1: *$E_{ox1/2}$, $E_{red1/2}$, E_{HOMO}, E_{LUMO} determined from CV data. $E_{ox1/2}$ and $E_{red1/2}$ are the midpoints of the first oxidation and first reduction, respectively, in the cyclic voltammograms. E_{HOMO} and E_{LUMO} are determined [127, 135] using $E_{HOMO} = E_{ox1/2} + 4.4$ and $E_{LUMO} = E_{red1/2} + 4.4$.*

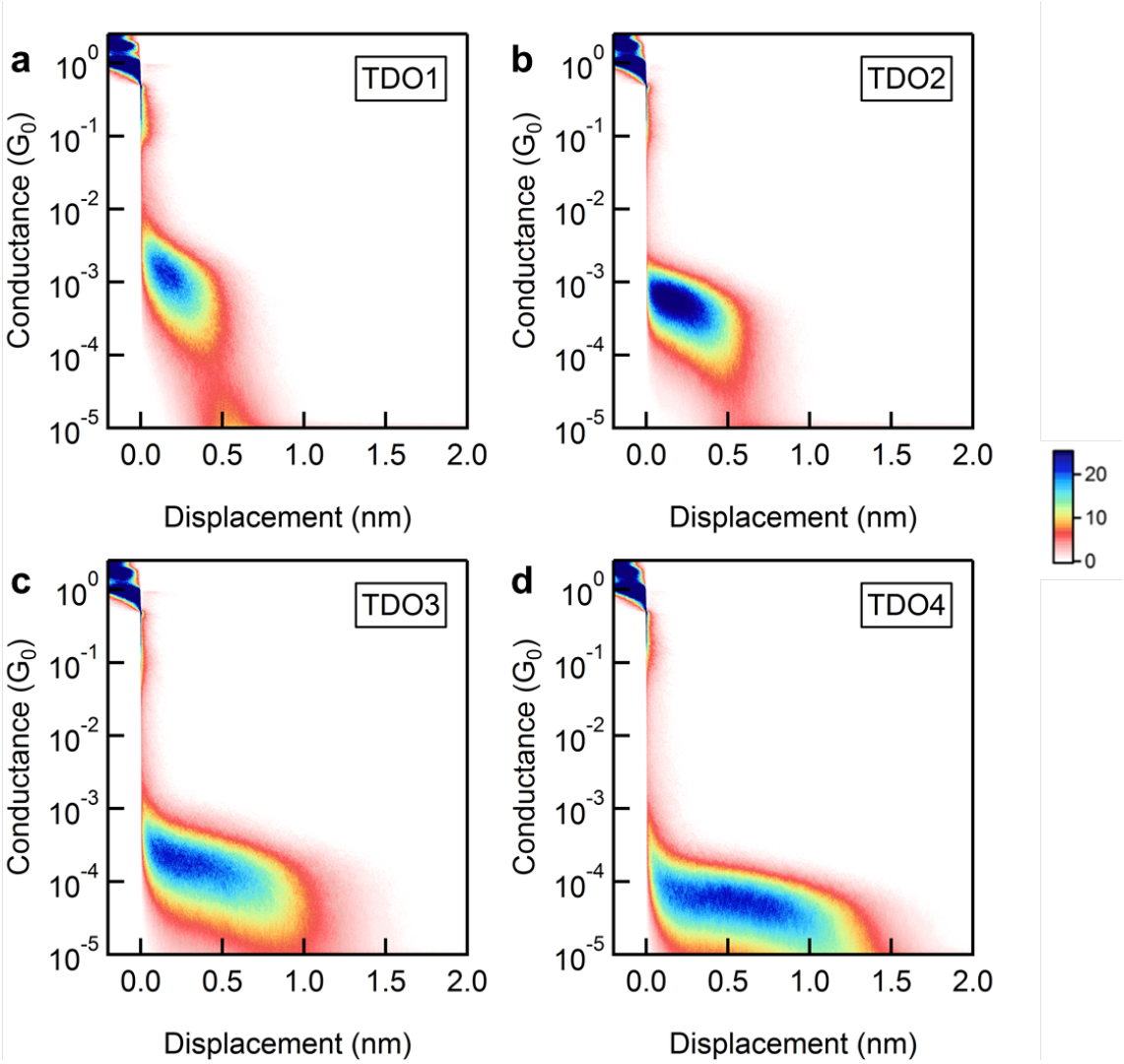

Figure 2.22: ***Two-dimensional conductance versus displacement histograms for TDOn.***

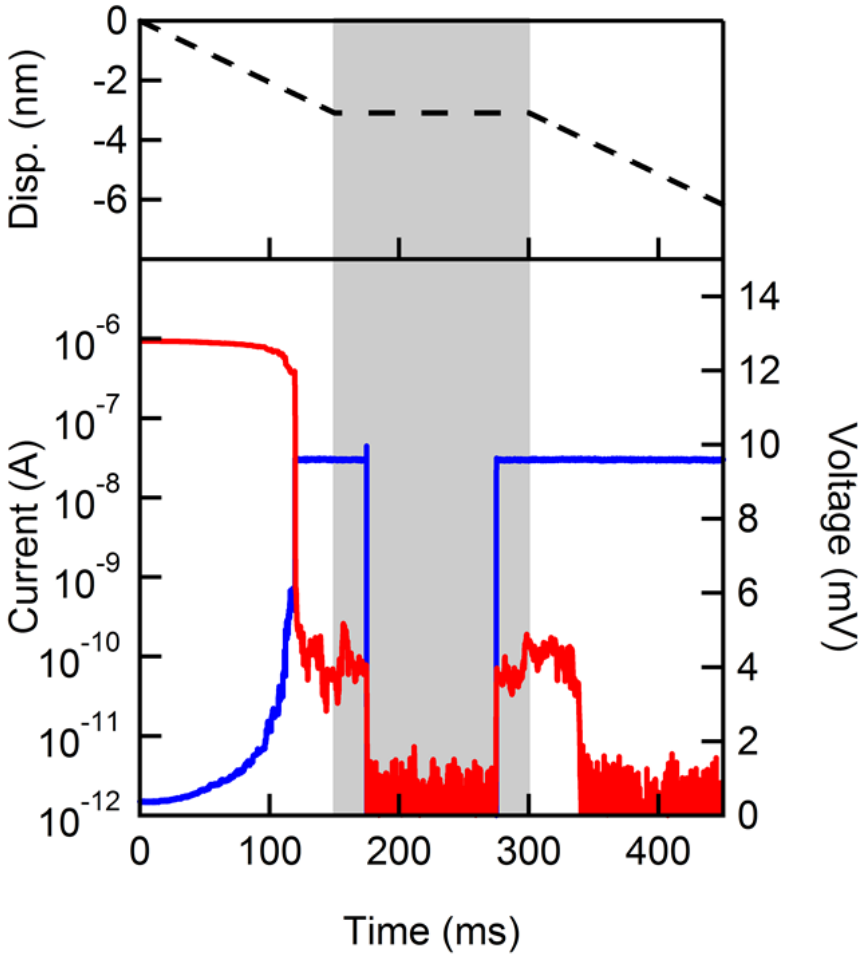

Figure 2.23: ***Sample single-molecule thermopower measurement.*** *Top Panel: Sample piezo ramp used in collecting thermopower data. The hold is shown in the gray shaded area. Bottom Panel: Sample current vs. displacement trace (red) and voltage vs. displacement trace (blue) for TDO3.*

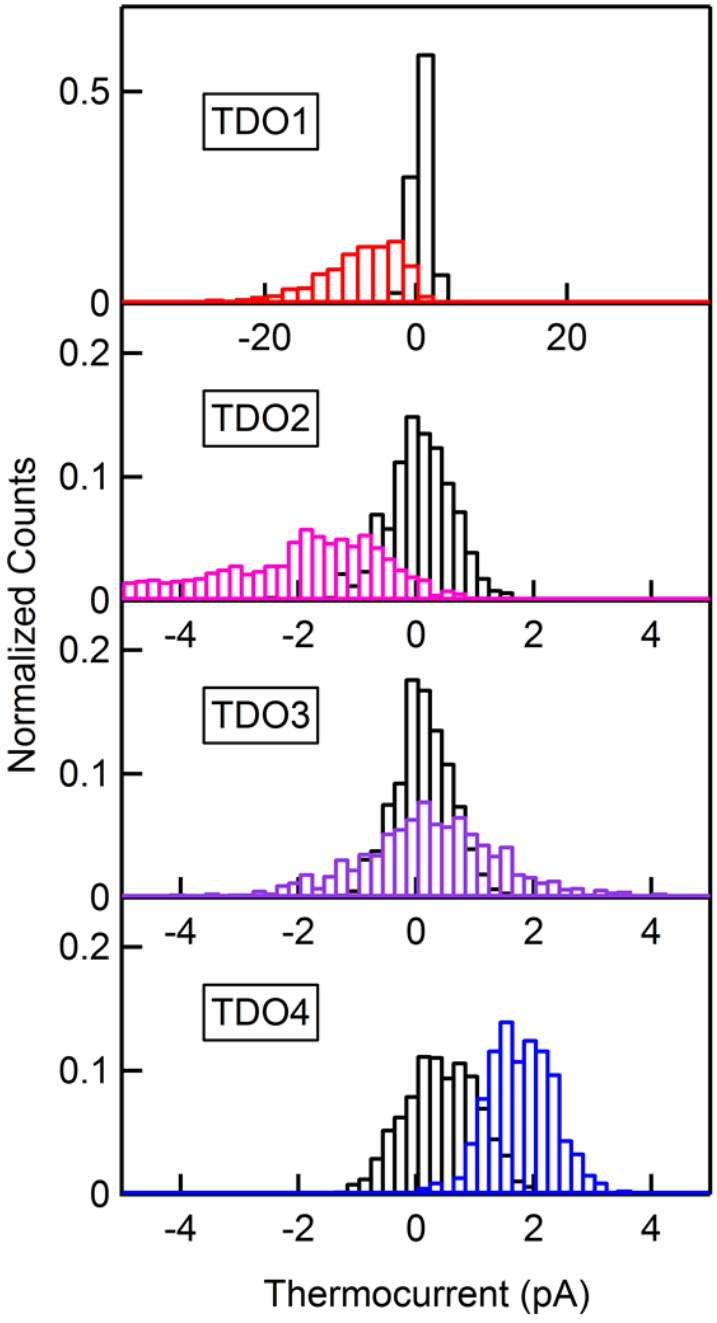

Figure 2.24: ***Thermoelectric current histograms for the TDOn series.*** *Histograms in black correspond to a ΔT of 0K, while colored histograms correspond to a ΔT of 16K. At ΔT=0K, the number of traces selected (following the procedure above) is 264 for TDO1, 520 for TDO2, 586 for TDO3 and 1,141 for TDO4. At ΔT=16K, the number of traces selected is 793 for TDO1, 891 for TDO2, 1,346 for TDO3, and 468 for TDO4.*

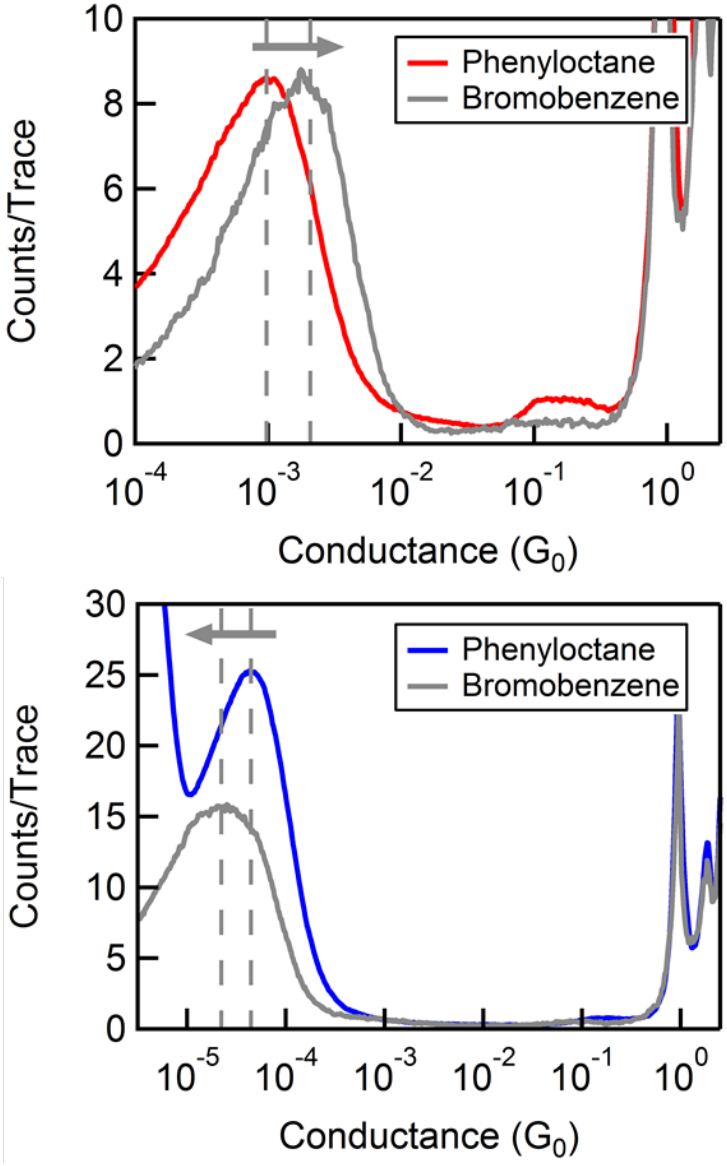

Figure 2.25: ***Solvent induced conductance shifts for TDO1 and TDO4.*** *(**a**) TDO1 conductance histogram measured from a 1 mM solution in bromobenzene and phenyloctane. The peak shifts to a higher conductance in bromobenzene implying HOMO dominated transport. (**b**) TDO4 shows a decrease in conductance upon changing the solvent from phenyloctane to bromobenzene, implying LUMO transport. [54]*

2.2.5.3 Additional Analysis

Single-Lorentzian Model Charge transport through a single-molecule junction can be analyzed in terms of a transmission function which details the probability that an electron incident on the molecular barrier is transmitted through the junction. Often, when one molecular orbital is dominant in this tunneling process, the transmission function, $T(E)$, can be approximated by a single Lorentzian of the form: [136]

$$T(E) = \frac{\Gamma^2/4}{(E - \Delta E)^2 + \Gamma^2/4}$$

Here, ΔE is the electronic molecular level alignment ($\Delta E = E_{resonance} - E_F$) and Γ is the coupling strength of the conducting orbital to the leads. Using this form of transmission, along with the definitions of conductance (G) and the Seebeck coefficient (S), expressions for ΔE and Γ can be obtained as:

$$\Delta E = -2\frac{S_0}{S}\left(1 - \frac{G}{G_0}\right)$$

$$\Gamma = 4\frac{S_0}{S}\sqrt{\frac{G}{G_0}\left(1 - \frac{G}{G_0}\right)}$$

where G_0=7.74x 10-5/Ω and S_0 = 7.25eV x 10-6 V/K at 300K.**[8]**

From our thermopower measurements, we conclude that transmission through TDO1 and TDO4 is dominated by HOMO and LUMO respectively, and assume that the transmission can be approximated by the Lorentzian function described above. (TDO2 and TDO3 have significant contributions from both orbitals, and therefore their transmission cannot be approximated by a single Lorentzian.) Using the above equations, we determine ΔE and Γ for TDO1 and TDO4 (Table 2.2).

	ΔE (eV)	Γ(eV)
TDO1	-2.0	0.13
TDO4	0.7	0.01

Table 2.2: *ΔE and Γ for TDO1 and TDO4 as determined from conductance and Seebeck measurements, assuming a single-Lorentzian as representative of transmission.*

I-V Measurements and Analysis In order to test whether our ΔE and Γ values are reasonable, we perform I-V measurements on TDO1 and TDO4 in 1,2,4-trichlorobenzene. The measurement procedure has been described before. [137] Briefly, after contact, the Au tip is retracted from the substrate for 150 ms, before being held at constant displacement for another 150 ms. During this hold, a saw-tooth voltage ramp is applied, ranging from -1 to +1V. After, the tip is retracted further in order to rupture the molecular junction.

We only consider traces which have a molecular feature present during the entirety of the voltage ramp. We select out approximately 1,400 such I-V traces for TDO1, and 3600 traces for TDO4. These are then compiled into logarithmically binned two dimensional current-voltage (2D IV) plots as shown in Figure 2.26a,b. In order to determine an average I-V curve for the two molecules, we fit each vertical line slice of the 2D IV with a Gaussian, and plot the peak value. We then plot these I-V curves on a linear scale (colored curves) in Figure 2.26c,d. We qualitatively compare the measured average I-V curve with I-V curves that have been generated from our single-Lorentzian transmission functions by integrating the area under the transmission curve, assuming a symmetric bias window and T=0K. Visually comparing the measured IV curve with the IV curve generated from our model Lorentzian transmission functions, we find excellent agreement between the two at low biases. The model IV curves underestimate the measured current at voltages greater than 0.5V, but at high biases there are multiple physical effects which cause deviations of the junction transmission from its low bias form. These effects include (a) a Stark shift that moves the resonances closer to E_F at high biases, (b) the polarizability of the molecular orbitals under bias, (c) bias induced changes in the junction geometry and (d) Coulomb blockade effects.

Tight Binding Model We seek to show that an exponential decay in conductance with molecular length can arise even when one orbital does not remain dominant across a molecular series. In order to demonstrate this, we use a tight binding model to determine a Hamiltonian matrix and then use a non-equilibrium Greens Function formalism in order to qualitatively model transmission through the molecular junctions. [55] We use an n-site model in which each site is represented by two orbitals of energy ϵ_H and ϵ_L (an occupied

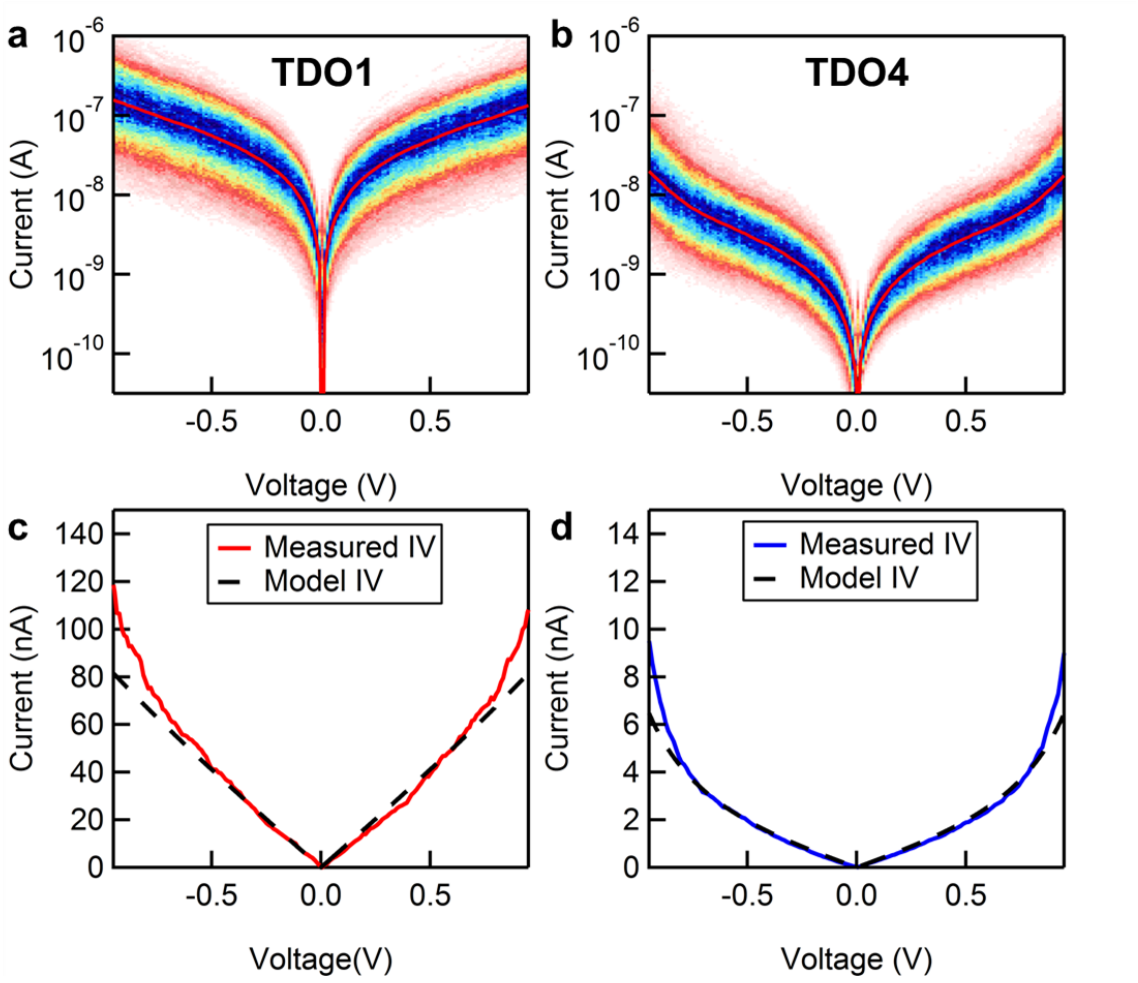

Figure 2.26: ***Current-Voltage (IV) measurements and analysis for TDO1 and TDO4.*** *(**a**) 2D current voltage plot for TDO1. (**b**) 2D current voltage plot for TDO4. (**c**) Average measured IV compared with single Lorenztian model IV for TDO1. (**d**) Average measured IV compared with single Lorenztian model IV for TDO4.*

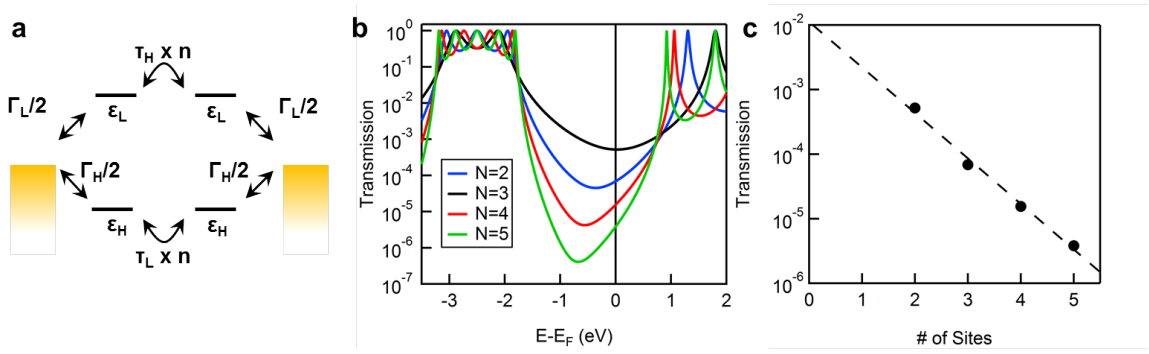

Figure 2.27: ***Two level tightbinding model for transport through TDOn junctions.*** *(**a**) Schematic of tight binding model showing the Fermi level in relation to each sites HOMO and LUMO and the coupling between them. (**b**) Computed transmission functions using parameters described in text. (**c**) Transmission vs site number, along with an exponential fit to the values.*

and an unoccupied orbital). Nearest neighbors have occupied orbitals coupled by τ_H and unoccupied orbitals coupled by τ_L (Figure 2.27a). Terminal sites have their occupied and unoccupied orbitals each coupled to the leads by an imaginary, energy independent, self-energy term $i\Gamma_H/2$ (and $i\Gamma_L/2$). In order to compute molecular transmission functions, we turn to the non-equilibrium Greens Function formalism. The retarded Greens function for the molecular junction is defined as $G(E) = [EI - H]^{-1}$, and transmission is then given as $T(E) = Tr(\Gamma_L G \Gamma_R G)$, which is computed numerically. Here, Γ_L and Γ_R are coupling matrices coupling the molecule to the left and right leads, respectively.

Using the model, we calculate transmission functions for molecular junctions where N ranges 2 sites to 5 sites, and show representative transmission functions in Figure 2.27b. To calculate these transmission functions, we choose ϵ_H = -2.5eV, ϵ_L = 3eV, τ_H = -0.4eV, τ_L = -1.2eV, Γ_H = -0.25eV, and Γ_L = 0.1eV. We plot conductance versus $T(E = E_F)$ versus number of sites in Figure 2.27c. The straight line relationship (on a log-scale) observed in Figure 2.27c demonstrates that an exponential decay in conductance is possible even with two contributing orbitals. We find that generally conductance decays exponentially with increasing length as long as the Fermi energy is not close to any resonance despite a change in the dominant transport channel going from N=2 to N=5 in this model. However, we expect to see a deviation from this clear exponential dependence especially if either resonance gets closer to E_F.

Chapter 3

Electrolyte Gating of Single-Molecule Junctions

In this chapter, we modulate the conductance of electrochemically inactive molecules in single-molecule junctions using an electrolytic gate to controllably tune the energy level alignment of the system. Molecular junctions that conduct through their highest occupied molecular orbital (HOMO) show a decrease in conductance when applying a positive electrochemical potential, and those that conduct though their lowest unoccupied molecular orbital (LUMO) show the opposite trend. We fit the experimentally measured conductance data as a function of gate voltage with a Lorentzian function, and find the fitting parameters to be in quantitative agreement with self-energy corrected density functional theory calculations of transmission probability across single-molecule junctions. This work shows that electrochemical gating can directly modulate the alignment of the conducting orbital relative to the metal Fermi energy, thereby changing the junction transport properties.

This chapter is based on the manuscript entitled *Tunable Charge Transport in Single-Molecule Junctions via Electrolyte Gating* by Brian Capozzi, Qishui Chen, Pierre Darancet, Michele Kotiuga, Marisa Buzzeo, Jeffrey B. Neaton, Colin Nuckolls, and Latha Venkataraman. Synthesis of materials was performed by Qishui Chen of Prof. Nuckolls' group. Theoretical work was carried out by Pierre Darancet and Michele Koriuga of Prof. Neaton's group. Prof. Buzzeo assisted with electrochemical studies. I performed the break junction

experiments and the data analysis.

3.1 Introduction

There has been significant interest in the field of single molecule electronics both from the standpoint of learning fundamental physics and for potentially leading to a further miniaturization of electronic components. [1] While molecular junctions- individual molecules attached to two metal electrodes- are most commonly studied in a source-drain device geometry, [2,4,138,139] a molecular junction with a gate electrode in a transistor configuration gives an additional knob with which to tune the transport characteristics. Creating such molecular transistors in a three-terminal geometry is not trivial, as it is very challenging to fabricate an effective gate electrode in close enough proximity to the conducting molecular junction. Recent experiments which have relied on electro-migration fabrication techniques, have demonstrated some gating in such three terminal devices. [16, 17, 23, 26] An attractive alternative to back gating is electrolyte gating, where large gate efficiencies can be achieved. Recently, both organic and semiconductor field effect transistors and nanotube or graphene devices [140, 141] made using ionic liquids, electrolyte solutions, or polymer electrolytes as gate dielectrics have received significant attention due to their ability to generate large interfacial capacitances on the nano-scale, thereby enhancing gate efficiencies. [67–69, 142–144] These large capacitances result from the formation of electric double layers at solution/material interfaces, whose width is on the order of the electrolyte size (few nm) allowing large electric fields to develop across this layer.

For nano-scale molecular junctions in particular, electrolytic gating should enable much more efficient electrostatic coupling since the electric double layer will exist regardless of the position of the gate electrode in solution. While several groups have applied an electrochemical gating technique to study transport in electrochemically active molecules that change their charge state, [145–149] the continuous modulation of the conductance of a non-redox active molecule has not been demonstrated. Here, we present the electrolytic gating of several molecules that reproducibly and consistently change their conductance upon application of gate biases despite being electrochemically inactive in the potential

ranges studied. In particular, we show that the conductance of a molecular junction can be tuned with an electrochemical gate potential analogous to what can be achieved using an electrostatic gate. We find that molecules that conduct through the lowest unoccupied molecular orbital (LUMO, n-type) show an increase (decrease) in conductance with positive (negative) gate potentials, while molecules that conduct through the highest occupied molecular orbital (HOMO, p-type) show the opposite trend. Furthermore, modeling the transmission functions of these molecules with a single Lorentzian line-shape, we are able to extract orbital coupling and molecular resonance position that agree well with self-energy corrected density functional theory (DFT) calculations. This quantitative agreement between experiment and theory demonstrates that, in gating the molecular junctions, we are indeed probing transport as a function of energy along the transmission curve.

3.2 Results and Discussion

3.2.1 Break-Junction Measurements in Ionic Media

In order to study the conductance ($G = I/V$) of single molecule junctions, we use the scanning tunneling microscope-based break junction (STM-BJ) technique. In this technique, a mechanically cut Au tip is repeatedly driven into and out of contact with an Au-on-mica substrate in a solution of a target molecule using a custom STM set-up that has been described in detail previously. [4] Electrolytic gating is implemented using an Au substrate and an Apiezon wax coated Au tip [70] which serve as the source and drain electrodes, and a Pt wire electrode which serves as the gate electrode as illustrated in Figure 3.1a. [140] The Au electrodes can also be considered the working electrode in our system while the Pt wire can be considered the counter electrode. The exposed areas of the insulated tips are 1μm. Conductance measurements are then carried out in a fluid cell with 1mM solutions of the target molecule in propylene carbonate, with tetrabutylammonium perchlorate (0.1M) serving as the supporting electrolyte. For each molecule, two to three thousand conductance traces are collected at multiple gate electrode potentials (that is, our gate potential is applied to the Pt electrode), with the source-drain bias fixed at 25 mV.

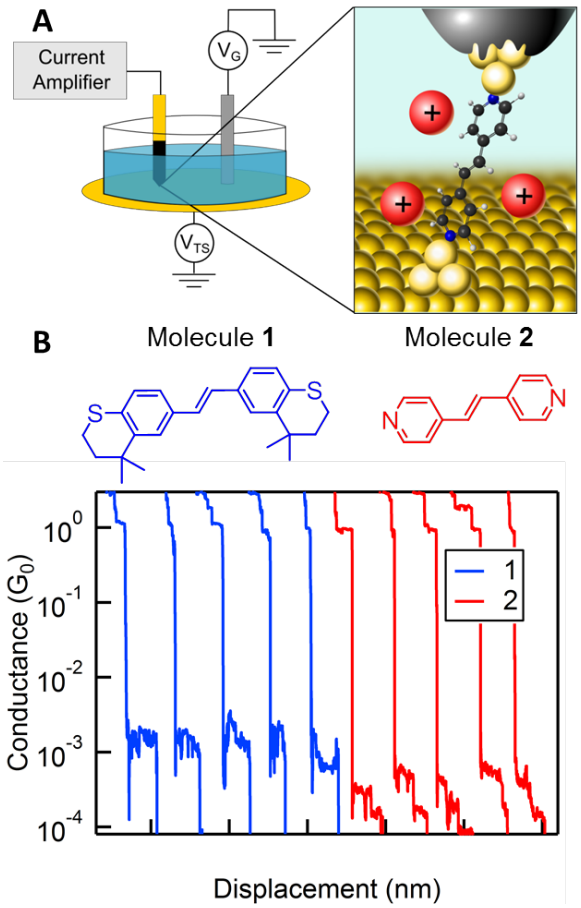

Figure 3.1: ***Single-molecule conductance measurements under electrochemical control.*** *(**A**) Schematic of experimental set-up and cartoon of a single molecule being gated in a junction. (**B**) Molecular structures of **1** and **2** along with several sample conductance traces for each molecule measured with a tip-sample voltage of 25 mV and at zero gate potential.*

We carry out break junction measurements on 1,2-bis(4,4-dimethylthiochroman-6-yl)ethylene (**1**), which is synthesized following procedures detailed previously, [15] and 1,2-bis(4-pyridyl)ethylene (**2**), which is obtained from Sigma-Aldrich and used without further purification (Fig 3.1b). Molecule **1** conducts through the HOMO while molecule **2** conductance through the LUMO as determined by calculations detailed below in the manuscript. Conductance traces display plateaus near integer multiples of the quantum of conductance (G_0,$2e^2/h$), with an additional plateau in a molecule-specific range below G_0; these additional features indicate the formation of metal-molecule-metal junctions (Fig 3.1c). In order to analyze the data,

each set of traces at a given gate potential is compiled into a linearly binned conductance histogram (without data selection) where frequently occurring conductance values now appear as peaks in the histogram. The most probable junction conductance is then obtained by fitting a Lorentzian to the conductance peak. [4] We note here that the conductance histograms for all molecules studied here are very similar to those carried out in without a gate electrode or the supporting electrolyte. [15, 150]

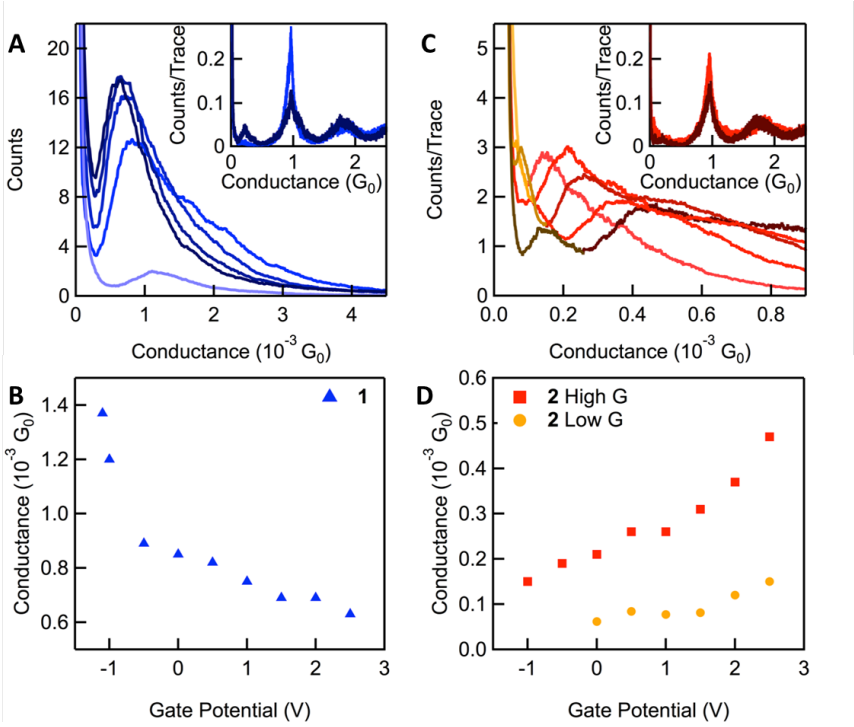

Figure 3.2: ***Gating HOMO and LUMO dominated molecular junctions.*** *(**A**) and (**C**) Sample conductance histograms at gate potentials V_G = 2.5V, 2V, 1V, 0V, -1V darkest to lightest for molecule **1** and **2** respectively. Note: for molecule **2**, red shades indicate the high-G conductance feature while orange shades indicate the low-G conductance feature. Inset: Conductance histograms at two gate potentials showing the continued formation of Au point contacts (peak at $1G_0$). (**B**) and (**D**) Peak conductance values vs applied gate potential for **1** and **2**, respectively.*

For **1**, the HOMO conducting molecule, the peak present in the conductance histogram clearly shifts to lower values as the applied gate potential is increased from -1.1V to 2.5V (Fig. 3.2a). Fig. 3.2b displays the conductance histogram peak values against the applied gate potential, where a conductance change by roughly a factor of 2 over the entire gate

potential range can be observed. The inset of Figure 3.2a shows full conductance histograms at two gate potentials, showing clear peaks at integer multiples of G_0 indicating that Au point contacts form regardless of gate potential. We note that the height of the molecular conductance peak decreases with application of increasingly negative gate potentials due to a decrease in length of the plateaus seen in individual traces as the gate potential is made to be more negative (see two-dimensional histograms shown in the supplementary information, SI, Fig. 3.6. For molecule **1**, we find that the applied potential can vary from -1.1V to +2.5 V; we do not see molecular conductance plateaus outside this window. At gate potentials more negative than -1.1V, we attribute the lack of plateaus to a weakening of the Au-S donor acceptor bond that anchors the molecule to the gold leads. Since molecule **1** binds through HOMO, as the gate potential is made more negative, the HOMO gets closer to the Fermi level, E_F, as will be discussed in detail below. This increases charge transfer between the molecule and the electrode and weakens the Au-S donor-acceptor bond. At applied gate potentials more positive than +2.5V, we no longer observe junction formation, possibly due to the Au getting oxidized and preventing junctions from forming.

The LUMO conducting molecule, **2**, shows two peaks in its conductance histograms, corresponding to two distinct binding configurations [150]: a higher conducting, tilted geometry (high-G), and a lower conducting, vertical geometry (low-G). Both peaks shift toward higher conductance values as the applied gate potential is increased from -1V to +2.5V (Fig. 3.2c), and for both geometries, the conductance peak shifts by approximately a factor of 3 over the entire gate voltage range (Fig. 3.2d). The inset of Fig. 3.2c shows conductance histograms at two gate potentials, displaying the continued formation of gold point contacts. In contrast to the conductance peak of molecule **1**, the peak heights for both high- and low-G features of molecule **2** do not change dramatically over the range of gate potentials. This difference can be rationalized by considering the location of the HOMO orbital for **2** relative to E_F. Since the HOMO orbital for **2** is far from E_F, [150] small changes in its alignment due to the applied gate do not result in a weakening of the Au-N donor acceptor bond. As the gate voltage is made more negative than -1V however, the low-G peak drops below the instrument noise and the high-G peak becomes a shoulder against the noise background. At positive gate voltages beyond 2.5V, we stop observing

junctions as in the measurements with **1**. Again, neither molecule undergoes a redox event in this gate bias window (see CV curves in SI Fig. 3.5), yet we clearly see that the gate bias modulates the measured conductance. This same procedure was repeated for 4,4'-bipyridine (see SI Fig. 3.7).

3.2.2 Modeling and Comparison with Theory

To understand these directional conductance shifts, we consider the effect of the gate potential on the alignment of frontier orbital resonance energy relative to the tip/substrate Fermi energy. Applying a positive potential to the gate electrode causes a buildup of anions ($-ve$) about the gate electrode while inducing a buildup of cations ($+ve$) about the Au electrodes and the molecular junction (a negative gate potential results in a build up of anions about the Au electrodes and the molecular junction). The double layer formed at the Au electrodes and about the molecular junction alters the energy difference between the electrode Fermi energy and the relevant junction frontier resonance energy (i.e. the molecular HOMO or LUMO which can be thought of as the molecules "valence band" and "conduction band", respectively). Analogous to a field effect transistor, the build-up of charge about the molecule and electrodes acts to electrostatically shift the molecular orbitals relative to the vacuum level and to E_F of the electrodes. Placing more positive (negative) charge in the vicinity of the molecule causes a downshift (upshift) in the molecular orbitals, bringing LUMO (HOMO) closer to E_F while pushing HOMO (LUMO) further away. Concomitantly, a layer of positive charge on the electrodes raises the energy required to remove an electron, thereby increasing the work function of the electrode. The arrangement of electrolyte both near the molecule and on the electrodes cooperatively changes the local potential at the molecule, altering level alignment and conductance. Along similar lines, a change in electrode work function has been previously shown to explain the variation in conductance observed for molecules in different solvents. [54]

Based on this discussion, we can now use the gate dependent conductance data to determine the alignment of the conducting orbital to E_F. We first relate the applied gate potential (applied between the Pt counter electrode and the instrument ground) to the potential drop at the working electrode (tip and substrate), as we also have, in these mea-

surements, a significant potential drop across the Pt electrode/solution interface. We relate the applied potential to the potential drop at the working electrode by comparing linear sweep voltammograms of a solution of ferrocene (1mM) and tetrabutylammonium perchlorate (counter ion, 0.1M) in propylene carbonate measured with just two electrodes (insulated tip and Pt counter electrode) and three electrodes (substrate, insulated tip, and Pt counter electrode). In the two-electrode system, the area of the insulated tip is significantly smaller than the area of the Pt counter electrode, so all of the applied potential will drop across the working electrode. This arrangement results in the blue voltammogram shown in Fig. 3.3, with the midpoint of ferrocene oxidation at an applied potential of 0.5 V. Repeating the measurement with the three-electrode arrangement yields the red curve (current is still measured through the tip, while the substrate electrode is grounded and thus provides a current pathway). In this case, because of the extra surface area, only a fraction of the applied potential actually drops across the working electrodes (tip and substrate), and the current from the ferrocene oxidation reactions doesn't peak until an applied potential of 2.5V. Although current is passing through both the tip and the substrate, we are still only concerned with measuring the current through the tip. Comparing the onset of current between the 2 curves, we determine that the applied gate potential needs to be scaled by a factor of 5. Additionally, we have carried out measurements using a geometry where the Pt gate electrode is much larger than the Au tip/substrate (source/drain) electrodes (see SI Fig. 3.8). Indeed we find that by changing the area ratios, we are able to impact how the gate potential drops across the molecular junction.

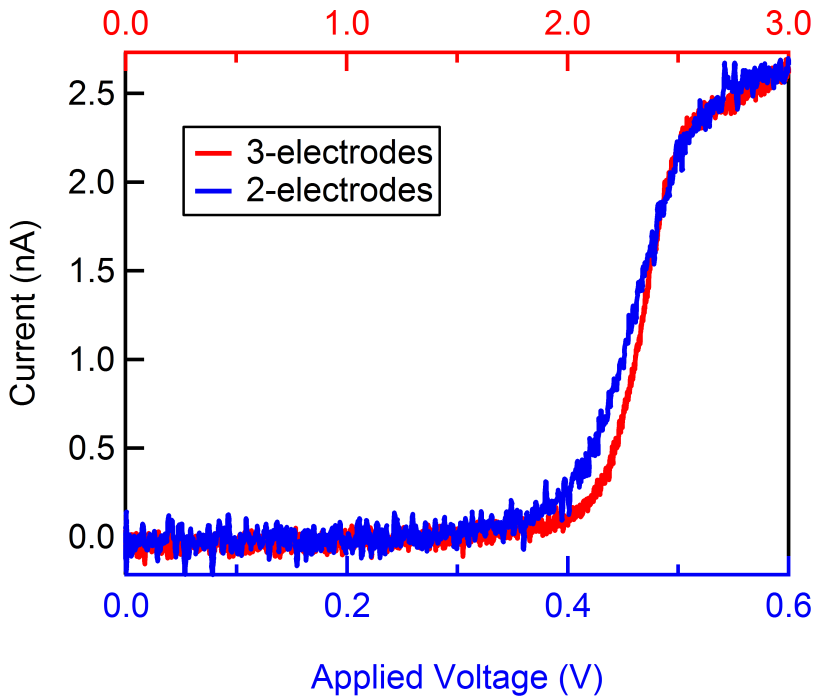

Figure 3.3: ***Cyclic voltammograms using the break junction geometry.*** *Linear sweep voltammograms of ferrocene (1mM) in propylene carbonate with tetrabutylammonium perchlorate (0.1M). In the 2-electrode circuit (blue curve, bottom axis), current is measured through the STM tip while applying the voltage to the Pt gate electrode keeping the substrate floating (unconnected). In the 3-electrode circuit (red curve, upper axis), the same measurement is performed while grounding the substrate, allowing for a current path through the substrate. Both voltammograms are recorded at a sweep rate of 100mV/s.*

We show in Fig. 3.4, the conductance peak positions measured for both molecules against the scaled gate potential (markers) and fit this data to a single-Lorentzian line shape peaked at an energy ϵ from E_F, with a full width at half maximum of Γ, which describes transport for the two molecules (solid lines, including high-G and low-G for molecule **2**). We determine, from this fit, the coupling Γ of the conducting orbital to the leads, and ϵ, the energy difference between conducting orbital and E_F without a gate. For molecule **1**, we find that a coupling Γ of 0.12 eV and a resonance position of 2.0 eV relative to E_F. For molecule **2**, we get Γ and ϵ of 0.04 eV and 1.5 eV for the high-G junctions and 0.02 eV

and 1.4 eV for the low-G junctions. We see that for molecule **2**, the high-G junctions are better coupled (larger Γ) than the low-G junctions, in agreement with previous work on 4,4'-bipyridine junctions. [9]

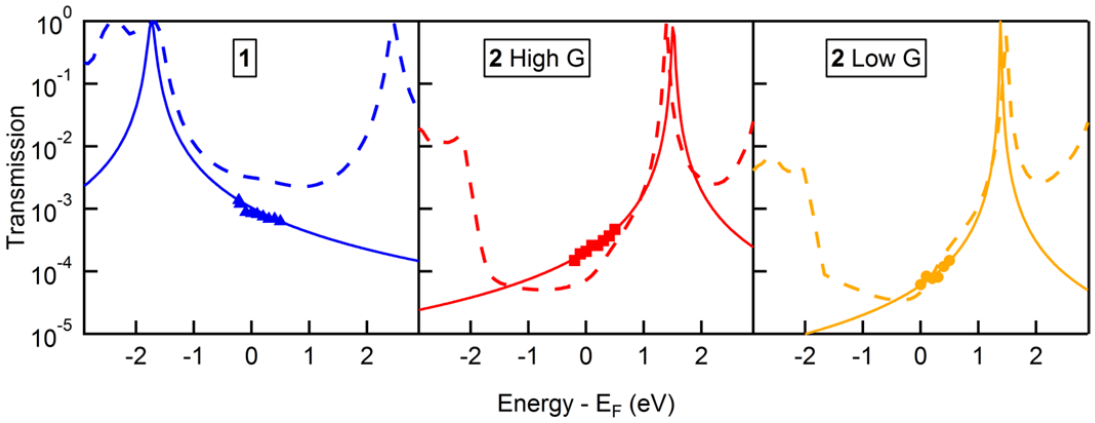

Figure 3.4: ***Comparison of experimental gating data with DFT+Σ calculated transmission functions.*** *Conductance data for molecules **1** and **2** plotted against the potential drop at the working electrode (markers) fit with a single-Lorentzian transmission model (solid lines). The DFT+Σ calculated transmission functions are overlaid as dashed lines.*

We further compare these fits with transport calculations based on a parameter-free, scattering-states, self-energy corrected density functional theory (DFT+Σ) approach (dashed lines in Fig. 3.4, see methods for details). We model the junctions with a unit cell of 7 layers of 16 (4x4) gold atoms with the molecule bound to a trimer Au tip structure on both sides. Initial geometries for both molecules **1** and **2** are adapted form previous work. [42,151] Relaxed geometries are obtained using density functional theory (DFT) with a gradient-corrected exchange-correlation functional (GGA-PBE) using a double-ζ-basis set implemented in the SIESTA package. [152–154] Transmission functions are calculated using a self-energy corrected scattering-states approach DFT+Σ [60, 155], implemented in the SCARLET code [156] as detailed in the supplementary information section 3.4. We overlay, in Fig. 3.4, the calculated transmission curves for molecule **1** and **2** (high G and low G) and find a good agreement in both the position of the resonance and its width between experiment and theory.

3.3 Conclusions

Such transmission functions as described above detail the probability that an electron of a given energy incident upon the molecular junction will be transmitted from one lead to the other through the molecule. Transport through such junctions occurs via a tunneling mechanism, and therefore, in a very simple picture, the probability of transmission is dependent upon how E_F of the leads is aligned with either the HOMO or LUMO of the molecule. By applying an electrolyte gate, we are able to modulate this relative alignment, bringing the relevant orbitals closer or further from resonance; this is essentially modifying the barrier for tunneling experienced by the electrons. In our experiments, since a small source-drain bias (25 mV) is applied to the molecular junction, the measured conductance essentially corresponds to transmission at one point along the energy axis. Upon gating the molecular junctions, the transmission function is rigidly shifted with respect to E_F [140, 157, 158], and we can see the segment of the transmission function that is mapped out during these measurement.

In summary, we have tuned the conductance of electrochemically inactive molecules using an electrolytic gate. Qualitatively, we see that conductance shifts in the expected direction, upon application of positive and negative gate potentials, for junctions whose transport is dominated by HOMO or LUMO resonances. Furthermore, using quantitative self-energy corrected DFT-based conductance calculations, we have demonstrated that the experimentally obtained conductance values as a function of gate potential trace out the predicted molecular junction transmission functions.

3.4 Supplementary Information

3.4.1 Additional Figures

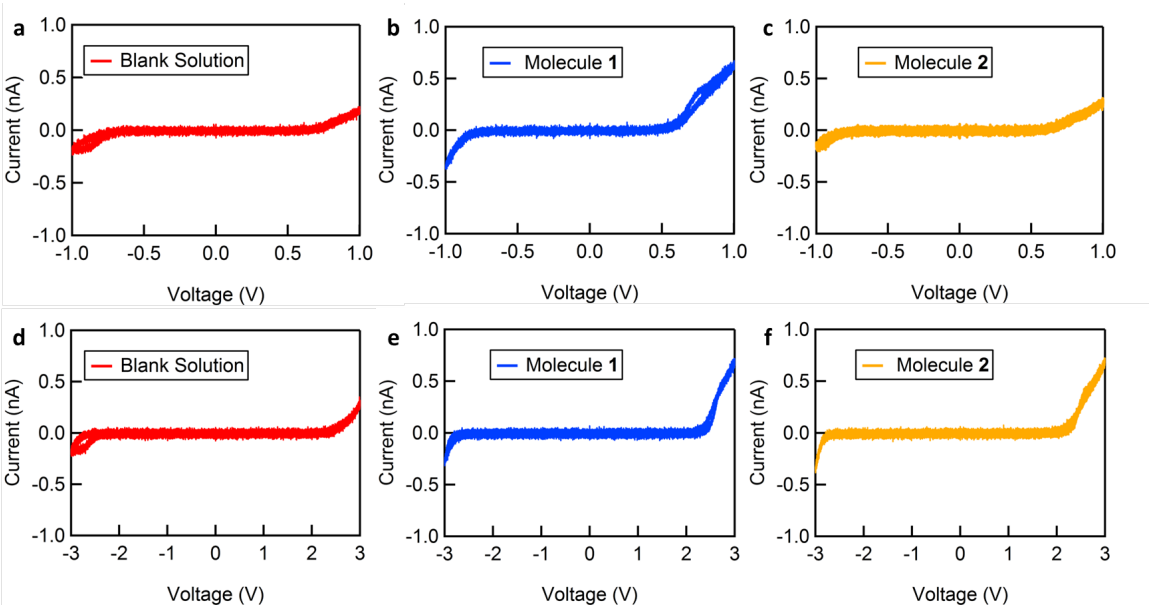

Figure 3.5: ***Cyclic voltammograms for gated molecules.*** *Cyclic voltammograms for a blank solution (solvent and electrolyte), a solution with molecule* ***1*** *and a solution with molecule* ***2*** *, demonstrating the lack of electrochemical activity for all systems in the range -1V to 2.5V. Plots (**a**), (**b**), (**c**) measured using the 2-electrode arrangement as detailed in the text, while plots (**d**), (**e**), (**f**) recorded using the 3-electrode arrangement as detailed in the text. All curves recorded at a scan rate of 100mV/s.*

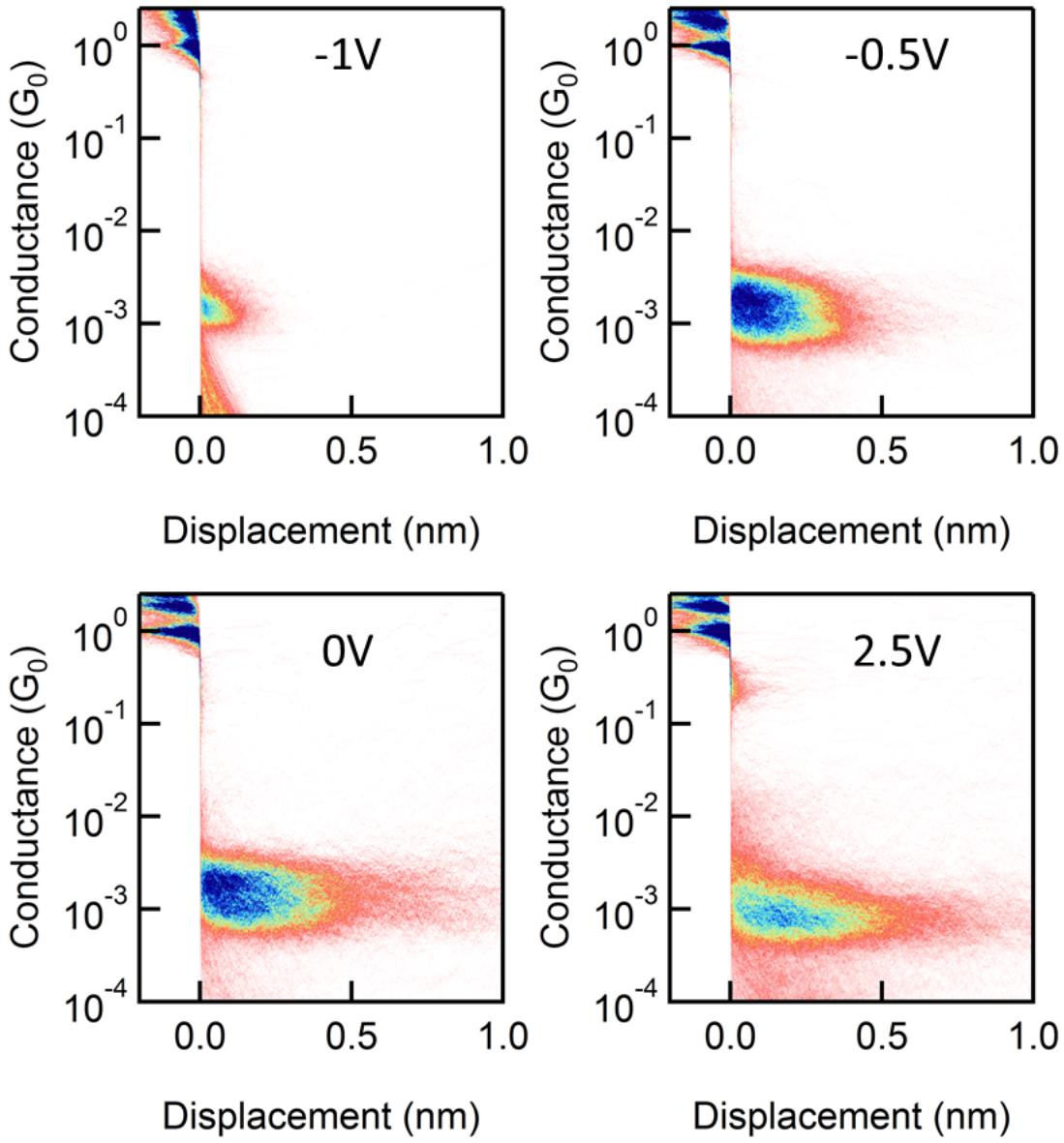

Figure 3.6: ***Influence of gating on molecular step-length.*** *Two-dimensional histograms for molecule* ***1*** *at selected gate potentials. The histograms were created by aligning each trace just after the* $1G_0$ *break (0 displacement is just after this break) and then overlaying all traces at the given gate potential without selection. A systematic decrease in plateau length can be observed as the gate potential is made more negative.*

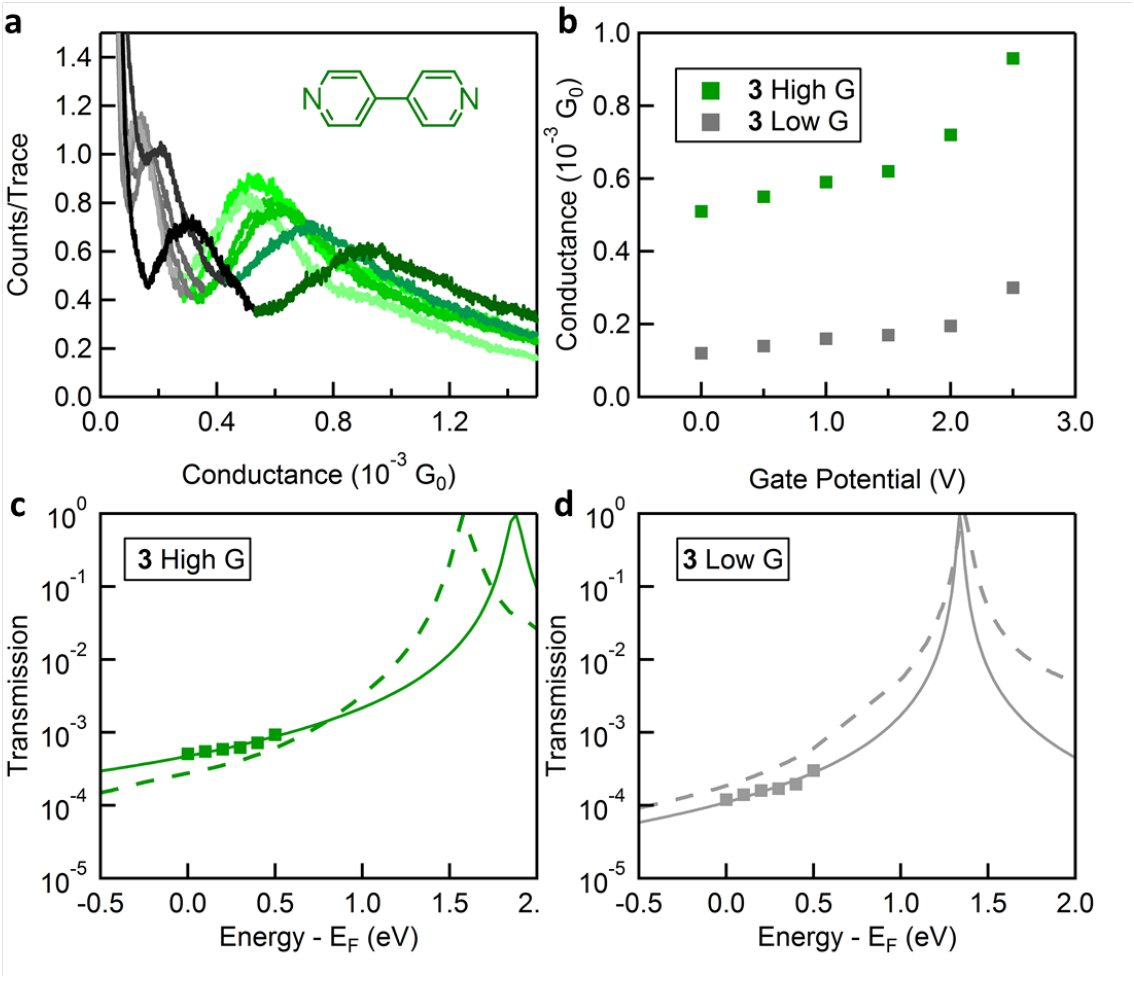

Figure 3.7: ***Gating data for 4,4'-bipyridine.*** *(**a**) Conductance histograms for 4,4-bipyridine taken at gate potentials VG = 2.5V, 2V, 1.5V, 1V, 0.5V, and 0V darkest to lightest. Note: green shades indicate the high-G feature for this molecule while grey shades indicate the low-G feature. Inset is the molecular structure. (**b**) Peak conductance values vs applied gate potential. (**c**) and (**d**) Conductance data for molecules 3 plotted against the potential drop at the working electrode (markers) fit with a single-Lorentzian transmission model (solid lines) for the high-G and low-G geometries respectively. The DFT+Σ calculated transmission functions are overlaid as dashed lines. For this molecule, we get Γ and ϵ of 0.08 eV and 1.83 eV for the high-G junctions and 0.028 eV and 1.34 eV for the low-G junctions.*

3.4.2 Control Gating Experiment

Gating measurements for molecules **1** and **2** were also carried out in an arrangement where the Au source and drain electrodes had a much smaller area than the Pt gate electrode. In order to accomplish this, the substrate was also insulated using Apiezon wax, leaving only a small area (5mm in diameter) exposed in order to carry out the break junction measurements. The Pt wire gate electrode was replaced with a much larger coiled piece of Pt wire in order to increase the surface area relative to the Au. With this arrangement, the majority of the applied gate potential is dropped across the Au electrodes as opposed to the Pt gate electrode. Conductance histograms were collected under applied gate potentials in 100mV intervals from 400mV to -100mV. As can be seen in SI Figure 3.8 below, much smaller gate potentials are needed in order to elicit a conductance change in this configuration. The gate potential applied here was also calibrated against oxidation of ferrocene in a similar manner to what is shown in Figure 3.3 of the manuscript. We found that the ferrocene oxidation peak in this case to be at 0.5 V indicating that the entire gate potential drops at the working electrode.

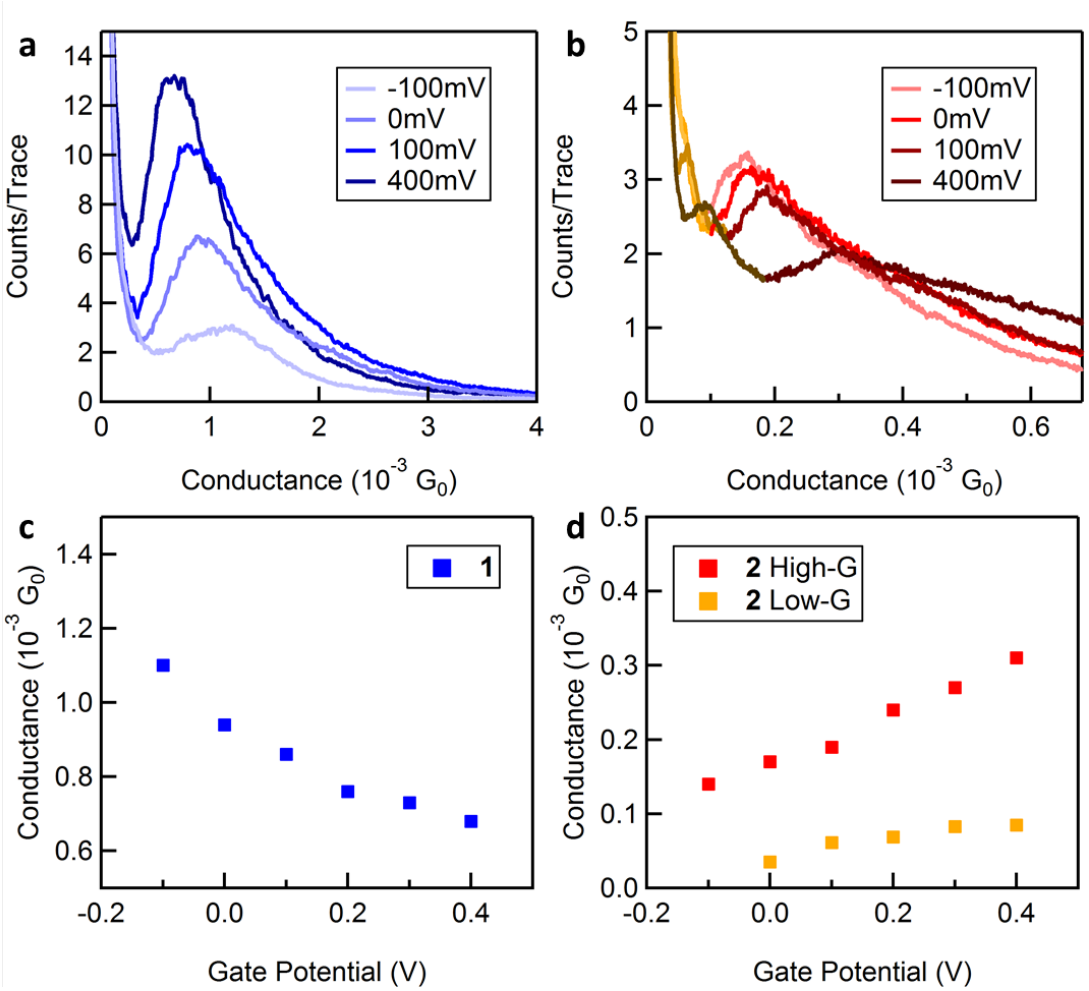

Figure 3.8: ***Gating experiments with alternative sized electrodes.*** *Gating data for molecules **1** & **2** using a large (with respect to the source drain electrodes) Pt gate electrode. (**a**) and (**b**) Sample conductance histograms at gate potentials VG = 400mV, 100mV, 0mV, -100mV darkest to lightest for molecule **1** and **2** respectively. Note: for molecule **2**, red shades indicate the high-G conductance feature while orange shades indicate the low-G conductance feature. (**c**) and (**d**) Peak conductance values vs applied gate potential for **1** and **2**, respectively.*

3.4.3 Calculation Details

We obtain the transmission functions using a parameter-free scattering-state approach based on DFT as implemented in the SCARLET package. [156] For all junctions, the transmission functions are calculated using a 16x16k$_{//}$-mesh and a 200-point energy grid in the energy range (E_F-4eV, E_F+4eV). The DFT molecular orbital energies in the junctions are cor-

rected using the DFT+Σ method. [60, 155] Specifically, we correct the gas-phase gap with a ΔSCF calculation, and correct for the lack of static nonlocal correlation effects in the junction through an electrostatic image charge model. PBE resonance energies are obtained by diagonalizing the junction Hamiltonian projected on the molecular subspace, as defined by the numerical orbitals centered on the atoms of the molecule. The DFT+Σ-corrected frontier orbitals for **1** and **2** LowG and HighG are at and E_F-1.52eV (Σ=-0.61eV), E_F+1.54eV (Σ=+1.42eV) and E_F+1.45eV (Σ=+1.27eV) respectively. XYZ coordinates for the studied junctions can be found in the supplementary information of reference [18].

Chapter 4

Environmentally Enabled Single-Molecule Diodes

In this chapter, we develop a new technique for creating a single-molecule diode. We do this by performing measurements in an electrolytic solution with electrodes of drastically different areas. The electric double layers that form about the source and drain electrodes of the molecular junction are of considerably different charge densities, yielding an asymmetric environment about the junction that can result in current rectification through the molecular junction. This method serves as an improvement over previous single-molecule diode designs, where an asymmetry is typically built into the molecule of interest. Diodes created using this design rule have suffered from poor performance, primarily because the asymmetry in the molecule is often enforced by having a portion of the molecule behave as an insulator. Our design scheme circumvents this issue, and has resulted in the highest performing single-molecule diodes to date.

This chapter is based on the manuscript entitled *Single Molecule Diodes with High Rectification Ratios through Environmental Control* by Brian Capozzi, Jianlong Xia, Olgun Adak, Emma J. Dell, Zhen-Fei Liu, Jeffrey C. Taylor, Jeffrey B. Neaton, Luis M. Campos, and Latha Venkataraman. Synthetic procedures and material characterizations were carried out by Jianlong Xia and Emma J. Dell of Prof. Luis M. Campos' group. Calculations were performed by Zhen-Fei Liu of Prof. Jeffrey B. Neaton's group. Olgun Adak and Jeffrey C.

Taylor of Prof. Latha Venkataraman's group assisted with measurements.

4.1 Introduction

Molecular electronics offers the promise of the ultimate miniaturization of electronic devices. Active components could be accessed through bottom-up fabrication using sub-nanometer scale elements. [159–161] A single-molecule diode, a circuit element that directs current flow, [162] was first proposed [1] with an asymmetric molecule comprising a donor-bridge-acceptor architecture to mimic a semiconductor p-n junction. Several single-molecule diodes have been realized in junctions featuring asymmetric molecular backbones, [13, 14, 163] molecule-electrode linkers, [15] or electrode materials. [164] Despite these advances, molecular diodes have had limited potential for applications due to low conductance values, low rectification ratios, extreme sensitivity to junction structure, and high operating voltages. [12–15, 165] Here, we demonstrate a powerful approach to induce current rectification in symmetric single-molecule junctions using two electrodes of the same metal, but breaking symmetry by exposing considerably different electrode areas to an ionic medium. This allows us to control the junctions electrostatic environment in an asymmetric fashion by simply changing the bias polarity. With this method, we reliably and reproducibly achieve rectification ratios in excess of 200 at operating voltages as low as 370mV using a symmetric oligomer of thiophene-1,1-dioxide. [117, 134] By taking advantage of an ionic environment, this method provides a general route for tuning nonlinear nanoscale device phenomena, that can be applied in systems beyond single-molecule junctions.

4.2 Results and Discussion

4.2.1 An Environmentally Enabled Molecular Rectifier

In this work, we use the scanning tunneling microscope-based break junction technique [2] (STM-BJ) in order to rapidly and reproducibly measure the conductance and current-voltage characteristics of thousands of single-molecule junctions (see the Supplementary Information, SI section 4.4, Fig. 4.6). We demonstrate rectification in single-molecule

junctions with this technique by carrying out measurements in propylene carbonate (PC), a polar solvent. We use an STM tip insulated with Apiezon wax [70] to reduce its area to ca. 1 μm^2 and a gold substrate that has an area greater than 1 cm^2 (Figure 4.1a). The insulation on the tip serves to reduce any background capacitive and faradaic electrochemical currents stemming from the ionic environment, but more importantly, it gives us control of the electrostatic environment around tip and substrate.

We first demonstrate exceptionally high and statistically reproducible single-molecule junction rectification in an oligomer consisting of four thiophene-1,1-dioxide units flanked by two gold-binding methyl-sulfide bearing thiophenes [134] (TDO4), as shown in Figure 4.1a. Sample conductance versus displacement traces for TDO4 measured in PC are shown in the inset of Figure 4.1b. Under the conditions described above, there is a significant difference in single-molecule junction conductance when measurements are performed at +180mV or -180mV (tip relative to substrate). When we compile thousands of conductance traces, without data selection, into one-dimensional log-binned conductance histograms (Figure 4.1b), it is clear that the conductance measured at -180mV exceeds that measured at +180mV by a factor of 3.25; this is a significant difference for such a low-bias measurement. This bias polarity dependent conductance is not observed when TDO4 is measured in a non-polar and non-ionic solvent (i.e. 1,2,4-trichlorobenzne, TCB, SI Fig. 4.7).

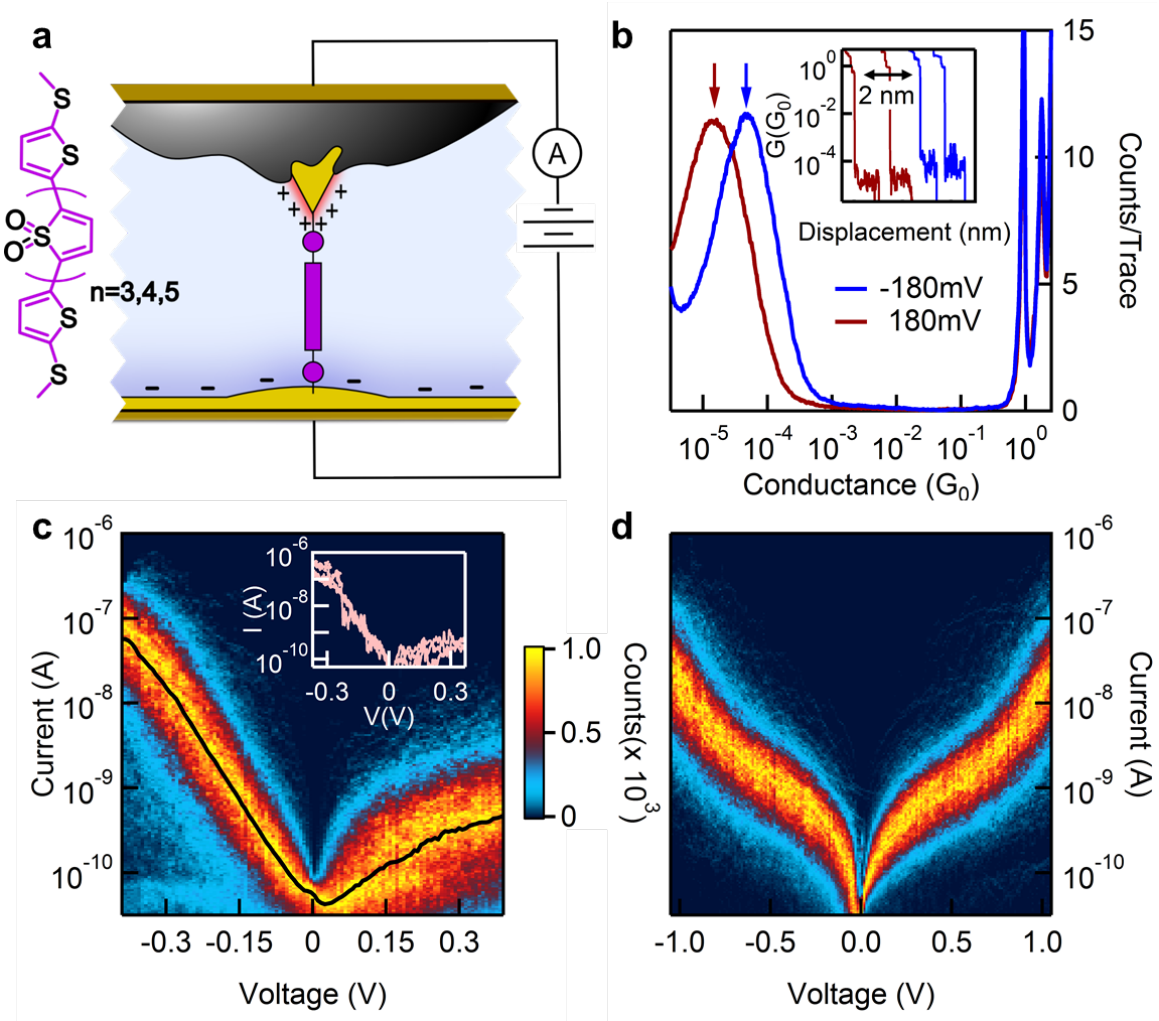

Figure 4.1: ***Environmentally enabled single-molecule diodes.*** *(**a**) TDOn molecular structure (alkyl side chains omitted for clarity) and schematic of molecular junction created using asymmetric area electrodes, not drawn to scale. (**b**) Log-binned conductance histograms for TDO4 taken at 180mV and +180mV created using 3000 traces each and 100 bins/decade. The arrows indicate the most probably measured conductance at each bias. Sample conductance versus displacement traces are inset and laterally offset for clarity. (**c**) Two-dimensional absolute current versus voltage histogram for TDO5 in PC, with examples of exceptionally rectifying junctions inset (3 selected traces). (**d**) Two-dimensional absolute current versus voltage histogram for TDO5 in TCB. Average IVs for TDO5 are overlaid on (**c**) and (**d**) in black.*

We next demonstrate the highest achieved rectification ratios in single-molecule junctions by performing current-voltage (IV) measurements on TDO5 (Figure 4.1a) in PC.

Thousands of individual IVs are obtained, and only traces containing a molecular feature that sustains the entire voltage ramp are considered (typically 500-1000 traces per molecule, see Methods). These traces are then overlaid and compiled into a two-dimensional (2D) current versus voltage histogram (Figure 4.1c). The plot illustrates a clear asymmetry in current with the sign of the bias, indicating a much higher current (flowing from tip to substrate) at negative voltages than at positive voltages (tip relative to substrate). Results from analogous IV measurements in TCB, where no asymmetry is observed, are shown in Figure 4.1d.

In order to obtain a quantitative value for the rectification ratio (I_{on}/I_{off}), each vertical slice of the 2D histogram is fit with a Gaussian, and a most probable current value is determined at each voltage to obtain an average IV curve (overlays in Figures 4.1c and 4.1d). We find a rectification ratio for TDO5 that is greater than 200 at +/-370mV in PC. While this average rectification ratio is already the highest reported for single-molecule junctions, several single-trace plots of these junctions display exceptionally high rectifying behavior,in excess of 500, as shown in the inset of Figure 4.1c. Although high rectification ratios have been observed in systems consisting of many-molecule junctions, [166, 167] the number of molecules involved in transport is generally unknown in these systems. Moreover, past reports have relied on asymmetric molecules, electrodes and chemical linker groups, unlike the design described here.

4.2.2 Mechanism for Rectification

We hypothesize that the highly asymmetric IV curves are due to the formation of an asymmetric, bias-dependent electric double layer. We note that a polar ion-soluble solvent is essential to observing rectification (SI Fig. 4.8). Indeed, measurements in PC with an added electrolyte (SI Fig. 4.9) do not differ significantly from those shown in Figure 4.1. The only source of asymmetry in our experiment is the disparate areas of the two electrodes exposed to the solvent. Since molecular junctions are formed after rupturing a gold-gold contact with a conductance greater than $5G_0$, with electrodes of the same metal and symmetric molecules, the metal-molecule-metal structure at the nanometer scale must, on average, be completely symmetric. We therefore postulate that electric double layers at

the tip and substrate, formed when ions dissolved in the polar solvent [168] move to screen out the electric field due to charges on the metal, influence the electrostatic environment around the junction. Specifically, the asymmetry in electrode areas exposed to the solvent results in the formation of a denser double layer on the tip electrode when compared with the substrate. [64] Experimental evidence for the existence of a dense double layer around the tip can be obtained from a cyclic voltammogram of ferrocene dissolved in PC measured using the same tip/substrate system used for the rectification measurements. As shown in SI Fig. 4.10 a clear, reversible ferrocene oxidation peak is observed at positive tip voltages providing definitive proof that the oxidation process occurs at the tip which is surrounded by dense double layer.

To understand rectification in these junctions in more detail, we consider a Landauer-like expression for current, assuming coherent off-resonant tunneling through the junction, a non-interacting mean field picture, and zero temperature, i.e.,

$$I = \frac{2e^2}{h} \int_{-eV/2}^{eV/2} T(E, \epsilon, \Gamma) dE \tag{4.1}$$

where e is the fundamental unit of charge, h is Plancks constant, V is the applied voltage and $T(E, \epsilon, \Gamma)$ is the energy-dependent (E) transmission function for the junction. We model transmission here with a single Lorentzian peaked at an orbital energy ϵ and with a constant width Γ as: [57]

$$T(E, \epsilon, \Gamma) = \frac{\Gamma^2/4}{(E-\epsilon)^2 + \Gamma^2/4} \tag{4.2}$$

Despite a clear asymmetry in $T(E, \epsilon, \Gamma)$ about the junction Fermi energy ($E = E_F$), for a symmetric junction under bias, V, current, evaluated through Equation 4.1, will be independent of the bias polarity.

We hypothesize that the double layer causes a bias polarity-dependent shift of the molecular resonance energy within the junction, leading to rectification. This bias-dependent environmental asymmetry can be modeled by replacing the resonance energy ϵ in Equation 4.2 with $(\epsilon + \alpha eV)$. The parameter α describes the impact of the applied voltage on the resonance position analogous to a first-order Stark shift coefficient. In Figure 4.2, we illustrate this model with a series of energy level diagrams where we assume, for simplicity, that α=0.5. At zero bias (Figure 4.2a), the resonance is located at an energy ϵ relative to

both the tip and substrate chemical potential. When a negative voltage V is applied to the tip relative to the substrate, the bias window will open symmetrically, consistent with a locally-symmetric junction geometry. However, due to the tip-substrate asymmetry of the double layer, we hypothesize the resonance shifts by an amount equal to αeV towards the tip chemical potential as shown in Figure 4.2b. When the tip is biased positively, the resonance shifts by the same amount, but in the opposite direction as is shown in Figure 4.2c. We stress that, under either bias polarity, the resonance position does not change relative to the substrate chemical potential, but only relative to the tip chemical potential. As long as $T(E, \epsilon, \Gamma)$ is asymmetric about E_F, the current, indicated by the shaded areas in Figures 4.2b and 4.2c, depends on the bias polarity yielding rectification. Figure 2d illustrates a non-rectifying case in solvents such as TCB where the resonance position does not move relative to the junction E_F.

The mechanism described above implies the observation of several additional phenomena. First, rectification ratios should in general be higher for junctions composed of molecules with a sharp resonance positioned closer to E_F. Second, the molecular orbital energy closest to E_F should generally dictate the direction of rectification: highest occupied molecular orbital (HOMO)- dominated junctions should turn on at the bias polarity that turns off lowest unoccupied molecular orbital (LUMO)-dominated molecules. Junctions possessing resonances with large Γ and/or ϵ should yield little or no rectification, as the transmission function about E_F will be relatively flat within accessible bias windows. Finally, this rectification should occur in any polar/ionic environment.

In Figure 4.3a, we show IV measurements from a family of derivatives containing TDO units (TDO3-TDO5) measured in PC. For junctions in this series, it has been previously shown that the LUMO moves closer to E_F by the addition of TDO units. [134] We find that all three IV curves display strong asymmetries, with significantly more current, reaching close to 0.1 μA at negative tip bias for TDO5. For all molecules, under positive tip bias, the IV exhibit a more linear dependence of current on voltage indicative of a rather flat transmission in this bias range, while the negative bias portions display highly non-linear behavior (particularly for TDO4 and TDO5), indicative of a resonance getting closer to the bias range.

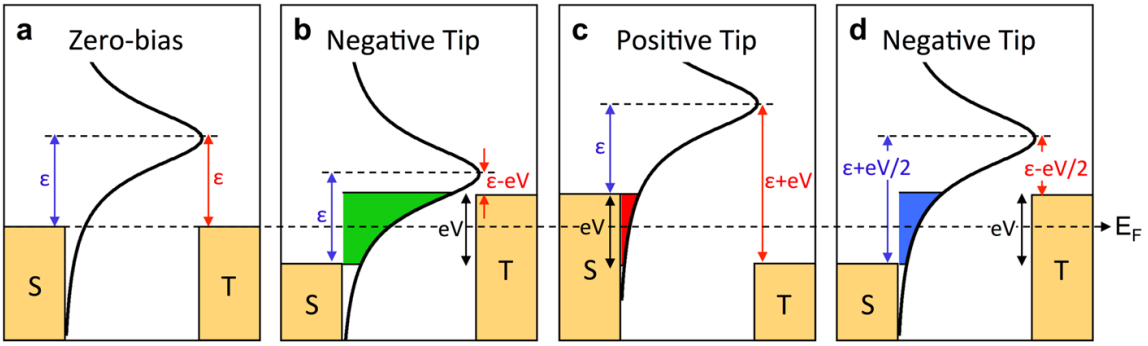

Figure 4.2: ***Energy-level diagram illustrating rectification mechanism for a LUMO conducting molecular junction.*** *(**a**) Zero-bias schematic depicting a molecular resonance with peak energy ϵ relative to the tip (T) and substrate (S) Fermi levels, E_F. (**b**) In polar media, when the tip is biased negatively relative to the substrate, the molecular resonance is at $\epsilon - eV$ relative to the tip chemical potential and at ϵ relative to the substrate chemical potential (α is taken to be 0.5 here). For this system, a large area of the resonance falls within the bias window, and the current is high. (**c**) When the tip is biased positively relative to the substrate, the molecular resonance again remains pinned to the substrate chemical potential, but is at $\epsilon + eV$ relative to the tip chemical potential. A small area of the resonance falls within the bias window and the current is low. (**d**) A similar schematic illustrating level alignment in a non-polar solvent (α is 0) with the tip biased negatively relative to the substrate. Here, the resonance does not shift in response to the applied bias, while both tip and substrate chemical potentials shift relative to the resonance position. The area under the resonance that falls within the bias window is independent of the bias polarity.*

The rectification ratio for each molecule as a function of the magnitude of the applied voltage is shown in the inset of Figure 4.3a. We find rectification ratios of 4 at 0.6V for TDO3, 90 at 0.42V for TDO4, and 200 at 0.37V for TDO5. We again emphasize that these high rectification ratios occur at exceptionally low operating voltages. The analogous IV measurements carried out in TCB are shown in Figure 4.3b, where we observe symmetric IV curves that become increasingly non-linear at higher applied voltages. Evaluating these data, we confirm our first prediction: as E_F aligns closer to a molecular resonance, the rectification ratio at a given bias increases.

Next, we consider the impact of the dominant transport orbital on the orientation of the diode. We perform IV measurements on three molecules that do not belong to the TDO family (see Figure 4.4a): 4,4-bipyridine (**1**), 4-4-diamino-p-terphenyl (**2**), 2,9-dithiadecane

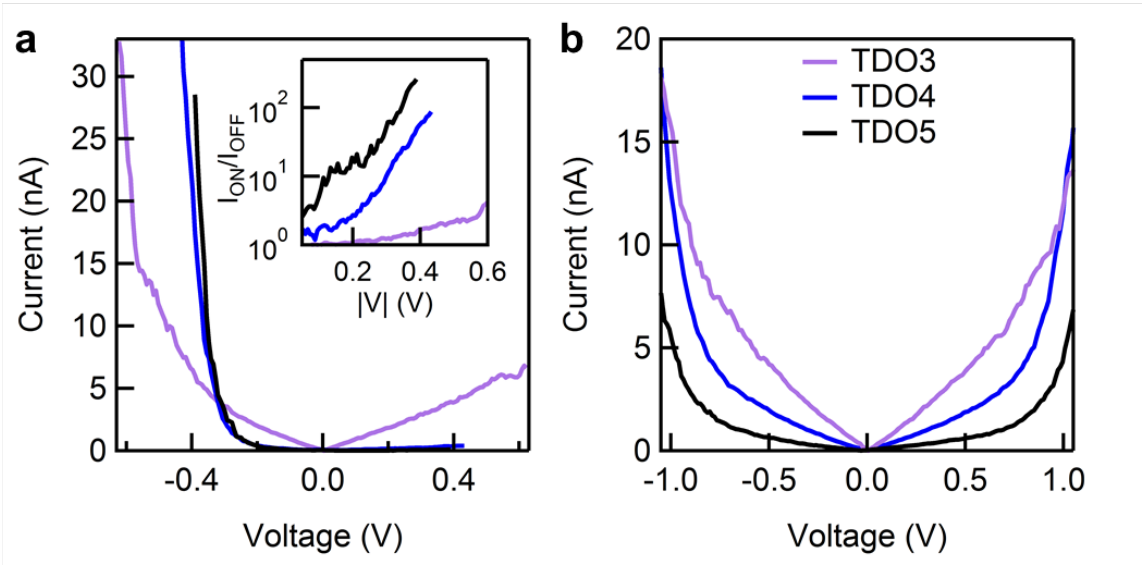

Figure 4.3: ***High rectification ratios in TDOn Junctions.*** *(**a**) Average IVs for TDOn with n=3-5 measured in PC. Inset: Rectification ratio (I_{on}/I_{off}) versus magnitude of applied voltage for curves. We find rectification ratios of 4 at 0.6V for TDO3, 90 at 0.42V for TDO4, and 200 at 0.37V for TDO5. We also note that the junctions rupture when the bias is increased beyond a molecule dependent critical voltage (-0.65V for TDO3, -0.42V for TDO4 and -0.39V for TDO5). We hypothesize that at this critical voltage, the LUMO resonance is at or very close to the bias window limit. This would imply that we are significantly charging the molecule and potentially breaking the linker-Au donor-acceptor bonds to the electrodes. See SI Figures 4.11 and 4.12 for 2D IV maps. (**b**) Average IVs for TDO3-5 measured in TCB. Note: IV curves show absolute value of current for clarity. Junctions formed in TCB are typically able to withstand twice the voltage of those in PC, becoming unstable and rupturing beyond 1.1V.*

(**3**). The characteristic IVs for these measured in PC are shown in Figure 4.4b. It is clear that **1** and **2** display on behavior at opposite bias polarities, while **3** does not show any discernible rectification. Within our model, this suggests that the two molecules should have transport dominated by different orbitals. Indeed, past work has shown that **1** conducts through the LUMO [60] while **2** conducts through the HOMO, [155] in agreement with our hypothesized rectification mechanism. The low rectification ratios observed for **1** and **2** further suggest that the dominant transport orbitals are rather far from E_F. The large gap alkane, **3**, does not rectify, indicating a flat transmission around E_F.

In Figure 4.4c, we compare measurements of **1** in different polar media and in TCB . The IVs measured in polar media are asymmetric, with on currents occurring at negative tip bias polarities demonstrating that the rectification is observable in all polar media. These results show clearly that our method of creating a molecular rectifier is not unique to either the TDO family or to PC as a solvent; a single-molecule diode can be created out of any molecule in any polar solvent (so long as the junction transmission function is asymmetric about the metals E_F). All experimental results presented here support our hypothesis that the bias-dependent double layer around the tip modifies the electrostatic environment at the junction to alter the relative alignment of the molecular orbital and the tip chemical potential.

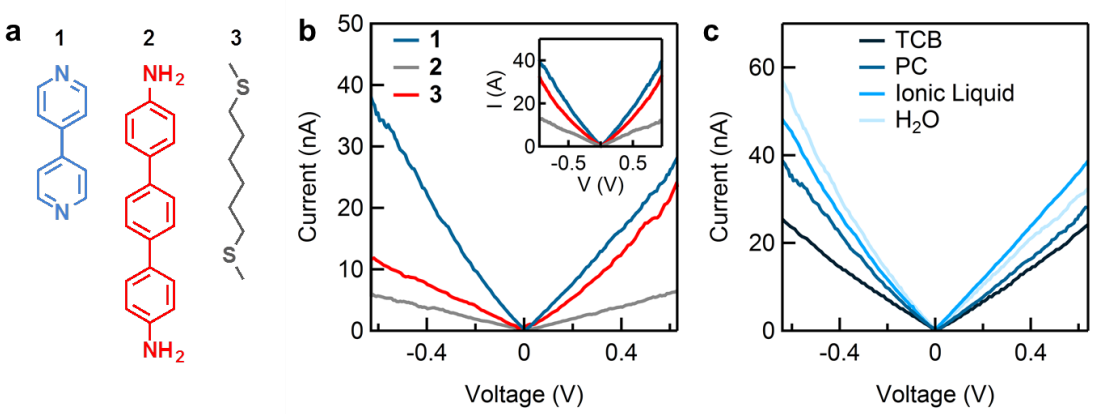

Figure 4.4: ***Rectification with Other Molecule/Solvent Systems.*** *(**a**) Molecular structures for additional molecules studies: 4,4-bipyridine (**1**), 4-4-diamino-p-terphenyl (**2**), and 2,9-dithiadecane (**3**). (**b**) IV curves for the three molecules measured in PC and in TCB (inset). A rectification ratio of 1.4 and 2.1 is seen for **1** and **2** at 0.62V, while **3** does not show any discernible rectification. See SI Figure 4.13 for corresponding 2D IV plots. (**c**) IV curves measured for 1 in TCB, PC, an ionic liquid (N,N-diethyl-N-(2-methoxyethyl)-N-methylammonium bis-(trifluoromethylsulphonyl-imide, DEME-TFSI) and dionized (18MΩ). Asymmetry, and therefore rectification, is only observed in the polar media, whereas a symmetric IV is measured in TCB. See SI Figure 4.14 for corresponding 2D IV plots. Slightly different currents (and therefore rectification ratios) are observed in the various solvents. This is attributed to a solvent effect, [54] where the work functions of the electrodes are altered by the presence of different solvent molecules adsorbed on the surface. Note: IV curves show absolute value of current for clarity.*

4.2.3 Assessing Energy-Level Alignment

After confirming the predictions implicit in our model, we now demonstrate that we can determine the parameter to provide quantitative support for the rectification mechanism proposed here. We use a recently developed AC technique described briefly in the SI, section 4.4, (manuscript under review, O.A, R. Korytar, A. Y. Joe, F. Evers, and L.V.) to determine the location of the conducting orbital (ϵ) and its coupling (Γ) to the Au electrodes for TDO4 in PC and TCB. The values obtained are then checked against zero bias self-energy corrected density functional (DFT+Σ) theory calculations. [155, 169] We show in Figure 4.5a and 4.5b that on average ϵ_{TCB} is 0.6 eV while the coupling, Γ_{TCB}, is 7 meV. Gamma is small, indicating that a mean-field approximation may not be adequate particularly as the molecule charges under bias. In PC, we solve these two equations by allowing α to vary from 0 to 0.5 in steps of 0.05. For each value of α we obtain the average value of Γ_{PC} and ϵ_{PC}. Note that the coupling of the LUMO to the leads should not be altered in different solvent environments as it primarily depends on the Au density of states, which is flat in the relevant energy window. Based on the results from these AC measurements, we find that the average Γ_{PC} is the same as Γ_{TCB} when $\alpha = 0.5$. Furthermore, we find that there is a 0.2 eV shift in ϵ_{PC} towards E_F compared with ϵ_{TCB}, which we attribute to a solvent-induced shift. [54] Using these experimentally determined ϵ and Γ parameters, we generate IVs from Lorentzian transmission functions and compare these to experimentally measured IV curves in SI Figure 4.15. We find reasonable agreement with the measured IVs and rectification ratios. This simple Lorentzian model also enables us to derive an analytic form for the observed rectification ratios, which are in good agreement with the experiment (see the SI, section 4.4, for discussion and SI Fig. 4.16).

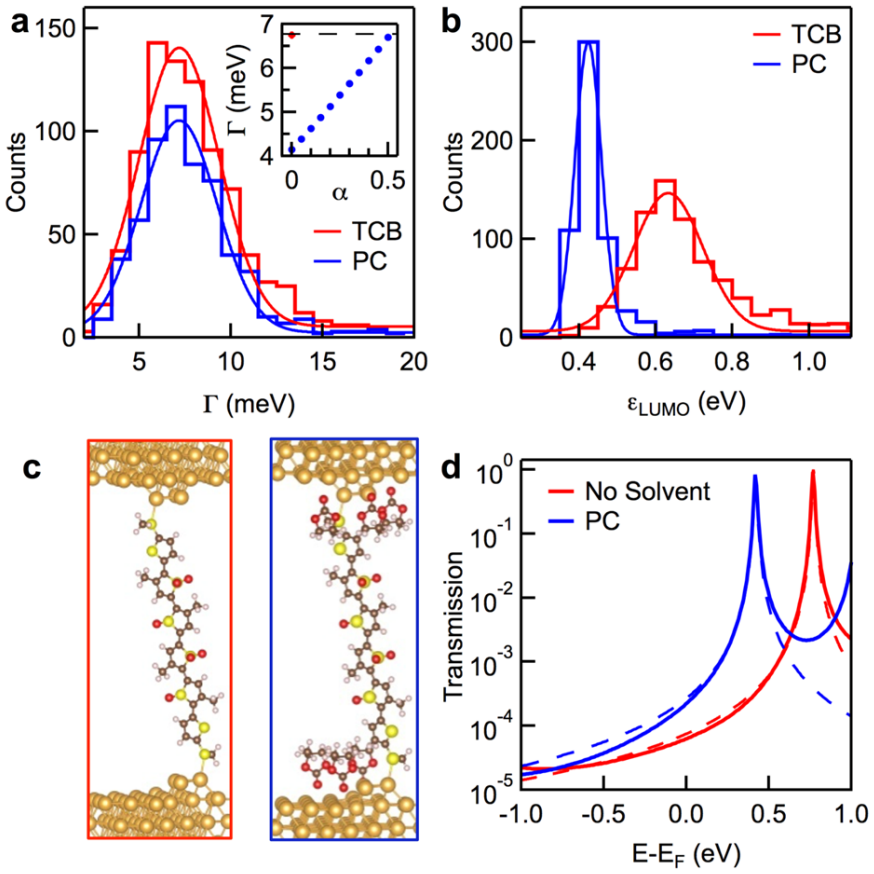

Figure 4.5: *Experimental determination of (**a**) orbital coupling strength and (**b**) energy level alignment for TDO4 in TCB and PC as determined using AC techniques. The inset of (**a**) shows the orbital coupling as a function of the bias asymmetry parameter α. The average value of the coupling for TCB junctions (red asterisk) is only achieved for $\alpha = 0.5$, which corresponds to a resonance that is pinned to the substrate chemical potential. The dashed line is a guide for the eye to make the comparison more apparent (**c**) Junction structures used to compute transmission characteristics. (**d**) DFT + Σ calculated transmission functions for TDO4 in a junction with no solvent molecules (red) and with propylene carbonate on both electrodes (blue). Dashed lines indicate Lorentzian fits to these transmission functions. These fits yield identical coupling strengths for the conducting orbital (Γ of 13 meV) for both junctions, and show a decrease in orbital position relative to EF when adding PC about the junction (ϵ of 440 meV (blue) and 760 meV (red)).*

We now turn to DFT+Σ calculations to validate three aspects of our measurements: (1) that the transmission function for TDO4 is well described by a Lorentzian function; (2)

that PC alters the level alignment in the junction but not the coupling; and (3) that adding a dipole layer on one electrode shifts the resonance position. We show the calculated zero-bias transmission functions for a TDO4 junction with and without PC (structures shown in Figure 4.5c) in Figure 4.5d. We find that these transmission curves are well described by a single Lorentzian form dominated by the LUMO, that these have a similar Γ, and that they show a relative shift in ϵ of about 0.3 eV. To model a dipole layer on one electrode, we add a layer of HF molecules within the unit cell oriented with the dipole pointing toward or away from the electrode and compute transmission through the TDO4 junction. Results from these calculations are shown in SI Figure 4.17. The presence of a dipole oriented with the negative charge close to the electrode shifts the resonance position closer to E_F. We stress here that these are zero-bias calculations, and as such cannot be used to quantitatively address the shift in the resonance position due to an applied bias since this depends on the double layer density. A first principles determination of the α parameter would require computing the impact of the double layer around the tip on the resonance position. To explain how the applied voltage yields an asymmetric double layer at an atomistic scale requires modeling of the electrodes and their associated double layers at a length scale that is well beyond what DFT, with current computational and algorithmic limitations, can handle.

4.3 Conclusions

While we note that we do not have a full atomistic model for the observed rectification effects, the results from the AC measurements and the DFT+Σ calculations support our postulated rectification mechanism. To summarize, two factors are needed to observe rectification: electrodes of different areas and an ion containing polar medium in which the transport measurements are performed. Due to the presence of ions in the environment, an electric double layer forms at each electrode/solution interface to screen out any applied bias. The disparate areas of the electrodes result in a denser layer of charge at the smaller tip electrode. This results in the pinning of the molecular orbitals to the chemical potential of the substrate, yielding a current dependence on the polarity of the applied bias.

We have demonstrated an unconventional technique by which to create single-molecule diodes with unprecedented rectification ratios at low operating voltages using symmetric molecules. This appealing and simple method enables the creation of single-molecule junctions by self-assembly, without the tedious chemical modifications that have been commonly employed to control molecule directionality in a junction. [13] Given the observed mechanism of rectification, we envision that this method can be easily implemented in other junctions beyond the STM-BJ test bed, for example, using other electrode materials including carbon nanotubes [170] or graphene [171] will yield rectifying behavior. By exploiting this tunable asymmetry in the electrostatic environment, this new approach offers a wealth of possibilities for translation into device fabrication.

4.4 Supplementary Information

4.4.1 Experimental Methods

Conductance Measurements Conductance measurements were carried out using the Scanning Tunneling Microscope-based break junction (STM-BJ) technique,**[1]** and have been described in detail before.**[2]** Conductance measurements for the TDOn family (synthetic details in Single-Molecule Diodes with High Rectification Ratios through Envrionmental Control) are carried out in dilute solutions (10μM-100μM) in propylene carbonate and 1,2,4-trichlorobenzene. Measurements for all other molecules (obtained from commercial sources, with over 95% purity) were carried out from 1mM concentration solutions. The insulated tips are created by driving a mechanically cut gold tip through Apiezon wax.**[3]** One dimensional conductance histograms are constructed using logarithmic bins (100 per decade) without any data selection.

Current-Voltage (IV) Measurements I-V measurements are performed using the STM-BJ, with a slightly modified procedure. [137] Instead of continuously retracting the tip from the substrate, the tip is withdrawn for 150 ms, held for 150 ms and then withdrawn for an additional 200 ms to fully rupture the molecular junction. A constant voltage is applied during the initial and final segments, as well as during the first and last 25 ms when the

tip position is held fixed. During the central 100 ms while the tip is held, a voltage ramp is applied. Current is measured during the entire 500ms procedure (sample trace in SI Figure 4.6). IV data is analyzed by first selecting traces with a molecular junction that sustains the entirety of the voltage ramp. Traces are selected by using an automated algorithm that requires the conductance during the first and last 25 ms of the hold to be within the width of the molecular conductance histogram. IVs in TCB were collected over a range of +/-1.05V, while IVs in PC were collected over smaller molecule-dependent voltage ranges. After trace selection, all IVs for a given molecule are used to construct a two-dimensional current versus voltage histogram. A most probable IV is obtained by fitting each vertical line slice of the two-dimensional IV histogram with a Gaussian and recording the peak current. This is then converted to its linearly scaled IV curve following the procedure detailed in Huber et al. [172]

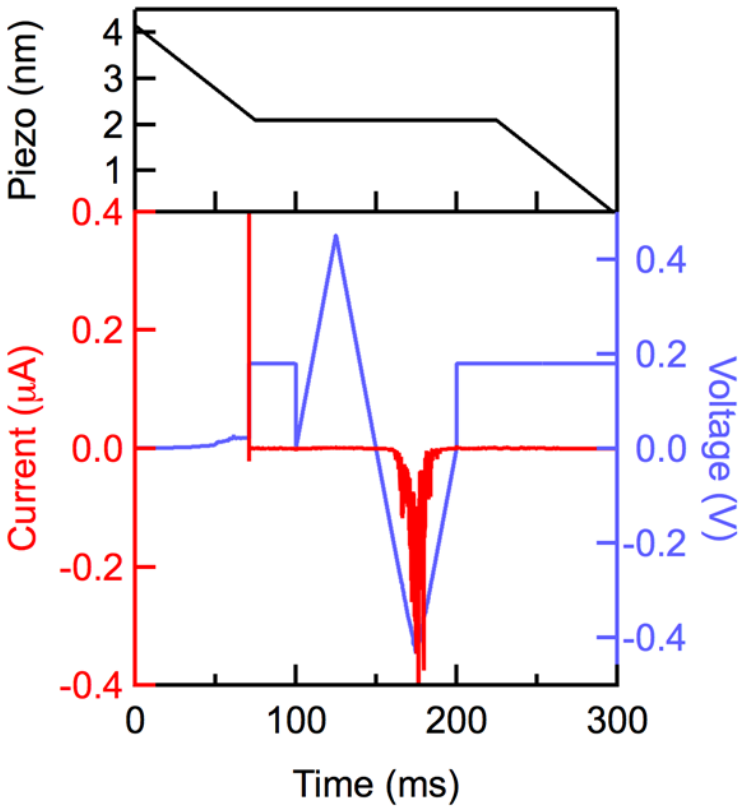

Figure 4.6: ***Sample IV measurement.*** *Top panel: Piezo ramp during a segment of the IV measurement. Bottom panel: Voltage applied to the tip (blue) and current flowing into the substrate (red) as a function of time for a single TDO4 trace in PC (same trace as in above panel). At -0.4V, a current of 0.4 μA is measured, while at +0.4V, the current is very small.*

4.4.2 Additional Data and Analysis

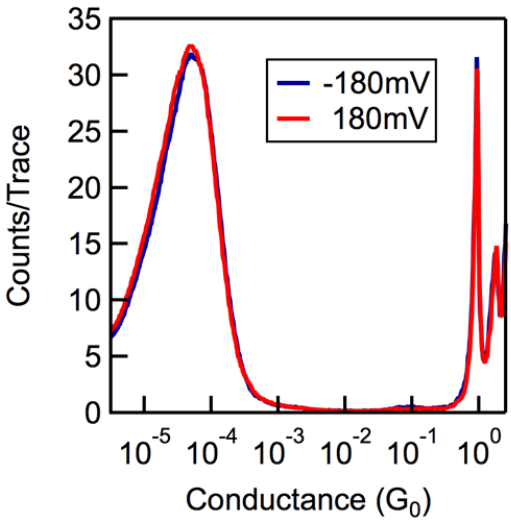

Figure 4.7: ***Bias polarity dependent conductance of TDO4 in TCB.*** *Log-binned conductance histograms for TDO4 measured in 1,2,4-trichlorobenzene at +/- 180mV using 100 bins/decade. In contrast with the data shown in Figure 4.1b, there is no change in conductance at the two different polarities.*

Non-polar Solvent with Insulated Tip Measurements of 4,4"-Diamino-*p*-terphenyl were carried out in phenyl octane (PO, non-polar) and in propylene carbonate (PC, polar) with a coated tip (glue coated for PO, and wax coated for PC). We collected 3000 conductance traces at +450mV and -450mV in both PC and PO (SI Figure 4.7). A clear shift in conductance is observed in PC while no change is seen in PO. We also note that 4,4"-Diamino-*p*-terphenyl has previously been shown to conduct through the highest occupied molecular orbital (HOMO)[**1**]; its conductance shifts up at positive tip biases in PC.

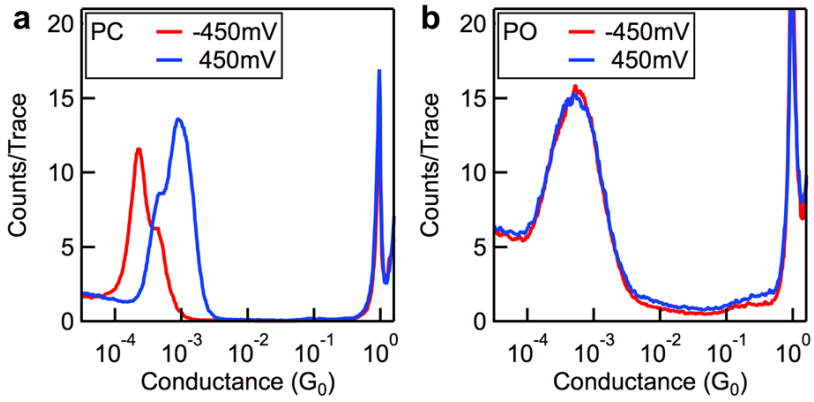

Figure 4.8: ***Comparison of conductance measurements taken with insulated tips in polar and non-polar solvents.*** *Log-binned conductance histograms for 4,4-diamino-p-terphenyl in (**a**) propylene carbonate (PC) and (**b**) phenyl octane (PO) created using 100 bins/decade. Both measurements were made with an insulated tip at 450mV and at -450mV. A clear polarity dependence is observed only in PC.*

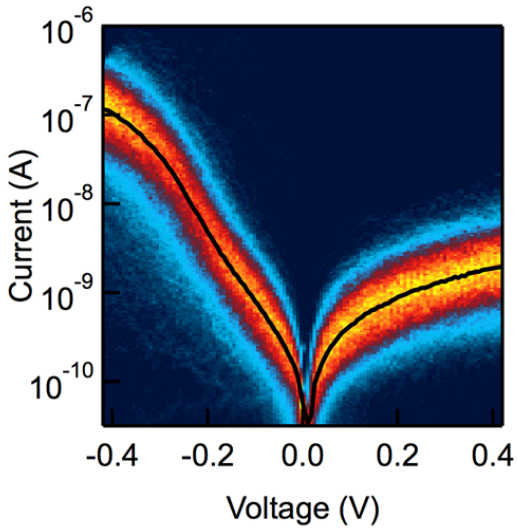

Figure 4.9: ***IV measurements on TDO4 in an electrolytic solution.*** *Two-dimensional IV histogram for TDO4 measured in propylene carbonate with an additional 0.1M of tetrabutylammonium perchlorate. Histogram is constructed from 2671 traces.*

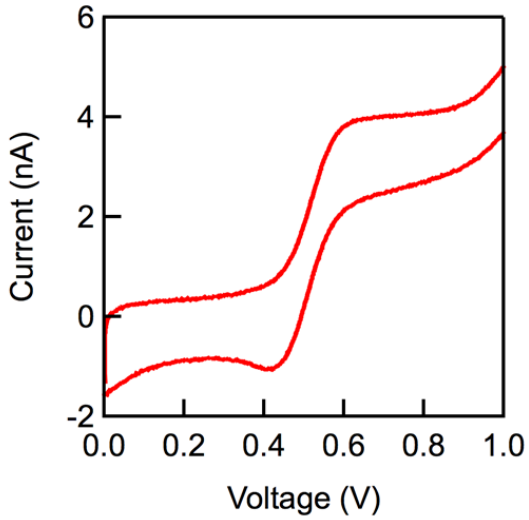

Figure 4.10: ***Cyclic voltammogram using two-electrode break junction geometry.*** *Cyclic voltammogram taken using the break-junction geometry with a solution of 1mM ferrocene in propylene carbonate (there is no added supporting electrolyte). An insulated gold tip serves as our working electrode while a large gold substrate serves as our counter electrode.*

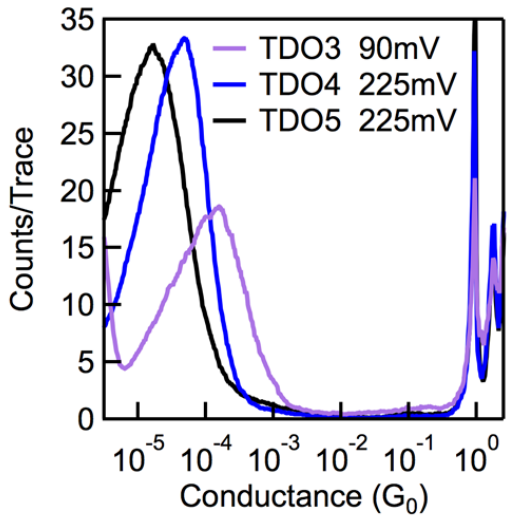

Figure 4.11: ***TDO conductance histograms in TCB.*** *Conductance histograms for TDO3-5 measured 1,2,4-trichlorobenzene (TCB). All histograms were measured prior to IV curves being collected.*

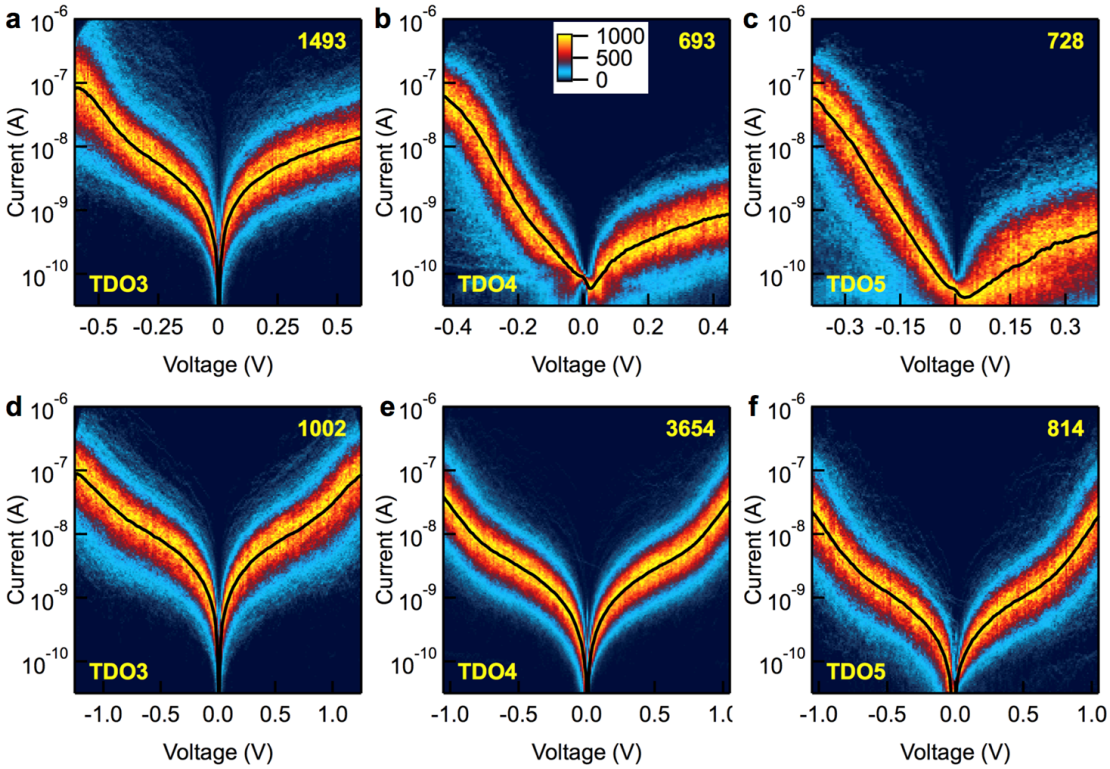

Figure 4.12: ***Two dimensional IV maps for TDO3-5.*** *Two-dimensional IV histograms for TDO3-TDO5 in propylene carbonate (**a-c**) and 1,2,4-trichlorobenzene (**d-e**). Histograms were constructed from the number of traces indicated in the figures. Average IV curves are overlaid as solid black lines.*

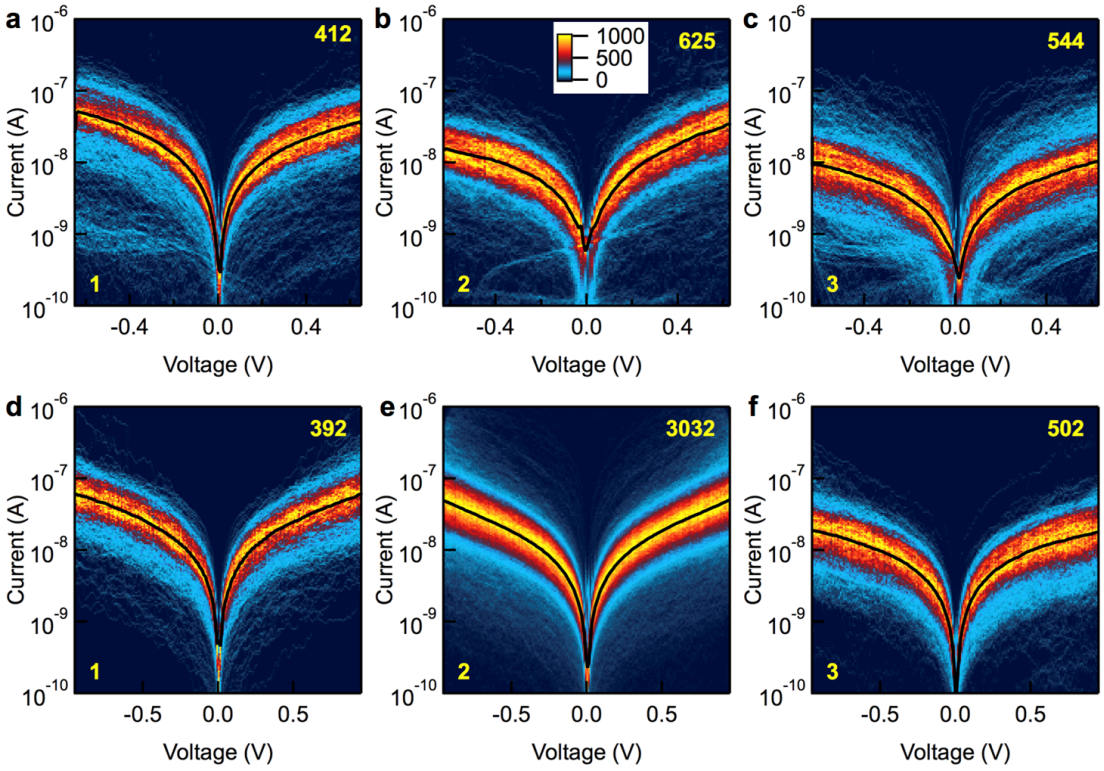

Figure 4.13: ***Two-dimensional IV maps for additional molecules.*** *Two-dimensional IV histograms for 4,4-bipyridine (**1**), 4-4-diamino-p-terphenyl (**2**), and 2,9-dithiadecane (**3**) in propylene carbonate (**a-c**) and 1,2,4-trichlorobenzene (**d-e**). Histograms were constructed from the number of traces indicated in the figures. Average IV curves are overlaid as solid black lines.*

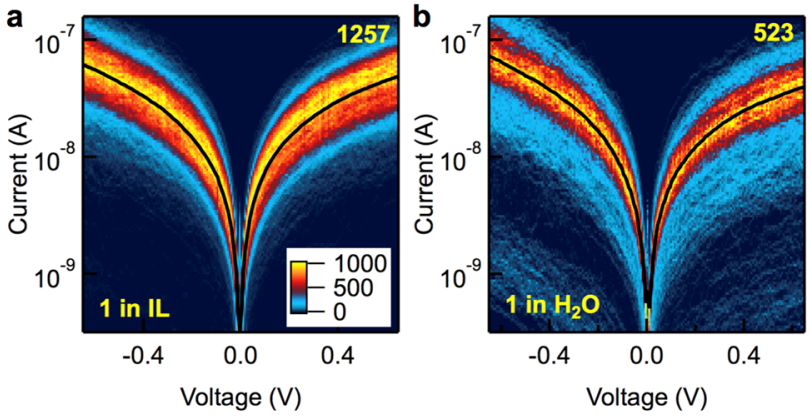

Figure 4.14: ***Two-dimensional IV histograms for 4,4-bipyridine (1) in additional polar media*** *Two-dimensional IV histograms for 4,4-bipyridine (**1**) in additional polar media: (**a**) an ionic liquid (DEME-TFSI) and (**b**) H_2O. Histograms were constructed from the number of traces indicated in the figures. Average IV curves are overlaid as solid black lines.*

4.4.3 Experimental Determination of Energy Level Alignment

In order to determine the orbital alignment and orbital coupling strength in TDO4 single-molecule junctions, we make use of the following recently developed technique (manuscript under review, O.A, R. Korytar, A. Y. Joe, F. Evers, and L.V.):

1) Measure the conductance, G, and the derivative of conductance with respect to voltage (dG/dV) for a single molecule junction.

2) Obtain analytical expressions for these two quantities in terms of orbital energy and orbital coupling strength.

3) Iteratively solve a pair of non-linear equations to determine the two values.

G and dG/dV are obtained by using a modified break-junction technique, similar to that of the IV measurements (see above). However, instead of applying a saw-tooth bias ramp while the tip is held at a fixed distance from the substrate, an additional AC voltage (65 mV at 16 kHz and 130 mV at 14 kHz in PC and TCB respectively) is applied on top of a DC voltage (-220 mV and 500 mV in PC and TCB respectively). As with IV measurements, we only analyze traces that have a molecule present in the junction while the hold is applied. We do this by checking that the conductance of the junction (just prior to the AC voltage being applied) falls within a standard deviation of the conductance histogram peak.

The frequency domain representation of the current while the AC voltage is applied is obtained using the discrete Fourier transform. The zero frequency signal corresponds to the DC current while the signal at the fundamental frequency (16 kHz and 14 kHz) corresponds to the AC current. The AC current consists of two components: the first is the tunneling current through the molecular junction and the second is the result of the capacitive coupling of the electrodes. We only consider the current in phase with the applied AC voltage in order to discard the capacitive component. We also measure currents resulting from any non-linearity in the conductance-voltage relationship; these are measured at the second harmonic frequency (32 kHz and 28 kHz). In order to see explicitly what is responsible for this signal, the current through the junction is Taylor expanded around the DC value up to third order terms to yield:

$$I = \left[I(V_{DC}) + \frac{1}{4}\frac{dG}{dV}\bigg|_{V_{DC}} V_{AC}^2\right] + \left[G\big|_{V_{DC}} + \frac{1}{8}\frac{d^2G}{dV^2}\bigg|_{V_{DC}} V_{AC}^2\right] V_{AC} sin(\omega_{AC} t) - \frac{1}{4}\frac{dG}{dV}\bigg|_{V_{DC}} V_{AC}^2 cos(2\omega_{AC} t)$$

Here, I is the current through the junction, V_{DC} is DC bias voltage, V_{AC} is the amplitude of the AC voltage, and ω_{AC} is the frequency of AC voltage.

The terms in the first bracket represent the DC current due to the DC voltage and a rectification term ($\frac{1}{4}\frac{dG}{dV}\Big|_{V_{DC}} V_{AC}^2$) due to a non-linearity in the conductance-voltage relationship. The second set of terms corresponds to the differential conductance (dI/dV) and a small contribution from second order conductance derivative with respect to voltage. The second harmonic term corresponds purely to the rectification term of the DC current. Thus, the second harmonic current measures dG/dV with small contributions from higher order terms. When the junction transmission function is well described by a single Lorentzian function (as given in Equation 4.2 of the manuscript), we can derive an analytic expression for the AC current that is in phase with the applied AC voltage at the fundamental frequency in terms of ϵ and Γ. Note that in this analysis, we explicitly include the dependence of the resonance position on the voltage through the α parameter as described in the main text. This gives one non-linear equation with two unknown parameters. Similarly, we derive a second analytic expression for the current at the second harmonic in terms of ϵ and Γ. Although not shown explicitly above, we include terms up to sixth order for the Taylor

series expansion. We solve these two non-linear equations using a non-linear least squares solver algorithm to determine ϵ and Γ in a single molecule junction.

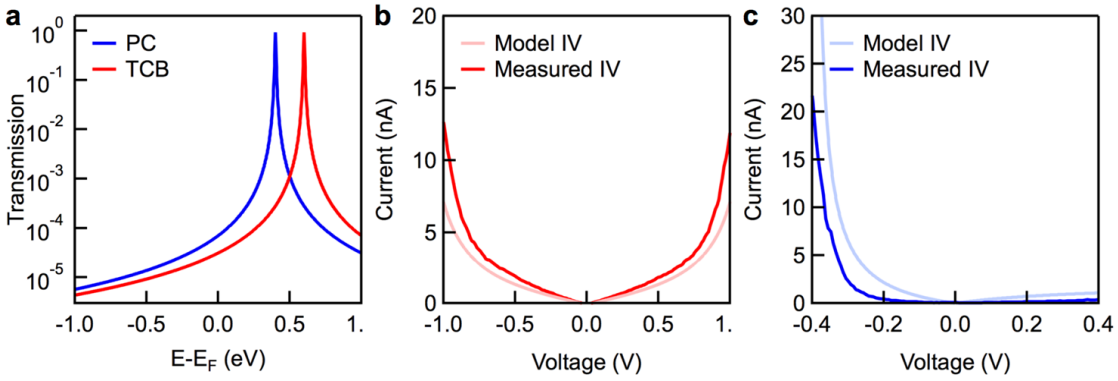

Figure 4.15: ***Computed IV curves using experimentally determined parameters and a single-Lorentzian model.*** *(**a**) Model transmission functions created using the and parameters extracted from AC measurements (see Figure 4.5). (**b**) Measured IVs for TDO4 in TCB compared with model IVs obtained by integrating the transmission function in (**a**) as detailed in the text. (**c**) The same analysis, using the model transmission function for PC. There is good agreement between the measured and calculated curves. Deviations between the model and measured IVs are primarily because IV measurements select a subset of junctions that sustain the entire bias ramp while the AC measurements are done at a fixed and smaller bias.*

Rectification and the Single-Lorentzian Model In cases where transmission can be indeed modeled as a single Lorentzian function over a reasonably wide energy range, we are able to obtain an analytic expression for the rectification ratio at a given voltage. Assuming a transmission function of the form:

$$T(E) = \frac{\Gamma^2/4}{(E - \epsilon - \alpha eV)^2 + \Gamma^2/4}$$

as defined in the main text. Assuming α=0.5, we find:

$$RR = \frac{\int_{-eV/2}^{eV/2} T(E - \epsilon + eV/2)dE}{\int_{-eV/2}^{eV/2} T(E - \epsilon - eV/2)dE}$$

$$RR = \frac{tan^{-1}\left(\frac{\epsilon}{\Gamma/2}\right) - tan^{-1}\left(\frac{\epsilon - eV}{\Gamma/2}\right)}{tan^{-1}\left(\frac{\epsilon + eV}{\Gamma/2}\right) - tan^{-1}\left(\frac{\epsilon}{\Gamma/2}\right)}$$

Plotting this function (see SI Figure 4.16), we find, not surprisingly, that we would expect very large rectification ratios as the bias window nears the molecular resonance. Indeed, this simple picture predicts ratios on the order of the ratios that we have measured experimentally.

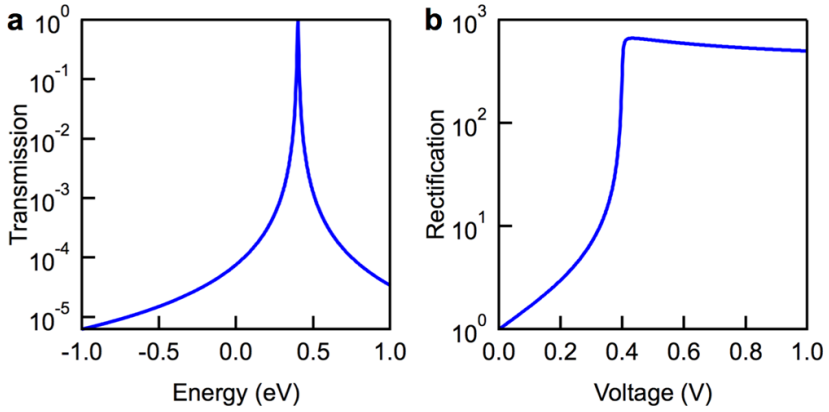

Figure 4.16: ***Model rectification ratios versus applied bias using a single-Lorentzian model.*** *(**a**) Single Lorentzian transmission function created using $\epsilon = 0.4$ eV and $\Gamma = 7$ meV. (**b**) Rectification ratio (I_{on}/I_{off}, RR) as a function of applied voltage using the analytic expression from above. Within our model, we find RRs ¿ 500 as the applied bias nears the value of the zero-bias molecular resonance in agreement with experiment.*

4.4.4 Computational Details

To compute the transport properties of the molecules, we employ an ab initio approach based on the combination of density functional theory (DFT), non-equilibrium Greens functions (NEGFs) [169], and a GW-based self-energy correction, [59] known as DFT+Σ. [155] To reduce computational cost, we replace the long C_6H_{13} chains in the molecules by CH_3. The molecules are placed between two gold leads consisting of seven Au (111) layers on each side, with 16 (44) atoms on each layer, to form molecular junctions. Due to the donor-acceptor nature of the Au-S bond, we use trimers as the binding motif, consistent with previous work. [155] The junction geometry is relaxed using the Perdew-Burke-Ernzerhof (PBE) [154] functional implemented in SIESTA. The Au basis set and pseudopotential are adapted from previous work. [155] The outer three layers of gold atoms are fixed in their bulk geometry during the relaxation. A 44 k-mesh is used and the atomic coordinates are

relaxed until all forces are below 0.04 eV/Å. The resulting Au-S bond lengths are about 2.85 Åand the angles between Au-S bond and the thiophene plane is about 20 degrees. After the junction geometry is relaxed, we compute the transport properties using DFT-NEGF formalism as implemented in TranSIESTA. [169] The outer three layers of gold atoms are the leads, and the extended molecule consists of four gold layers on each side. The PBE functional, a 66 k-mesh and 36 energy grids in the integration contour are used [169] to converge the non-equilibrium density matrix.

The DFT+Σ [155] method corrects the level alignments inherent to the Perdew-Burke-Ernzerhof (PBE) functional, [154] by adding a self-energy correction [59] to the converged PBE Kohn-Sham Hamiltonian and computing the transmission function with this modified Hamiltonian [59] The self-energy correction is based on the GW method, and includes two parts: (1) gas-phase contribution, correcting inaccuracies in PBE eigenvalues for isolated molecule; and (2) surface polarization effect that is approximated by a classical image-charge model. [59] For the TDO4 system, PBE places the LUMO, the dominant conducting orbital at 0.28 eV above E_F. The gas-phase correction shifts LUMO upwards by 1 eV and the surface polarization effect shifts LUMO downwards by 0.5 eV resulting in a net upward shift of 0.5 eV and placing the LUMO at about 0.78 eV above E_F. This LUMO position is in excellent agreement with the experimentally determined position in TCB as shown in Figure 4.5b.

To model the effect of PC molecules on level alignment in TDO4 molecular junction, we add three PC molecules on both gold surfaces in a unit cell oriented with the oxygen on the Au (111) surface. The distance between the oxygen atom of PC and the top Au (111) surface is about 2.5 and the binding energy between the PC molecule and the Au (111) surface is about 0.2 eV. When compared to junctions without PC, we find the LUMO peak in T(E) is shifted downwards by about 0.3 eV, again in excellent agreement with the experimentally determined shift of 0.2 eV (Figure 4.5b).

To model the effects of a dense electric layer on one electrode, we have computed zero bias transmission functions with the addition of 5 hydrofluoric acid (HF) molecules to one electrode, with the HF dipole being oriented either up or down (SI Figure 4.17). The HF molecules are added to the relaxed TDO4 junction; no further structural relaxation

is done after the HF is added. The HF bond (and therefore the dipole moment) is kept perpendicular to the Au surface. The lower atom in the HF molecule is kept 5 Åabove the surface to ensure that the molecule is not bound.

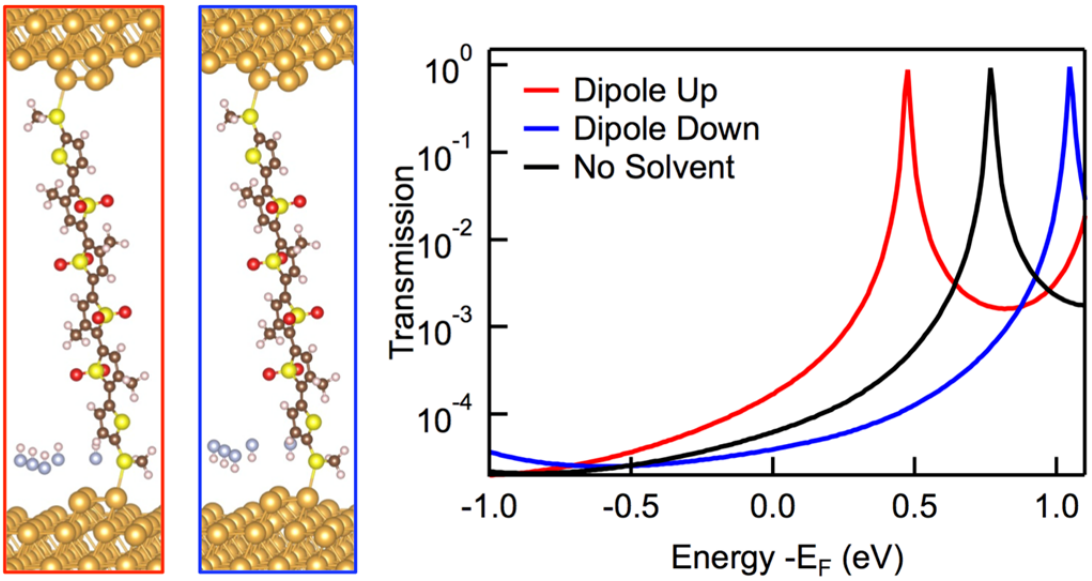

Figure 4.17: ***DFT+Σ calculated transmission functions with a dipole layer on one electrode.*** *Junction structures and junction transmission functions for TDO4, using hydrofluoric acid (HF) as a dipole to simulate the effects of a dense electric double layer on one electrode; the dipole orientation is used as a proxy to simulate the effects of an applied bias. Zero bias transmission functions are calculated without solvent (black), with the HF dipole oriented up (red) and with the HF dipole oriented down (blue). It can be clearly seen that the effect of the dipole is to shift the molecular resonance relative to* E_F.

4.4.5 Synthetic Details

Synthetic details for TDO5 can be found in the Supplementary Information section of *Single-Molecule Diodes with High On/Off Ratios Through Environmental Control.*

Chapter 5

Experimental Determination of Single-Molecule Junction Transmission Functions

The electronic transport characteristics of a single-molecule junction are governed by a transmission function which dictates the probability of an incident electron being conducted through the junction. Here, we present a new technique for measuring transmission functions over an energy range of 2eV around the metal Fermi energy, E_F. This technique is experimentally simple, does not require an assumed functional form for transmission, and provides access to a large region of the transmission landscape. In order to accomplish this, we create molecular junctions in an ionic environment with electrodes of different areas to create dissimilar density electric double layers at the source and drain electrodes. This then allows us to electrostatically shift the molecular resonance relative to the junction Fermi level to determine the dominant orbital for charge transport in the molecular junction and to map out the junctions transmission function. We demonstrate this technique using two groups of molecules, one with molecular resonances located relatively far from E_F and one with molecular resonance within the accessible gate voltage. Our results compare well with previous electrochemical gating data and calculated transmission functions. Furthermore, with the second group of molecules, we are able to examine the behavior of a molecular

junction as a molecular resonance falls within the gate bias window. This work provides a new, experimentally simple, route for exploring details of charge transport at the nanoscale.

This chapter is based on the manuscript entitled *Mapping the Transmission Function of a Single-Molecule Junction* by Brian Capozzi, Jonathan Z. Low, Jianlong Xia, Luis M. Campos, and Latha Venkataraman, which is currently under preparation. Synthetic procedures and material characterizations were carried out by Jonathan Z. Low and Jianlong Xia of Prof. Luis M. Campos' group. I performed the break junction measurements, data analysis, and modeling.

5.1 Introduction

Characterizing metal-molecule interfaces is a key step in developing organic electronic devices, as interfacial properties serve to dictate device properties. [30] The simplest interface that can be envisioned is that of a single metal-molecule bond: these interfaces can be readily created and studied using break junction techniques. [2, 37] Advances in the study of single-molecule circuits have led to a wealth of knowledge regarding the electronic and mechanical properties of such systems, as well as the mechanisms by which charge is transported. [160, 161, 173] For most systems investigated, charge transport occurs via coherent tunneling, and can therefore be described by a transmission function detailing the probability that an incident electron is conducted through the molecular barrier. [55] Several techniques have emerged to experimentally assess energy-level alignment at the metal-molecule interface in single-molecule junctions, providing insight into the transmission function. These methods include thermopower measurements [41–43], AC techniques [174], gating [16, 18, 19, 43], and measuring current-voltage curves [175, 176].

While these methods have indeed provided information about the transmission function beyond its value at the metal Fermi energy, E_F, ($G(E_F) = G_0T(E_F)$), the additional information has been limited. Thermopower measurements give access to two quantities: low-bias conductance and the Seebeck coefficient. These can then be related to the electron transmission probability at the E_F and the slope of the transmission function at E_F. [177] Using a recently developed AC method, currents can be measured at the first and second

harmonics of an applied AC voltage (this AC modulation is on top of a DC voltage); these values correspond to the first and second derivatives of the transmission function. [174] These two methods, however, provide only two data points of information about the transmission function; extracting the exact level-alignment further requires assuming a functional form for transmission, commonly a two-parameter single-Lorentzian, and solving for the parameters. These two techniques therefore fail when the single-Lorentzian approximation for transmission is not valid. [132]

Current-voltage (IV) characteristics can, in principle, be fit in order to obtain the transmission function since the measured current at a given voltage is proportional to the integral of the transmission function. Again, however, IV fitting requires a known functional form for transmission, and these fitting procedures are valid only if high-bias effects (such as stark shifted molecular levels [178]) can be excluded. Using a gate to electrostatically tune the energy-level alignment in the molecular junction, shifting molecular orbitals relative to the electrode E_F, can also be used to directly map the transmission function. [16, 18] Yet, gating techniques have proven difficult to implement at the single molecule level. Indeed, back- and side- gated devices require extensive fabrication processes and have typically had very low yields. [16,179–181] Electrolyte gating alleviates the problem of needing to place a gate electrode in close proximity of the molecular junction. [18,19] In principle, though, this technique then requires the usage of two additional electrodes in solution, a reference electrode and a counter electrode, which need to be controlled using a potentiostat; this makes it difficult to apply electrolyte gating to other electrode materials or device architectures.

Here, we demonstrate a simple new technique that can be used to probe transmission in single-molecule junctions over an energy range of about 2 eV. Taking advantage of an asymmetric environment created by carrying out transport measurements in an ionic medium with electrodes of considerably different areas, we are able to map the transmission function by simply performing conductance measurements over a range of source-drain biases. This removes the complications of needing additional electrodes and provides information about the transmission function without requiring knowledge of its functional form. We demonstrate this technique using two molecules which have resonances substantially far from E_F and two that have a molecular resonance accessible within the bias window. We find that as

the bias window approaches the resonance for one molecule, the junctions rupture while for the other, we are able to we pass the molecular resonance. In the latter case, we find that the current through the junction begins to decrease beyond the resonance. This implies that the line-shape of the transmission function is changed as the bias window approaches the molecular resonance. We hypothesize that this may occur due to increased electron-electron interactions as the highest occupied molecular orbital (HOMO) loses charge.

5.2 Results and Discussion

5.2.1 Single-Molecule Conductance Measurements

We study charge transport in single-molecule junctions using the scanning tunneling microscope based break junction (STM-BJ) technique. [2,4] Break junction measurements are carried out in a polar solvent (propylene carbonate, PC) using an Au tip insulated with Apiezon [70] wax in order to reduce any background electrochemical currents (schematic, Figure 5.1a). Conductance measurements are then performed by repeatedly driving the tip into and out of contact with the substrate; upon retracting the tip, the gold junction is thinned down to a single-atom contact, which subsequently ruptures and yields a sub-nanometer gap between two atomically sharp electrodes. When this process is repeated in the presence of molecules that are terminated with gold-binding groups, a single-molecule can bridge the gap and the conductance of the metal-molecule-metal junction can then be measured.

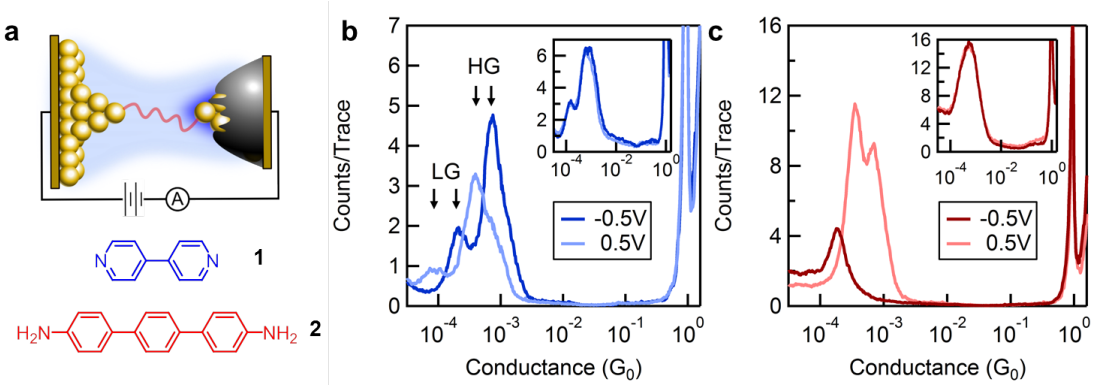

Figure 5.1: ***Break junction measurements in propylene carbonate.*** *(**a**) Schematic of molecular junction form with an insulated STM tip in an ionic environment. Molecular structures of 4,4-bipyridine (**1**) and 4,4-p-diaminoterphenyl (**2**). (**b**) Logarithmically binned histograms for **1** measured in propylene carbonate at -0.5V and 0.5V (tip relative to substrate). A clear difference in conductance for both LG and HG conductance features is observed, with higher conductances measured at the negative bias polarity. Inset are histograms measured at the same biases in phenyl octane; no difference in conductance is observed. (**c**) Same measurements performed in (**b**), but using molecule **2**. Again, in propylene carbonate different conductances are measured at the two polarities, but in phenyl octane (inset), the same conductances are observed. For this molecule, however, the higher conductance occurs at the positive tip polarity.*

We first measure the conductance of 4,4-bipyridine (**1**) and 4,4-p-diaminoterphenyl (**2**) under these conditions. Both are obtained from commercial sources (Sigma Aldrich and Alfa Aesar for **1** and **2**, respectively) and used without further purification. Measurements are compiled into logarithmically binned conductance histograms, which show peaks at molecule specific values. In Figure 5.1b, we show two histograms for **1** obtained when the tip is biased at +0.5V and -0.5V relative to the substrate. In both histograms, two conductance peaks are seen, which have been attributed to two distinct binding geometries for the molecule. The lower conductance (LG) corresponds to a fully elongated junction where the molecule is bound vertically between the Au electrodes through Au-N donor-acceptor bonds. The higher conductance (HG) corresponds to a tilted junction where there is an additional pi-coupling between the pyridine rings and the Au electrodes. [9, 182] For both junction geometries, there is a clear dependence on the conductance peak position with bias polarity, with a higher conductance observed at a negative applied bias. Such a

bias polarity-dependent conductance is only observed in the polar solvent. Measurements performed in 1-octylbenzene at +/-0.5V show no shift in the conductance peaks (see inset of Figure 5.1b). In Figure 5.1c, we show conductance histograms for **2** measured at +/ 0.5 V. We again see a clear shift in the conductance histogram peaks with bias polarity. We note that the conductance histogram for molecule **2** at +0.5 V in PC also displays a distinct double peak feature. Here, we attribute the second peak to a junction with two molecules in parallel as the higher conductance is almost exactly twice the lower one. Conductance histograms in PC are significantly narrower than their 1-octylbenzene counterparts, enabling the multi-molecule junctions to be resolved more clearly. For both one- and two-molecule junctions, the measured conductance is higher when the tip is biased positively relative to the substrate. Interestingly, the formation rate of two-molecule junctions (and indeed even of one molecule junctions) is greatly diminished at -0.5V. Again, this in contrast to measurements performed in 1-octylbenzene (inset Fig. 5.1c, which do not show any dependence on bias polarity.

5.2.2 Extracting the Transmission Function

We find that the bias polarity dependent conductance values that we have measured are in accord with our previous work [183] where we have shown that the conductance of a molecular junction, even one containing a symmetric molecule, in an ionic environment with electrodes of considerably different areas is dependent on both the magnitude and polarity of the applied bias. This occurs because of the formation of double layers at the solution/electrode interfaces. [64] The disparity in areas of the two electrodes yields a much denser double layer at the tip, which has a much smaller area exposed to the solvent. This dense double layer causes a bias polarity-dependent shift of the molecular junction resonance energy, leading to rectification. Considering a Landauer-like expression for current, and assuming coherent off-resonant tunneling through the junction and zero temperature, we have [55],

$$I = \frac{2e^2}{h} \int_{-eV/2}^{eV/2} T(E)dE \tag{5.1}$$

where e is the fundamental unit of charge, h is Plancks constant, V is the applied voltage and

$T(E)$ is the energy-dependent (E) transmission function for the junction. When the junction transmission is dominated by a single level that is equally coupled to both electrodes, $T(E)$ can be expressed as a Lorentzian of the form:

$$T(E) = \frac{\Gamma^2/4}{(E-\epsilon)^2 + \Gamma^2/4} \tag{5.2}$$

where ϵ is the position of dominant conducting orbital relative to the metal Fermi level and Γ the coupling of the molecular orbital to the electrodes. The bias-dependent environmental asymmetry can then be modeled by replacing the resonance energy ϵ in equation 5.2 with $(\epsilon + \alpha eV)$, where the parameter α describes the impact of the applied voltage on the resonance position, similar to that of a first-order Stark shift coefficient. With the strong asymmetry in the double layer density,(due to the large area mismatch between the tip and substrate) we find that α=0.5 in our measurements [183]. Within this picture, when the tip is biased negatively (positively) relative to the substrate, the molecular orbitals shift down (up) relative to E_F (i.e. the lowest unoccupied molecular orbital, LUMO (HOMO), nears E_F while HOMO (LUMO) moves further from E_F). We thus expect the conductance of a LUMO-dominated molecule, such as **1**, to increase as the tip becomes more negatively biased relative to the substrate, while we would expect the conductance of a HOMO-dominated molecule, such as **2**, to increase as the tip becomes more positively biased relative to the substrate.

We now take conductance measurements for **1** and **2** at tip bias voltages in intervals of 100mV (from -700mV to 500mV for **1** and from -500mV to 700mV for **2**, see conductance histograms in the Supplementary Information, SI, Fig. 5.5 and 5.6). We plot the peak conductance values versus applied voltage for the two molecules in Figures 5.2a and 5.2b. Negative biases yields higher conductance for **1** while positive biases yields higher conductance for **2**. From these measurements, we extract transmission values for the two molecules as a function of energy. We stress that the measured changes in conductance are due to measurements considering different regions of the transmission function, and that the extracted transmission values are not based on assuming a functional form for this transmission function. By making a change of variable (from E to $E' = E + eV/2$) and using α=0.5, equation 5.1 can be expressed as,

$$I = \frac{2e^2}{h} \int_0^{eV} T(E' - eV/2)dE' \tag{5.3}$$

Physically, the bias window is still opening symmetrically around E_F however, the mathematical formulation of equation 5.3 allows for the straightforward extraction of transmission function for a molecular junction as long as the transmission function does not change with applied bias. By performing measurements at regular intervals we can determine the current, and hence the transmission probability, for sufficiently small energy interval along the transmission function:

$$\frac{G(V_2) - G(V_1)}{V_2 - V_1} \approx T(\frac{E_2' + E_1'}{2}) \tag{5.4}$$

Using the conductance versus voltage data in Figures 5.2a and 5.2b, coupled with equation 5.4, we plot the extracted transmission values for molecules **1** and **2** in Figures 5.2c and 5.2d.

We compare our extracted transmission values with previously calculated DFT+Σ transmission functions from reference [18]. In Figure 5.2c, we overlay our transmission values with calculated transmission functions for both HG and LG geometries of molecule **1**, and find that the experimentally determined transmission values are slightly greater than the calculated transmission functions. For this system, it is also possible to approximate the transmission as a single-Lorentzian. [9, 18] When fitting the experimental data, the fitting parameters are also in good agreement with the values obtained from other methods. In Figure 5.2d, we overlay a calculated transmission function from reference [136] for molecule **2**; we again find excellent agreement between the measured transmission and the calculated function values. For two-molecule junctions, we divide the measured transmission values by 2 (accounting for two molecules in parallel, and assuming no cooperative effects) [184], and overlay these values on the one-molecule transmission data. Again, we find that the extracted transmission values are only slightly higher than the calculated transmission function. We also note that for molecule **2**, transmission cannot be approximated using a single-Lorentzian because of the presence of Au d-states at around -1.8 eV. [136]

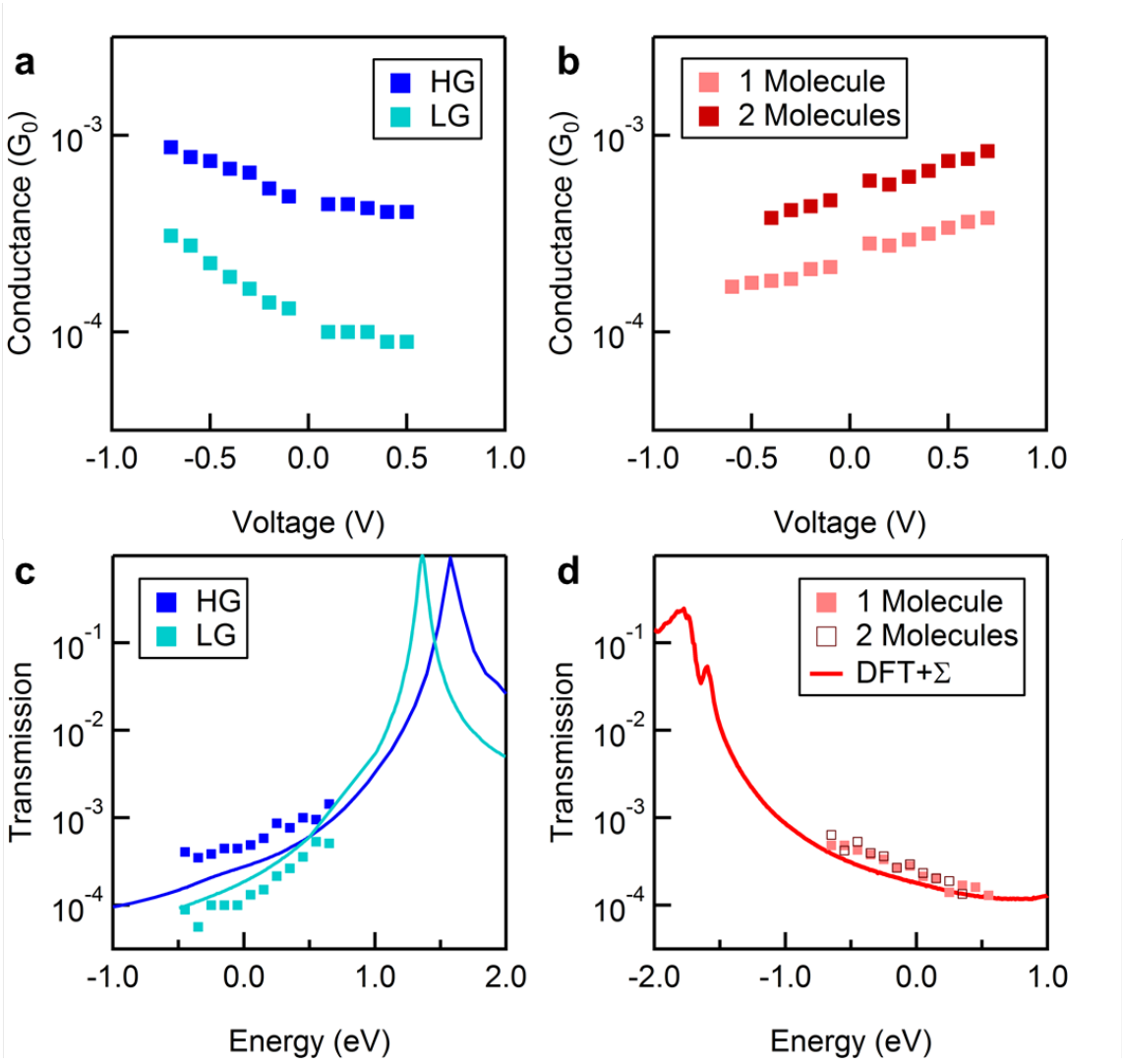

Figure 5.2: ***Extracting transmission for 4,4'-bipyridine and 4,4"-p-diaminoterphenyl.*** *(**a**) Peak conductance value versus applied voltage (tip relative to substrate) for low and high conductance states (LG and HG) for molecule **1**. The conductance increases with increasingly negative bias, indicating LUMO-dominated transport (**b**) Peak conductance value versus applied voltage for molecule **2**. Here, the conductance increases with increasingly positive bias, indicating HOMO-dominated transport.(**c**) Extracted transmission values for high and low conductance features (HG and LG, markers) for **1** along with DFT+Σ calculated transmission functions (adapted from reference [18]) for the two binding geometries (**d**) Extracted transmission values for one- and two-molecule junctions for **2** overlay a DFT+Σ calculated transmission function adapted from reference [136]. It can be seen that there is good agreement between calculated and measured values.*

5.2.3 Molecular Junctions near Resonance

Next, we can examine systems that have resonances located substantially closer to E_F than molecules **1** and **2**. For this, we turn to transport measurements on two small-gap thiophene-containing oligomers. Molecule **3** is composed of four thiophene dioxide (TDO) units flanked on either side by methyl-sulfide bearing thiophenes, while molecule **4** consists of a 3,4-ethylenedioxythiophene (EDOT) unit flanked by two thiophenes with the terminal thiophenes containing the gold-binding methyl sulfides (structures are inset in Figures 5.3a and 5.3b). We again perform conductance measurements at regular voltage intervals, and plot the resulting conductance values in Figures 5.3a and 5.3b (full conductance histograms can be found in the SI, Fig. 5.7 and 5.8). Examining the conductance behavior at different applied biases, we find that **3** has transport dominated by LUMO while **4** has transport dominated by HOMO. We further find that we are unable to form molecular junctions for molecule **3** when the voltage exceeds -0.4V, while for molecule **4**, when the voltage exceeds 0.8V, we find that the conductance begins to decrease with increasing bias.

In Figures 5.3c and 5.3d, we show transmission values extracted from the bias-dependent conductance values for **3** and **4**, respectively. Assuming a single-Lorentzian form for transmission, we find that **3** has a LUMO that is located only 0.42eV from E_F, while **4** has a HOMO that is located 0.75eV from E_F. This approximation has been shown to be reasonable for **3** [134, 183]. Given the high-lying HOMO of **4**, this approximation may also be reasonable since the HOMO will be much closer to E_F than the Au d-states at -1.8eV. As these ϵ values are well within our accessible source-drain bias range, we should be able to investigate resonant transport through molecules **3** and **4**. Interestingly, however, while molecule **3** no longer forms junctions when the applied voltage exceeds the estimated resonance position, molecule **4** continues to form junctions. We do note, however, that we clearly observe a decrease in the measured conductance as the applied bias exceeds +0.8V; we hypothesize that this decrease in conductance may be indicative of opening the bias window through a molecular resonance.

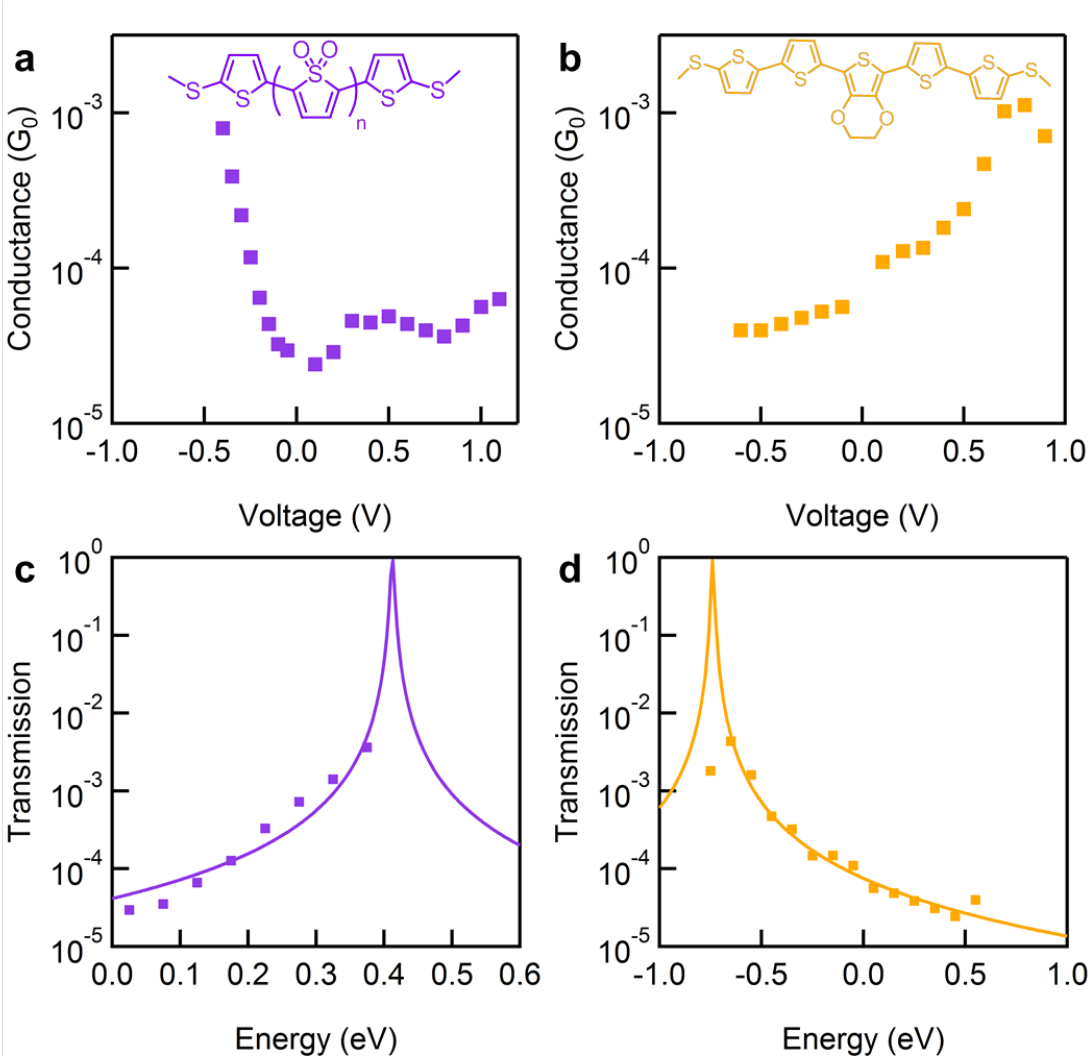

Figure 5.3: ***Extracting transmission for near resonant molecular junctions.*** *(**a**) Peak conductance value versus applied voltage (tip relative to substrate) for molecule **3** (molecular structure inset). (**b**) Peak conductance value versus applied voltage for molecule **4** (molecular structure inset).(**c**) and (**d**) are extracted transmission values for molecules **3** and **4**, respectively (markers). Overlaid curves are single-Lorentzian fits to the data.*

To further investigate the impact of the applied bias on the current across these junctions, we carry out current-voltage (IV) measurements on **3** and **4**. These are performed using a slightly modified break-junction procedure: the tip and substrate are pulled apart for 200ms at a speed of 16 nm/s, after which the tip-substrate distance is kept constant for 150ms. During this time, a voltage ramp is applied to the junction. The junction is

then pulled apart and broken. Since we are only interested in the behavior of the junction as the bias window approaches a molecular resonance, we only apply a negative voltage ramp for **3** (from 0V to -0.65V) and a positive voltage ramp for **4** (from 0 to 1.6V). We perform thousands of such measurements for each molecule, and analyze the IV data for junctions that start at a conductance that is representative of a molecular junction for the given molecule. Selected traces are then compiled into two-dimensional current vs. voltage histograms in Figure 5.4a and 5.4b for **3** and **4**, respectively. We also overlay an averaged current vs voltage trace that is determined by fitting a Gaussian function to each vertical line slice of the two dimensional histogram and plotting its peak value.

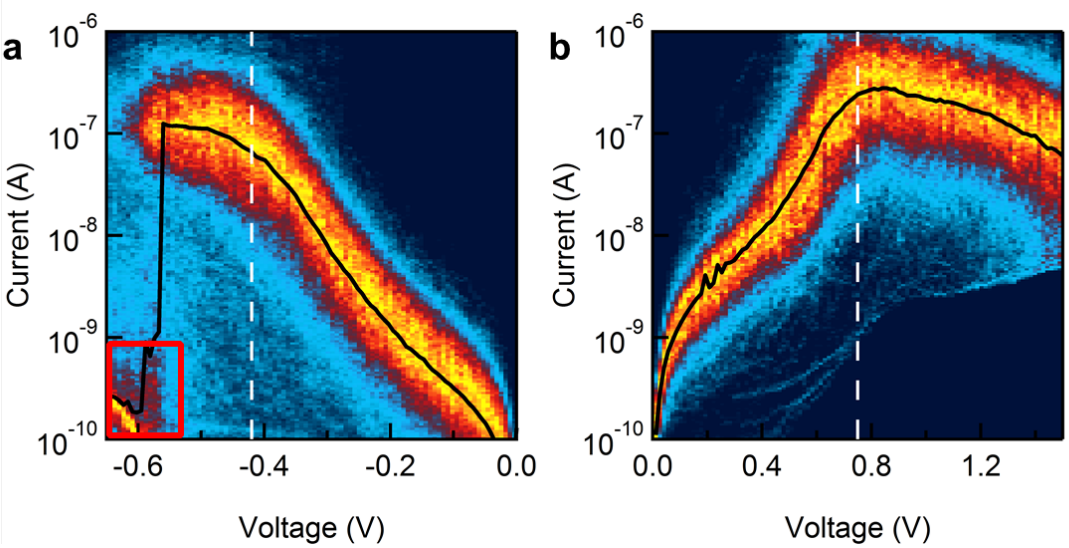

Figure 5.4: ***Approaching resonant transport in molecular junctions*** *(**a**) Two dimensional current-voltage (IV) histogram constructed from 1574 individual IV curves of molecule **3**. The dashed white line indicates the position of LUMO from conductance versus voltage measurements. It can be seen that molecular junctions always rupture beyond this point. The boxed area in the lower left hand corner shows background current present in junctions where the molecule-metal bond has ruptured. (**b**) Two-dimensional IV histogram constructed from 1147 IV curves of molecule **4**. The dashed white line again indicates the position of the molecular resonance, but in contrast to what is seen with molecule **3**, the junction persists when the applied voltage exceeds the molecular resonance position, and current is seen to now decrease with increasingly positive voltage.*

From these histograms, it is apparent that junctions with **3** rupture soon after the

bias window exceeds the estimated molecular resonance (Fig. 5.4a). A white dashed line is overlaid on the histogram to indicate the position of LUMO estimated from our transmission fit. When the applied bias exceeds this value, it can be seen that the measured current drops to instrumental noise. For molecule **4**, junctions persist even after the bias window exceeds the resonance position (again, indicated by a dashed white line). Indeed, for **4**, we find that the measured current begins to decrease as the bias window has exceeded the molecular resonance (Fig. 5.4b). In either case, as the molecular resonance enters the window between the chemical potentials of the two electrodes, substantial charging of the molecule occurs. For **3**, as the LUMO enters the bias window, it becomes partially occupied, leading to net negative charge on the molecule. For **4**, as the HOMO enters the bias window, it becomes partially unoccupied, yielding a net positive charge on the molecule. Since the orbitals responsible for transport become partially charged, one needs to consider the impact of electron-electron interactions on transport through these junctions. Given the size of these molecules, we estimate that the electrostatic charging energy is larger than the electronic coupling. From our single-Lorentzian fits, we find that $\Gamma \approx 5.3$meV for **3** and $\Gamma \approx 12.8$meV for **4**. We can estimate the charging energy, U, by first crudely approximating each molecule as a metal sphere with a radius equal to the length of the molecule. Then, the charging energy is equivalent to

$$U = \frac{e^2}{4\pi\epsilon_0 R} \tag{5.5}$$

where ϵ_0 is the permitivitty of free space and R is the length of the molecule. These U values are on the order of 1eV for **3** and **4**. Screening due to the leads in the junction will substantially reduce these values, but it is likely that U will still be larger than Γ.

The above discussion would imply that Coulomb blockade effects should be important, modifying the transmission function of the junction to one that includes the charging energy U. [185] In this case, the transmission function consists of two resonances peaked at e^2/h separated by a charging energy U. We would thus still expect an increase in current with bias voltage as we cross the first resonance and enter the blockaded region. However, this clearly is not what we observe in here. For **3**, we hypothesize that charging the molecule is responsible for rupturing the junction, perhaps because of strongly repulsive electrostatic

forces. For **4**, we find that the conductance decrease beyond the first resonance, which is at odds with the expected behavior for a transmission function with a bias independent line shape. We thus concluded that for **4**, the shape of the transmission must be altered as the bias is increased, leading to the experimentally measured trend.

5.3 Conclusions

We have presented a new, experimentally simple method for investigating the transmission function of a single-molecule junction. In addition to its simplicity, this method provides access to a large energetic region of the junction transmission function; in principle, this energy range should only be limited by the oxidation and reduction potentials of the solvent/electrode system with which the measurements are performed. This technique provides direct access to the transmission function, circumventing the need to *a priori* assume a functional form for transmission as has been done with thermopower measurements, AC measurements, and IV-fitting techniques. Given the control our method provides over level-alignment in the molecular junction, we are also able to drive charge transport into the resonant regime in junctions containing molecules with favorable initial level alignment. This opens up the exciting possibility to study transport phenomena associated with charged molecular conductors.

5.4 Supplementary Information

5.4.1 All Conductance Histograms

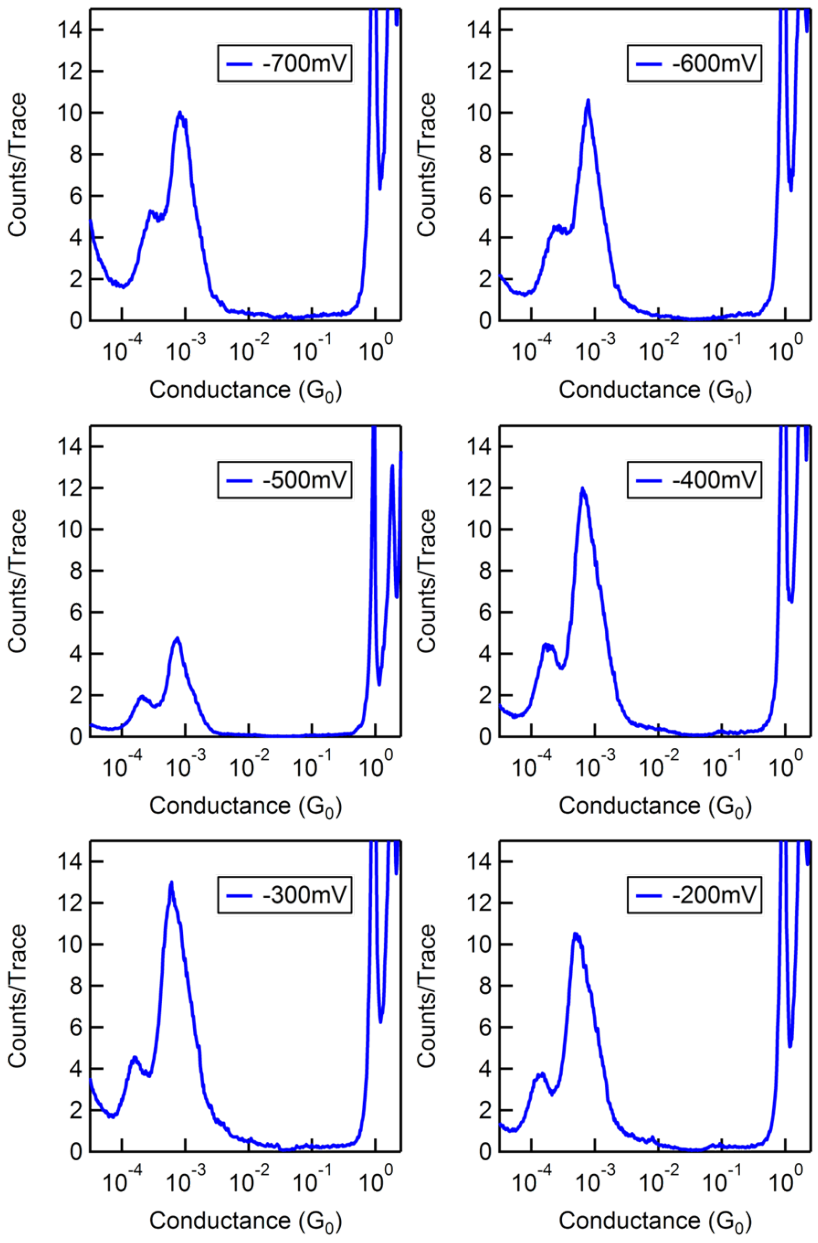

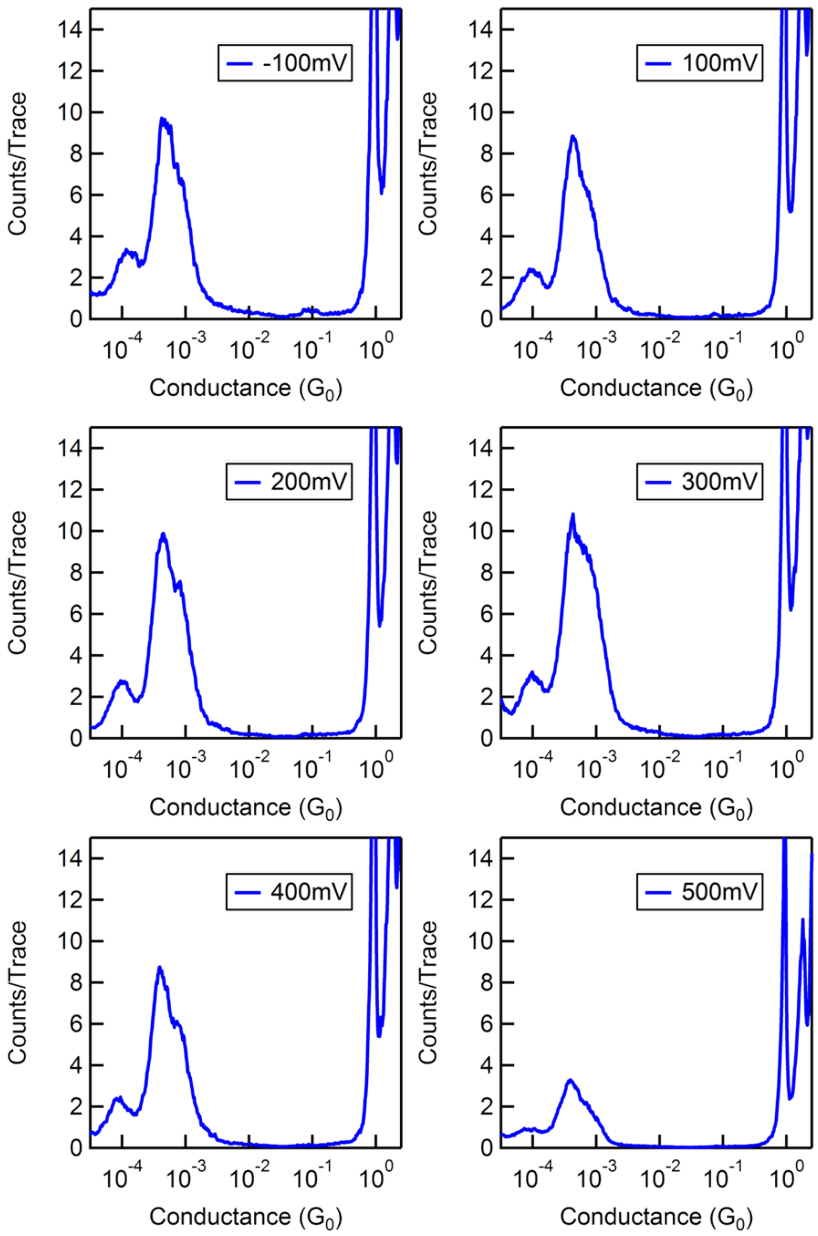

Figure 5.5: ***Conductance histograms for 1.*** *All logarithmically binned conductance histograms for molecule* ***1*** *at biases ranging from -700mV to 500mV in intervals of 100mV.*

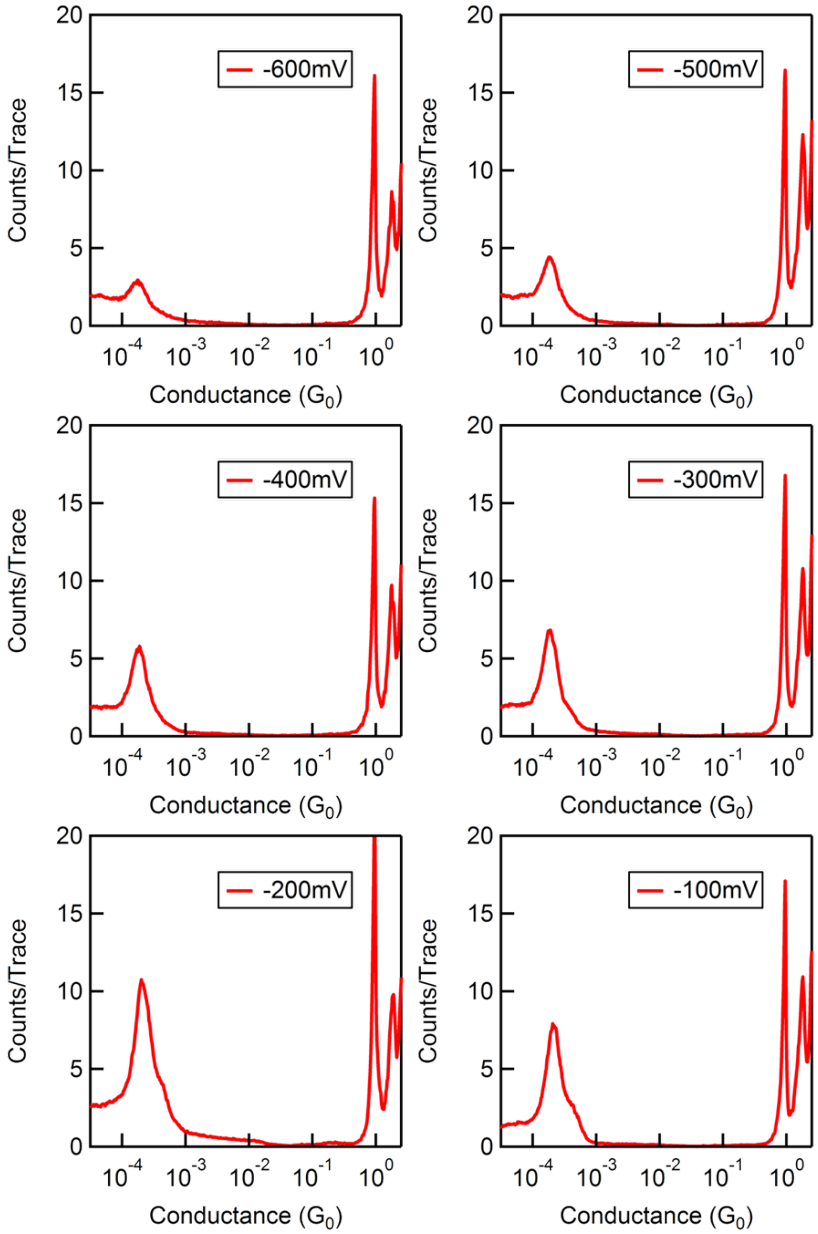
-600mV
-500mV
-400mV
-300mV
-200mV
-100mV
Counts/Trace
Conductance (G0)
0
5
10
15
20
10-4
10-3
10-2
10-1
100

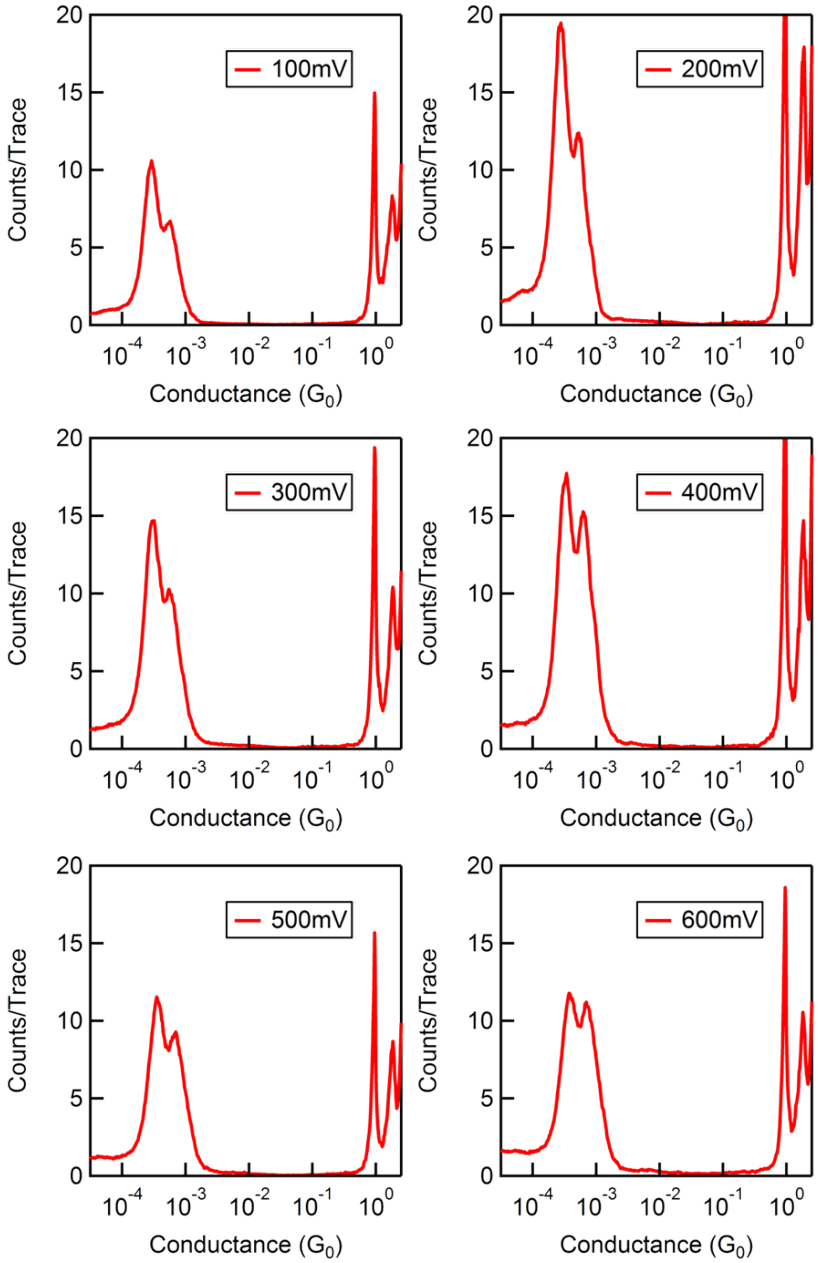
100mV
200mV
300mV
400mV
500mV
600mV
Counts/Trace
Conductance (G0)
0
5
10
15
20
10-4
10-3
10-2
10-1
100

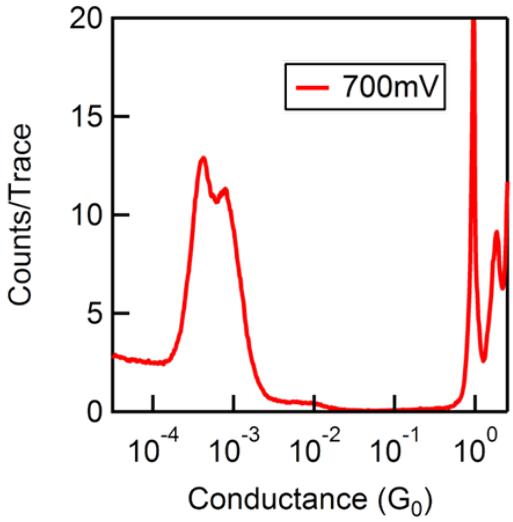

Figure 5.6: ***Conductance histograms for 2.*** *All logarithmically binned conductance histograms for molecule* ***2*** *at biases ranging from -600mV to 700mV in intervals of 100mV.*

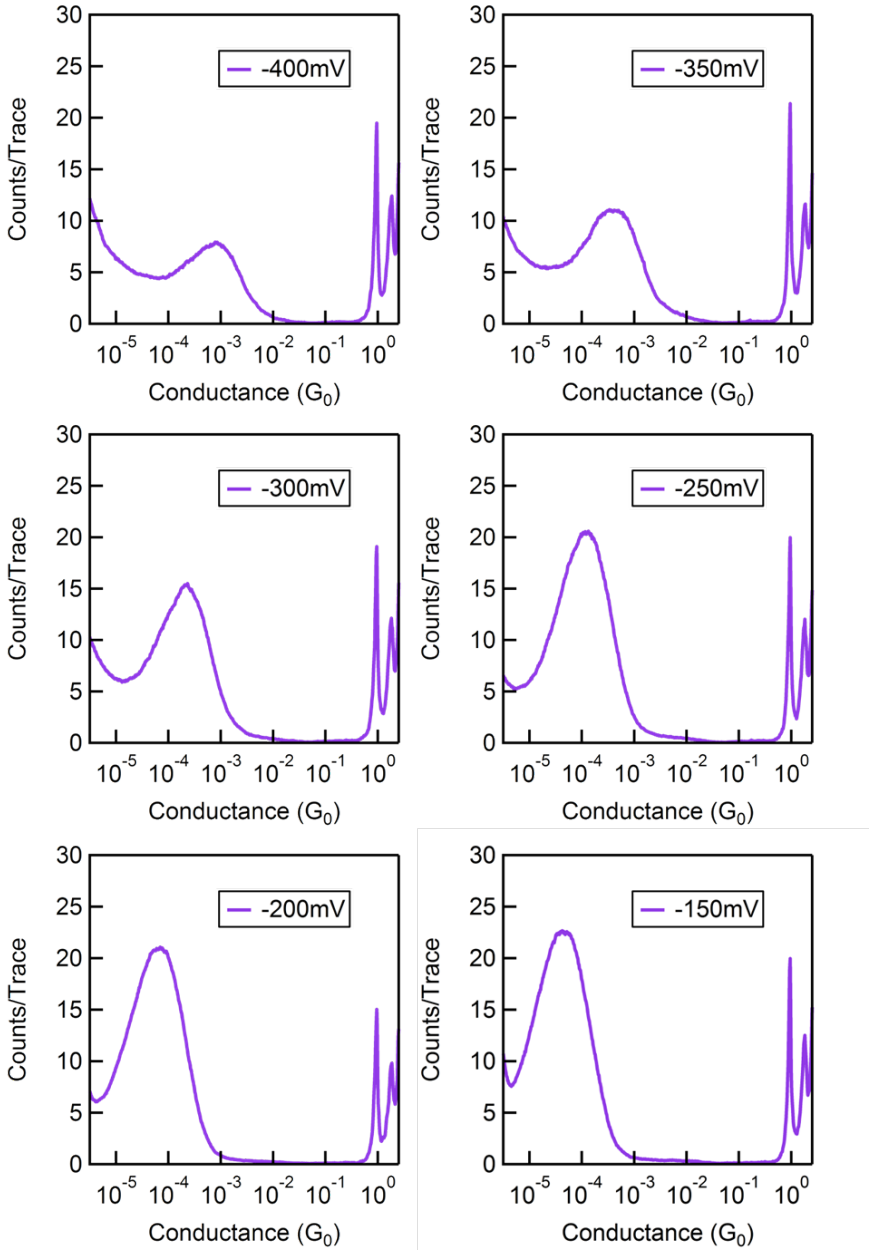
-400mV
-350mV
-300mV
-250mV
-200mV
-150mV
Counts/Trace
Conductance (G0)
0
5
10
15
20
25
30
10-5 10-4 10-3 10-2 10-1 100

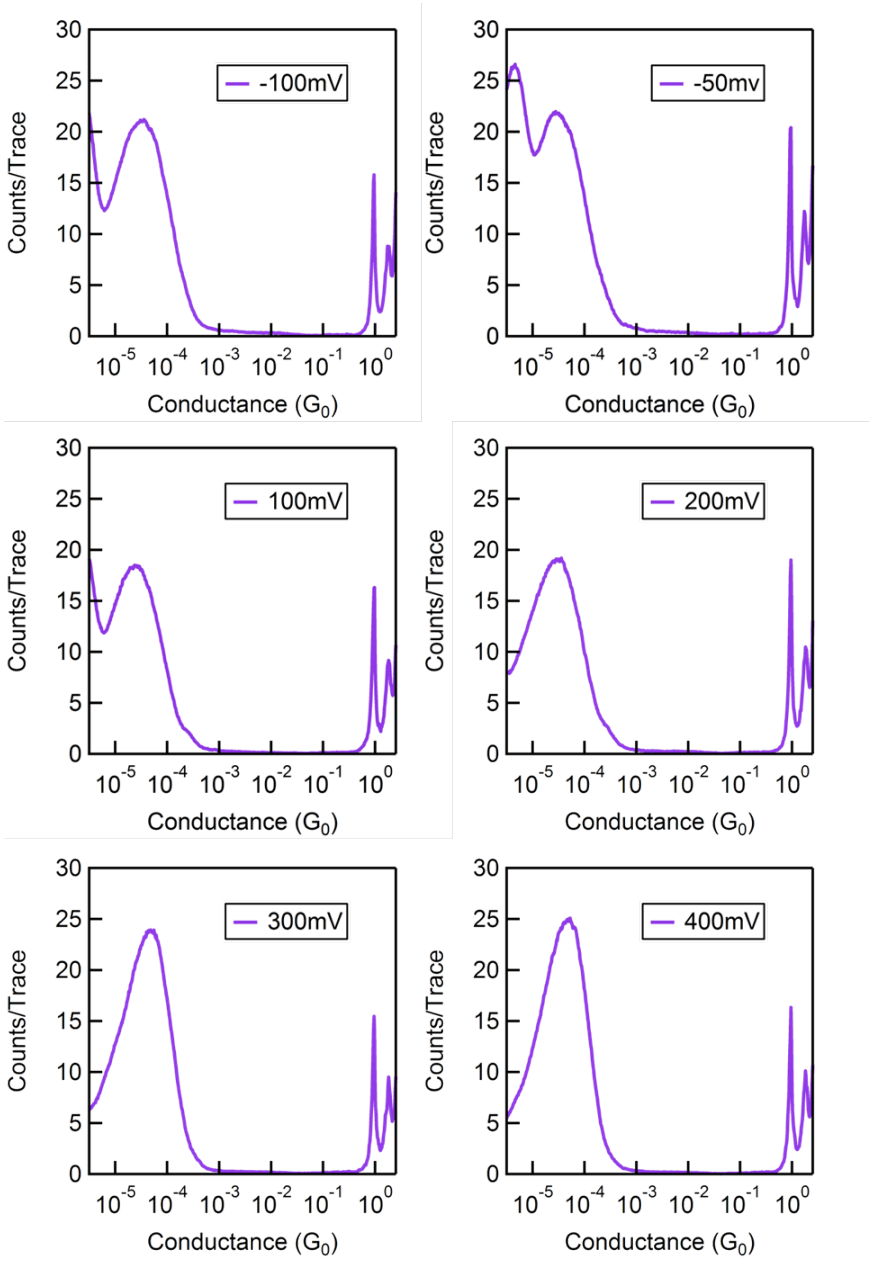
-100mV
-50mv
100mV
200mV
300mV
400mV
Counts/Trace
Conductance (G0)
0
5
10
15
20
25
30
10-5 10-4 10-3 10-2 10-1 100

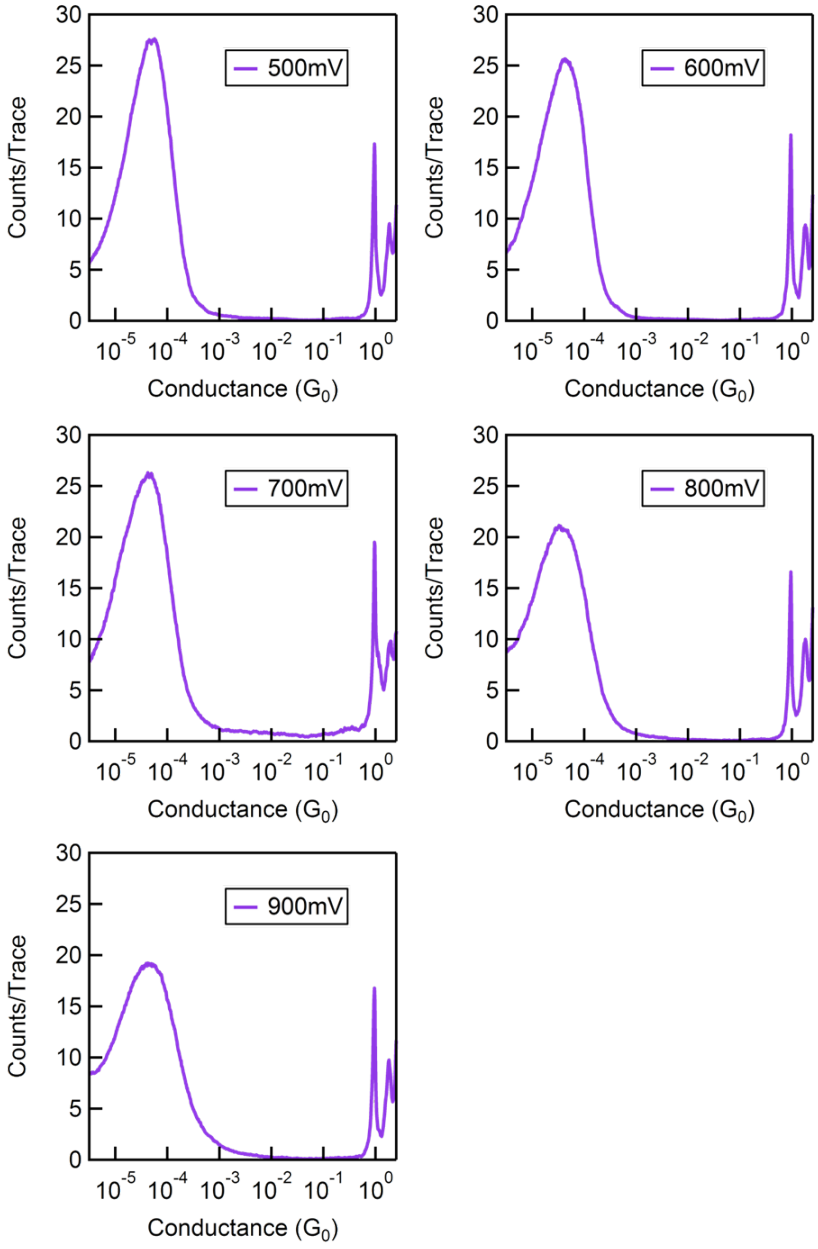

Figure 5.7: ***Conductance histograms for 3.*** *All logarithmically binned conductance histograms for molecule* ***3*** *at biases ranging from -400mV to 900mV.*

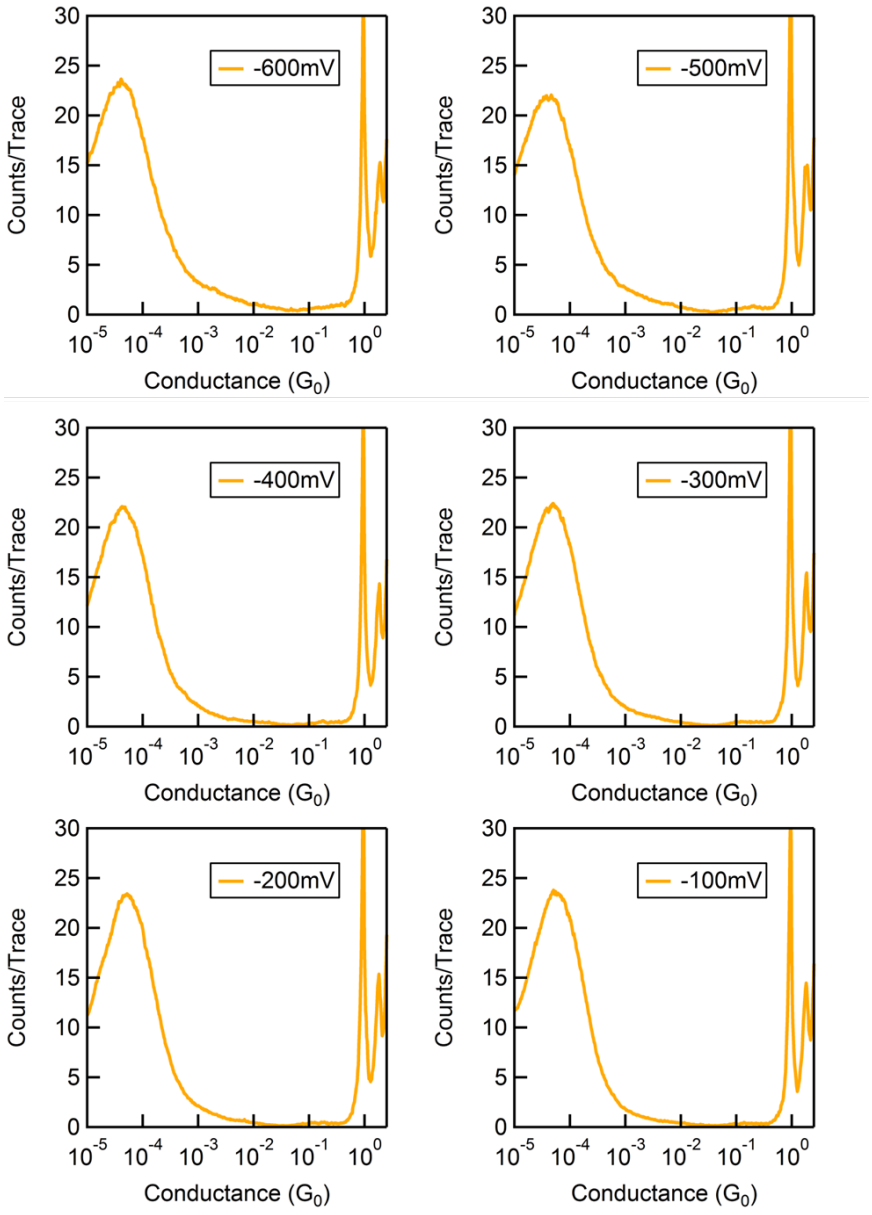
-600mV
-500mV
-400mV
-300mV
-200mV
-100mV
Counts/Trace
Conductance (G0)
0
5
10
15
20
25
30
10-5
10-4
10-3
10-2
10-1
100

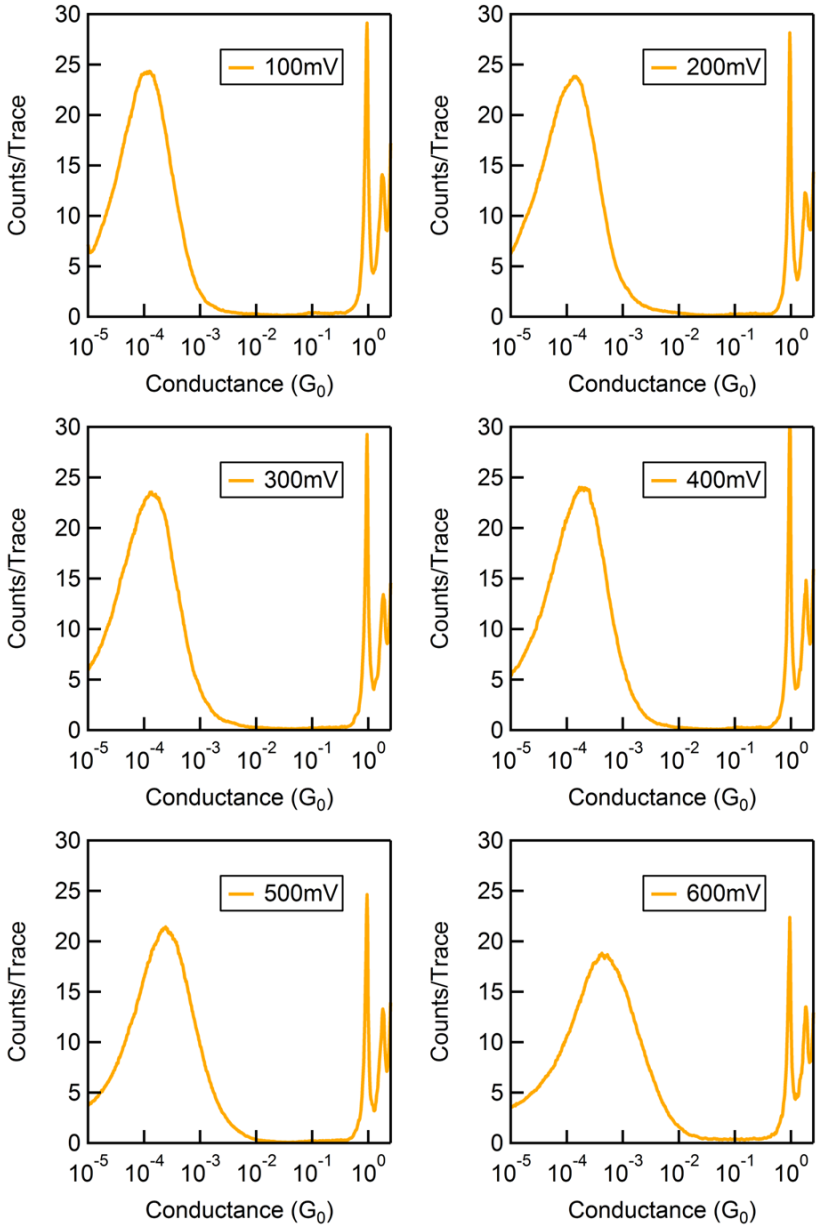
100mV
200mV
300mV
400mV
500mV
600mV
Counts/Trace
Conductance (G0)
0
5
10
15
20
25
30
10-5
10-4
10-3
10-2
10-1
100

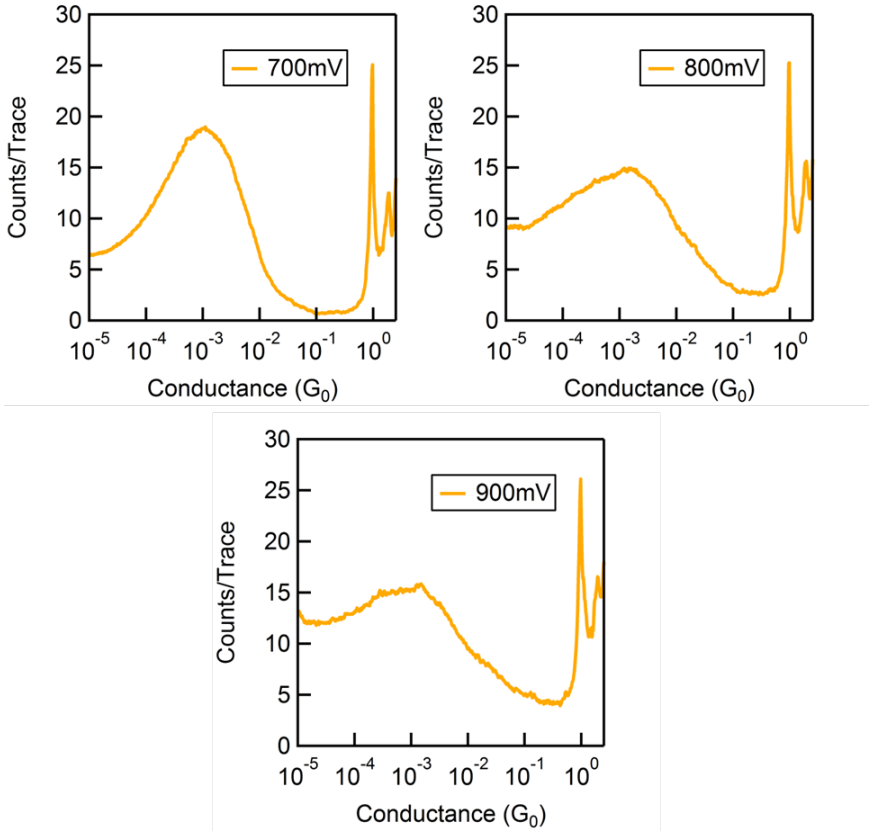

Figure 5.8: ***Conductance histograms for 4.*** *All logarithmically binned conductance histograms for molecule* ***4*** *at biases ranging from -600mV to 900mV in intervals of 100mV.*

Chapter 6

Conclusions and Outlook

6.1 Summary

This thesis has presented experimental studies detailing the manipulation of charge transport through a single-molecule junction by electrochemically controlling the junction's electrostatic environment. Through this work, we have shown the first gating of a non-redox active small-molecule junction, and have developed a novel method for creating a single-molecule diode. We have further been able to experimentally evaluate energy level alignment at metal-molecule interfaces, and have been able to probe large (2eV) regions of the transmission function which governs charge transport through the molecular junction; this has offered further insight into electronic structure of nanoscale devices.

We began by investigating two families of thiophene-based molecules with the intention of understanding how commonly used molecules in organic electronic devices conduct at the single-molecule level. We discovered that oligothiophenes are surprisingly poor candidates for single-molecule devices due to unfavorable conformational effects arising from their aromaticity and 5-fold symmetry. We found that a better class of molecules for single-molecule devices can be developed by oxidizing the thiophene unit, creating a thiophene dioxide unit. In studying these oxidized counterparts, we found an interesting family of molecules with high conductances, narrow conductance distributions, a shallow conductance decay with molecular length, and very narrow HOMO-LUMO gaps.

We next demonstrated gating functionality with the scanning tunneling microscope

break junction technique by incorporating a third electrode in an electrolytic solution. As ions in solution form compact double layers against charged metal electrodes, an applied voltage to the third electrode can be used to efficiently gate a single-molecule junction by altering the double layer density at the source and drain electrodes. We have shown the continuous modulation of the conductance of non-redox active molecules, and have shown that we can use this data to map the junction transmission function.

Removing the gate electrode and performing transport measurements in an electrolytic solution with source and drain electrodes of considerably different areas, we also found that we can induce rectification in otherwise symmetric molecular junctions. Due to the dissimilar areas of the electrodes, the double layer at the electrode with the smaller surface area is considerably denser, and therefore any applied bias preferentially impacts this electrode. This technique has general applications and results in current rectification in any molecular junction with a transmission function which is asymmetric about E_F. Coupling this technique with the small-gap oligothiophene dioxides, we created single-molecule diodes with the highest reported rectification ratios to date. We have found that this method provides a simple alternative to 3-electrode measurements for quantitatively investigating single-molecule junction transmission functions. Furthermore, this technique has allowed us to begin studying resonant transport, i.e. transport when a molecular orbital falls within the bias window, in molecular junctions.

6.2 Future Directions

While we have developed several methods for controlling the electrostatic environment surrounding a single-molecule junction, improvements can still be made. Gating measurements would greatly benefit from being performed with true electrochemical potential control. This would be accomplished by using a bipotentiostat, enabling accurate and independent control of the potentials of the tip and substrate electrodes relative to a reference electrode. The use of a bipotentiostat would enable complete control over the gating efficiency, and would provide no ambiguity in how much of the gate voltage impacted metal-molecule level alignment. Furthermore, utilizing a true reference electrode would allow for a more direct

comparison between orbital alignments determined via electrochemical measurements and via break junction measurements.

Measurements would also benefit from improvements to the tip insulation process. While Apiezon wax has worked well for the measurements presented here, its use is limited as it is readily dissolved by many polar organic solvents. This has restricted us to a narrow range of solvents, and having access to a greater variety would be beneficial. Furthermore, developing a method to enable more control over the electrode areas exposed to solution would allow us to further reduce background currents and enable measurements of lower conducting molecules.

With the approaches developed in this thesis, there are multiple directions for future studies. Being able to control the electrochemical potentials of the source and drain electrodes will allow for charge transport through charged single-molecule junctions to be studied. This charging can potentially happen in one of two ways. Molecules may possess orbitals which are decoupled to the leads, but which are energetically available to accept or donate a charge with gating. For this class of redox active molecules, we can hope to study the influence of an additional charge localized on the molecular backbone. Sometimes, redox events lead to drastic structural changes in the molecular backbone, allowing for the possibility of electrochemically enabled single-molecule switches. Alternatively, resonant charge transport can be studied in molecules which have a molecular orbital that is aligned near E_F and couples to the leads. Indeed, as discussed in Chapters 4 and 5, we have begun to investigate these types of systems and found several unexpected physical phenomena. Molecules which exhibit quantum interference effects (which suppress current and manifest as anti-resonances in transmission functions) may make interesting candidates for single-molecule diodes and transistors.

6.3 Complete List of Published Work

† indicates equal contributions

1. B. Capozzi, J. Z. Low, J. Xia, L. M. Campos, and L. Venkataraman, *Mapping the Transmission Function of a Single-Molecule Junction*, manuscript in preparation

2. B. Choi†, B. Capozzi†, S. Ahn, A. Turkiewicz, C. Nuckolls, M. L. Steigerwald, L. Venkataraman, X. Roy, *Solvent-Dependent Tunneling Decay Constants in Single Cluster Junctions*, submitted

3. B. Capozzi, J. Xia, O. Adak, E. Dell, Z. Liu, J.C. Taylor, J. B. Neaton, L. M. Campos and L. Venkataraman, *Single-Molecule Diodes with High Rectification Ratios through Environmental Control*, Nature Nanotechnology, in press.

4. E.J. Dell†, B. Capozzi†, J. Xia, L. Venkataraman, L. M. Campos, *Molecular Length Dictates the Nature of Charge Carriers in Single-Molecule Junctions*, Nature Chemistry, 7, 209214 (2015).

5. B. Capozzi†, E.J. Dell†, T.C. Berkelbach, D.R. Reichman, L. Venkataraman, L.M. Campos, *Length-Dependent Conductance of Oligothiophenes*, JACS, 136, 10486 (2014).

6. J. Xia†, B. Capozzi†, S. Wei, M. Strange, A. Batra, J. Moreno, R. Amir, E. Amir, G. Solomon, L. Venkataraman, L. Campos, *Breakdown of Interference Rules in Azulene, a Non-Alternant Hydrocarbon*, Nano Letters, 14, 29412945 (2014).

7. B. Capozzi, Q. Chen, P. Darancet, M. Buzzeo, J.B. Neaton, C. Nuckolls, L. Venkataraman, *Tunable Charge Transport in Single-Molecule Junctions via Electrolytic Gating*, Nano Letters, 14, 14001404 (2014).

8. E.J. Dell†, B. Capozzi†, K.H. DuBay, T.C. Berkelbach, J.R. Moreno, D.R. Reichman, L. Venkataraman, L.M. Campos, *Impact of Molecular Symmetry on Single-Molecule Conductance*, JACS, vol 135, p 11724-11727, (2013).

9. S. Ahn, S. V. Aradhya, R. S. Klausen, B. Capozzi, X. Roy, M. L. Steigerwald, C. Nuckolls, L. Venkataraman, *Electronic Transport and Mechanical Stability of Carboxyl Linked Single-Molecule Junctions* PCCP, 14, 1384113845, (2012).

Bibliography

[1] A. Aviram and M. A. Ratner, "Molecular rectifiers," *Chemical Physics Letters*, vol. 29, no. 2, pp. 277–283, 1974.

[2] B. Xu and N. J. Tao, "Measurement of single-molecule resistance by repeated formation of molecular junctions," *Science*, vol. 301, no. 5637, pp. 1221–1223, 2003.

[3] J. He, F. Chen, J. Li, O. F. Sankey, Y. Terazono, C. Herrero, D. Gust, T. A. Moore, A. L. Moore, and S. M. Lindsay, "Electronic decay constant of carotenoid polyenes from single-molecule measurements," *Journal of the American Chemical Society*, vol. 127, no. 5, pp. 1384–1385, 2005.

[4] L. Venkataraman, J. E. Klare, I. W. Tam, C. Nuckolls, M. S. Hybertsen, and M. L. Steigerwald, "Single-molecule circuits with well-defined molecular conductance," *Nano Letters*, vol. 6, no. 3, pp. 458–462, 2006.

[5] R. S. Klausen, J. R. Widawsky, M. L. Steigerwald, L. Venkataraman, and C. Nuckolls, "Conductive molecular silicon," *Journal of the American Chemical Society*, vol. 134, no. 10, pp. 4541–4544, 2012.

[6] P. Moreno-García, M. Gulcur, D. Z. Manrique, T. Pope, W. Hong, V. Kaliginedi, C. Huang, A. S. Batsanov, M. R. Bryce, C. Lambert, and T. Wandlowski, "Single-molecule conductance of functionalized oligoynes: Length dependence and junction evolution," *Journal of the American Chemical Society*, vol. 135, no. 33, pp. 12228–12240, 2013.

[7] F. Chen, J. He, C. Nuckolls, T. Roberts, J. E. Klare, and S. Lindsay, "A molecular switch based on potential-induced changes of oxidation state," *Nano Letters*, vol. 5, no. 3, pp. 503–506, 2005.

[8] P. Liljeroth, J. Repp, and G. Meyer, "Current-induced hydrogen tautomerization and conductance switching of naphthalocyanine molecules," *Science*, vol. 317, no. 5842, pp. 1203–1206, 2007.

[9] S. Y. Quek, M. Kamenetska, M. L. Steigerwald, H. J. Choi, S. G. Louie, M. S. Hybertsen, J. B. Neaton, and VenkataramanLatha, "Mechanically controlled binary conductance switching of a single-molecule junction," *Nat Nano*, vol. 4, no. 4, pp. 230–234, 2009.

[10] T. A. Su, H. Li, M. L. Steigerwald, L. Venkataraman, and C. Nuckolls, "Stereoelectronic switching in single-molecule junctions," *Nat Chem*, vol. 7, no. 3, pp. 215–220, 2015.

[11] E. Lörtscher, J. M. Tour, J. W. Ciszek, and H. Riel, "A single-molecule switch and memory element," *Journal of Physics: Conference Series*, vol. 61, no. 1, p. 987, 2007.

[12] M. Elbing, R. Ochs, M. Koentopp, M. Fischer, C. von Hnisch, F. Weigend, F. Evers, H. B. Weber, and M. Mayor, "A single-molecule diode," *Proceedings of the National Academy of Sciences of the United States of America*, vol. 102, no. 25, pp. 8815–8820, 2005.

[13] I. Díez-Pérez, J. Hihath, Y. Lee, L. Yu, L. Adamska, M. A. Kozhushner, I. I. Oleynik, and N. Tao, "Rectification and stability of a single molecular diode with controlled orientation," *Nat Chem*, vol. 1, no. 8, pp. 635–641, 2009.

[14] E. Lörtscher, B. Gotsmann, Y. Lee, L. Yu, C. Rettner, and H. Riel, "Transport properties of a single-molecule diode," *ACS Nano*, 2012.

[15] A. Batra, P. Darancet, Q. Chen, J. S. Meisner, J. R. Widawsky, J. B. Neaton, C. Nuckolls, and L. Venkataraman, "Tuning rectification in single-molecular diodes," *Nano Letters*, vol. 13, no. 12, pp. 6233–6237, 2013.

[16] H. Song, Y. Kim, Y. H. Jang, H. Jeong, M. A. Reed, and T. Lee, "Observation of molecular orbital gating," *Nature*, vol. 462, no. 7276, pp. 1039–43, 2009.

[17] M. L. Perrin, C. J. O. Verzijl, C. A. Martin, A. J. Shaikh, R. Eelkema, H. van EschJan, J. M. van Ruitenbeek, J. M. Thijssen, H. S. J. van der Zant, and D. Dulic, "Large tunable image-charge effects in single-molecule junctions," *Nat Nano*, vol. 8, no. 4, pp. 282–287, 2013.

[18] B. Capozzi, Q. Chen, P. Darancet, M. Kotiuga, M. Buzzeo, J. B. Neaton, C. Nuckolls, and L. Venkataraman, "Tunable charge transport in single-molecule junctions via electrolytic gating," *Nano Letters*, vol. 14, no. 3, pp. 1400–1404, 2014.

[19] R. J. Brooke, C. Jin, D. S. Szumski, R. J. Nichols, B.-W. Mao, K. S. Thygesen, and W. Schwarzacher, "Single-molecule electrochemical transistor utilizing a nickel-pyridyl spinterface," *Nano Letters*, vol. 15, no. 1, pp. 275–280, 2015.

[20] V. Kaliginedi, P. Moreno-García, H. Valkenier, W. Hong, V. M. García-Suárez, P. Buiter, J. L. H. Otten, J. C. Hummelen, C. J. Lambert, and T. Wandlowski, "Correlations between molecular structure and single-junction conductance: A case study with oligo(phenylene-ethynylene)-type wires," *Journal of the American Chemical Society*, vol. 134, no. 11, pp. 5262–5275, 2012.

[21] C. M. Guedon, H. Valkenier, T. Markussen, K. S. Thygesen, J. C. Hummelen, and S. J. van der Molen, "Observation of quantum interference in molecular charge transport," *Nat Nano*, vol. 7, no. 5, pp. 305–309, 2012. 10.1038/nnano.2012.37.

[22] J. Xia, B. Capozzi, S. Wei, M. Strange, A. Batra, J. R. Moreno, R. J. Amir, E. Amir, G. C. Solomon, L. Venkataraman, and L. M. Campos, "Breakdown of interference rules in azulene, a nonalternant hydrocarbon," *Nano Letters*, vol. 14, no. 5, pp. 2941–2945, 2014.

[23] J. Park, A. N. Pasupathy, J. I. Goldsmith, C. Chang, Y. Yaish, J. R. Petta, M. Rinkoski, J. P. Sethna, H. D. Abruna, P. L. McEuen, and D. C. Ralph, "Coulomb blockade and the kondo effect in single-atom transistors," *Nature*, vol. 417, no. 6890, pp. 722–5, 2002.

[24] L. H. Yu, Z. K. Keane, J. W. Ciszek, L. Cheng, M. P. Stewart, J. M. Tour, and D. Natelson, "Inelastic electron tunneling via molecular vibrations in single-molecule transistors," *Phys. Rev. Lett.*, vol. 93, p. 266802, Dec 2004.

[25] L. H. Yu and D. Natelson, "The kondo effect in c60 single-molecule transistors," *Nano Letters*, vol. 4, no. 1, pp. 79–83, 2004.

[26] W. Liang, M. P. Shores, M. Bockrath, J. R. Long, and H. Park, "Kondo resonance in a single-molecule transistor," *Nature*, vol. 417, no. 6890, pp. 725–729, 2002.

[27] J. J. Parks, A. R. Champagne, G. R. Hutchison, S. Flores-Torres, H. D. Abruña, and D. C. Ralph, "Tuning the kondo effect with a mechanically controllable break junction," *Phys. Rev. Lett.*, vol. 99, p. 026601, Jul 2007.

[28] S. Wagner, F. Kisslinger, S. Ballmann, F. Schramm, R. Chandrasekar, T. Bodenstein, O. Fuhr, D. Secker, K. Fink, M. Ruben, and H. B. Weber, "Switching of a coupled spin pair in a single-molecule junction," *Nat Nano*, vol. 8, no. 8, pp. 575–579, 2013.

[29] D. Rakhmilevitch, R. Korytár, A. Bagrets, F. Evers, and O. Tal, "Electron-vibration interaction in the presence of a switchable kondo resonance realized in a molecular junction," *Phys. Rev. Lett.*, vol. 113, p. 236603, Dec 2014.

[30] H. Kroemer, "Quasi-electric fields and band offsets: Teaching electrons new tricks (nobel lecture)," *ChemPhysChem*, vol. 2, no. 8-9, pp. 490–499, 2001.

[31] Y. S. Park, A. C. Whalley, M. Kamenetska, M. L. Steigerwald, M. S. Hybertsen, C. Nuckolls, and L. Venkataraman, "Contact chemistry and single-molecule conductance: A comparison of phosphines, methyl sulfides, and amines," *Journal of the American Chemical Society*, vol. 129, no. 51, pp. 15768–15769, 2007.

[32] Z. L. Cheng, R. Skouta, H. Vázquez, J. R. Widawsky, S. Schneebeli, W. Chen, M. S. Hybertsen, R. Breslow, and L. Venkataraman, "In situ formation of highly conducting covalent au-c contacts for single-molecule junctions," *Nat Nano*, vol. 6, no. 6, pp. 353–357, 2011.

[33] H. Park, A. K. L. Lim, A. P. Alivisatos, J. Park, and P. L. McEuen, "Fabrication of metallic electrodes with nanometer separation by electromigration," *Applied Physics Letters*, vol. 75, no. 2, pp. 301–303, 1999.

[34] D. R. Ward, G. D. Scott, Z. K. Keane, N. J. Halas, and D. Natelson, "Electronic and optical properties of electromigrated molecular junctions," *Journal of Physics: Condensed Matter*, vol. 20, no. 37, p. 374118, 2008.

[35] R. H. M. Smit, Y. Noat, C. Untiedt, N. D. Lang, M. C. van Hemert, and J. M. van Ruitenbeek, "Measurement of the conductance of a hydrogen molecule," *Nature*, vol. 419, no. 6910, pp. 906–909, 2002. 10.1038/nature01103.

[36] L. Venkataraman, J. E. Klare, C. Nuckolls, M. S. Hybertsen, and M. L. Steigerwald, "Dependence of single-molecule junction conductance on molecular conformation," *Nature*, vol. 442, no. 7105, pp. 904–907, 2006.

[37] C. Muller, J. van Ruitenbeek, and L. de Jongh, "Experimental observation of the transition from weak link to tunnel junction," *Physica C: Superconductivity*, vol. 191, no. 34, pp. 485 – 504, 1992.

[38] M. A. Reed, C. Zhou, C. J. Muller, T. P. Burgin, and J. M. Tour, "Conductance of a molecular junction," *Science*, vol. 278, no. 5336, pp. 252–254, 1997.

[39] B. Xu, X. Xiao, and N. J. Tao, "Measurements of single-molecule electromechanical properties," *Journal of the American Chemical Society*, vol. 125, no. 52, pp. 16164–16165, 2003.

[40] M. Frei, S. V. Aradhya, M. Koentopp, M. S. Hybertsen, and L. Venkataraman, "Mechanics and chemistry: Single molecule bond rupture forces correlate with molecular backbone structure," *Nano Letters*, vol. 11, no. 4, pp. 1518–1523, 2011.

[41] P. Reddy, S. Y. Jang, R. A. Segalman, and A. Majumdar, "Thermoelectricity in molecular junctions," *Science*, vol. 315, pp. 1568–1571, 2007.

[42] J. R. Widawsky, P. Darancet, J. B. Neaton, and L. Venkataraman, "Simultaneous determination of conductance and thermopower of single molecule junctions," *Nano Letters*, vol. 12, no. 1, pp. 354–358, 2011.

[43] Y. Kim, W. Jeong, K. Kim, W. Lee, and P. Reddy, "Electrostatic control of thermoelectricity in molecular junctions," *Nat Nano*, vol. 9, pp. 881–885, 11 2014.

[44] R. Yamada, M. Noguchi, and H. Tada, "Magnetoresistance of single molecular junctions measured by a mechanically controllable break junction method," *Applied Physics Letters*, vol. 98, no. 5, pp. 053110–3, 2011.

[45] Z. Liu, S.-Y. Ding, Z.-B. Chen, X. Wang, J.-H. Tian, J. R. Anema, X.-S. Zhou, D.-Y. Wu, B.-W. Mao, X. Xu, B. Ren, and Z.-Q. Tian, "Revealing the molecular structure of single-molecule junctions in different conductance states by fishing-mode tip-enhanced raman spectroscopy," *Nat Commun*, vol. 2, p. 305, 2011. 10.1038/ncomms1310.

[46] N. Agraït, A. L. Yeyati, and J. M. van Ruitenbeek, "Quantum properties of atomic-sized conductors," *Physics Reports*, vol. 377, no. 23, pp. 81 – 279, 2003.

[47] Z. Gai, Y. He, H. Yu, and W. S. Yang, "Observation of conductance quantization of ballistic metallic point contacts at room temperature," *Phys. Rev. B*, vol. 53, pp. 1042–1045, Jan 1996.

[48] J. L. Costa-Krämer, "Conductance quantization at room temperature in magnetic and nonmagnetic metallic nanowires," *Physical Review B*, vol. 55, no. 8, pp. R4875–R4878, 1997.

[49] J. L. Costa-Krämer, N. García, and H. Olin, "Conductance quantization histograms of gold nanowires at 4 k," *Phys. Rev. B*, vol. 55, pp. 12910–12913, May 1997.

[50] M. T. González, S. Wu, R. Huber, S. J. van der Molen, C. Schnenberger, and M. Calame, "Electrical conductance of molecular junctions by a robust statistical analysis," *Nano Letters*, vol. 6, no. 10, pp. 2238–2242, 2006.

[51] M. Burkle, J. K. Viljas, D. Vonlanthen, A. Mishchenko, G. Schön, M. Mayor, T. Wandlowski, and F. Pauly, "Conduction mechanisms in biphenyl dithiol single-molecule junctions," *Phys. Rev. B*, vol. 85, p. 075417, Feb 2012.

[52] E. J. Dell, B. Capozzi, K. H. DuBay, T. C. Berkelbach, J. R. Moreno, D. R. Reichman, L. Venkataraman, and L. M. Campos, "Impact of molecular symmetry on single-molecule conductance," *Journal of the American Chemical Society*, vol. 135, no. 32, pp. 11724–11727, 2013.

[53] M. Kamenetska, M. Koentopp, A. C. Whalley, Y. S. Park, M. L. Steigerwald, C. Nuckolls, M. S. Hybertsen, and L. Venkataraman, "Formation and evolution of single-molecule junctions," *Physical Review Letters*, vol. 102, no. 12, p. 126803, 2009.

[54] V. Fatemi, M. Kamenetska, J. B. Neaton, and L. Venkataraman, "Environmental control of single-molecule junction transport," *Nano Letters*, vol. 11, no. 5, pp. 1988–1992, 2011.

[55] S. Datta, *Electronic Transport in Mesoscopic Systems*. Cambridge Studies in Semiconductor Physics and Microelectronic Engineering, Untied Kingdom: Cambridge University Press, 1995.

[56] R. Landauer, "Spatial variation of currents and fields due to localized scatterers in metallic conduction," *IBM Journal of Research and Development*, vol. 44, pp. 251–259, Jan 2000.

[57] M. Paulsson and S. Datta, "Thermoelectric effect in molecular electronics," *Phys. Rev. B*, vol. 67, p. 241403, 2003.

[58] U. Peskin, "An introduction to the formulation of steady-state transport through molecular junctions," *Journal of Physics B: Atomic, Molecular and Optical Physics*, vol. 43, no. 15, p. 153001, 2010.

[59] J. B. Neaton, M. S. Hybertsen, and S. G. Louie, "Renormalization of molecular electronic levels at metal-molecule interfaces," *Physical Review Letters*, vol. 97, no. 21, p. 216405, 2006.

[60] S. Y. Quek, H. J. Choi, S. G. Louie, and J. B. Neaton, "Length dependence of conductance in aromatic single-molecule junctions," *Nano Letters*, vol. 9, no. 11, pp. 3949–3953, 2009.

[61] N. Ashcroft and N. Mermin, *Solid State Physics*. Philadelphia: Saunders College, 1976.

[62] M. X. Tan, P. E. Laibinis, S. T. Nguyen, J. M. Kesselman, C. E. Stanton, and N. S. Lewis, *Principles and Applications of Semiconductor Photoelectrochemistry*, pp. 21–144. John Wiley and Sons, Inc., 2007.

[63] J. Bockris and A. Reddy, *Modern Electrochemistry*. No. v. 2, pt. 1 in Modern Electrochemistry, Plenum Press, 1998.

[64] L. R. F. Bard, A. J., *Electrochemical Methods: Theory and Applications*. United States: Wiley, 2001.

[65] S. F. Nelsen, "Ionization potential, oxidation potential comparisons for compounds containing amino nitrogen," *Israel Journal of Chemistry*, vol. 18, no. 1-2, pp. 45–55, 1979.

[66] B. W. DAndrade, S. Datta, S. R. Forrest, P. Djurovich, E. Polikarpov, and M. E. Thompson, "Relationship between the ionization and oxidation potentials of molecular organic semiconductors," *Organic Electronics*, vol. 6, no. 1, pp. 11–20, 2005.

[67] M. J. Panzer and C. D. Frisbie, "Exploiting ionic coupling in electronic devices: Electrolyte-gated organic field-effect transistors," *Advanced Materials*, vol. 20, no. 16, pp. 3177–3180, 2008.

[68] S. H. Kim, K. Hong, W. Xie, K. H. Lee, S. Zhang, T. P. Lodge, and C. D. Frisbie, "Electrolyte-gated transistors for organic and printed electronics," *Advanced Materials*, vol. 25, no. 13, pp. 1822–1846, 2013.

[69] L. Kergoat, L. Herlogsson, B. Piro, M. C. Pham, G. Horowitz, X. Crispin, and M. Berggren, "Tuning the threshold voltage in electrolyte-gated organic field-effect

transistors," *Proceedings of the National Academy of Sciences*, vol. 109, no. 22, pp. 8394–8399, 2012.

[70] L. A. Nagahara, T. Thundat, and S. M. Lindsay, "Preparation and characterization of stm tips for electrochemical studies," *Review of Scientific Instruments*, vol. 60, no. 10, pp. 3128–3130, 1989.

[71] I. F. Perepichka and D. F. Perepichka, *Handbook of thiophene-based materials : applications in organic electronics and photonics*. Chichester, U.K.: Wiley, 2009.

[72] G. Dennler, M. C. Scharber, and C. J. Brabec, "Polymer-fullerene bulk-heterojunction solar cells," *Advanced Materials*, vol. 21, no. 13, pp. 1323–1338, 2009.

[73] H. Sirringhaus, N. Tessler, and R. H. Friend, "Integrated optoelectronic devices based on conjugated polymers," *Science*, vol. 280, no. 5370, pp. 1741–1744, 1998.

[74] H. Sirringhaus, P. J. Brown, R. H. Friend, M. M. Nielsen, K. Bechgaard, B. M. W. Langeveld-Voss, A. J. H. Spiering, R. A. J. Janssen, E. W. Meijer, P. Herwig, and D. M. de Leeuw, "Two-dimensional charge transport in self-organized, high-mobility conjugated polymers," *Nature*, vol. 401, no. 6754, pp. 685–688, 1999.

[75] J. Roncali, "Conjugated poly(thiophenes) - synthesis, functionalization, and applications," *Chemical Reviews*, vol. 92, no. 4, pp. 711–738, 1992.

[76] N. D. Treat, L. M. Campos, M. D. Dimitriou, B. Ma, M. L. Chabinyc, and C. J. Hawker, "Nanostructured hybrid solar cells: Dependence of the open circuit voltage on the interfacial composition," *Advanced Materials*, vol. 22, no. 44, pp. 4982–4986, 2010.

[77] Z. B. Henson, K. Mullen, and G. C. Bazan, "Design strategies for organic semiconductors beyond the molecular formula," *Nature Chem.*, vol. 4, pp. 699–704, 2012.

[78] L. Zhang, N. S. Colella, F. Liu, S. Trahan, J. K. Baral, H. H. Winter, S. C. B. Mannsfeld, and A. L. Briseno, "Synthesis, electronic structure,

molecular packing/morphology evolution, and carrier mobilities of pure oligo-/poly(alkylthiophenes)," *Journal of the American Chemical Society*, vol. 135, no. 2, pp. 844–854, 2012.

[79] F. P. V. Koch, M. Heeney, and P. Smith, "Thermal and structural characteristics of oligo(3-hexylthiophene)s (3ht)n, n = 436," *Journal of the American Chemical Society*, vol. 135, no. 37, pp. 13699–13709, 2013.

[80] B. Q. Xu, X. L. Li, X. Y. Xiao, H. Sakaguchi, and N. J. Tao, "Electromechanical and conductance switching properties of single oligothiophene molecules," *Nano Letters*, vol. 5, no. 7, pp. 1491–1495, 2005.

[81] R. Yamada, H. Kumazawa, T. Noutoshi, S. Tanaka, and H. Tada, "Electrical conductance of oligothiophene molecular wires," *Nano Letters*, vol. 8, no. 4, pp. 1237–1240, 2008.

[82] E. Leary, H. Hbenreich, S. J. Higgins, H. van Zalinge, W. Haiss, R. J. Nichols, C. M. Finch, I. Grace, C. J. Lambert, R. McGrath, and J. Smerdon, "Single-molecule solvation-shell sensing," *Physical Review Letters*, vol. 102, no. 8, p. 086801, 2009.

[83] Y. Le, M. Endou, S. K. Lee, R. Yamada, H. Tada, and Y. Aso, "Completely encapsulated oligothiophenes: Synthesis, properties, and single-molecule conductance," *Angewandte Chemie-International Edition*, vol. 50, no. 50, pp. 11980–11984, 2011.

[84] S. K. Lee, R. Yamada, S. Tanaka, G. S. Chang, Y. Asai, and H. Tada, "Universal temperature crossover behavior of electrical conductance in a single oligothiophene molecular wire," *Acs Nano*, vol. 6, no. 6, pp. 5078–5082, 2012.

[85] S. Gélinas, A. Rao, A. Kumar, S. L. Smith, A. W. Chin, J. Clark, T. S. van der Poll, G. C. Bazan, and R. H. Friend, "Ultrafast long-range charge separation in organic semiconductor photovoltaic diodes," *Science*, vol. 343, no. 6170, pp. 512–516, 2014.

[86] J.-L. Brédas, J. E. Norton, J. Cornil, and V. Coropceanu, "Molecular understanding of organic solar cells: The challenges," *Accounts of Chemical Research*, vol. 42, no. 11, pp. 1691–1699, 2009.

[87] V. B. Engelkes, J. M. Beebe, and C. D. Frisbie, "Length-dependent transport in molecular junctions based on sams of alkanethiols and alkanedithiols: Effect of metal work function and applied bias on tunneling efficiency and contact resistance," *Journal of the American Chemical Society*, vol. 126, no. 43, pp. 14287–14296, 2004.

[88] W. Chen, J. R. Widawsky, H. Vázquez, S. T. Schneebeli, M. S. Hybertsen, R. Breslow, and L. Venkataraman, "Highly conducting -conjugated molecular junctions covalently bonded to gold electrodes," *Journal of the American Chemical Society*, vol. 133, no. 43, pp. 17160–17163, 2011.

[89] J. S. Meisner, M. Kamenetska, M. Krikorian, M. L. Steigerwald, L. Venkataraman, and C. Nuckolls, "A single-molecule potentiometer," *Nano Letters*, vol. 11, no. 4, pp. 1575–1579, 2011.

[90] C. Li, A. Mishchenko, Z. Li, I. Pobelov, W. Th, X. Q. Li, F. Wrthner, A. Bagrets, and F. Evers, "Electrochemical gate-controlled electron transport of redox-active single perylene bisimide molecular junctions," *Journal of Physics: Condensed Matter*, vol. 20, no. 37, p. 374122, 2008.

[91] J. M. Beebe, V. B. Engelkes, L. L. Miller, and C. D. Frisbie, "Contact resistance in metal-molecule-metal junctions based on aliphatic sams: Effects of surface linker and metal work function," *Journal of the American Chemical Society*, vol. 124, no. 38, pp. 11268–11269, 2002.

[92] M. S. Hybertsen, L. Venkataraman, J. E. Klare, A. C. Whalley, M. L. Steigerwald, and C. Nuckolls, "Amine-linked single-molecule circuits: systematic trends across molecular families," *Journal of Physics: Condensed Matter*, vol. 20, no. 37, p. 374115, 2008.

[93] H. B. Akkerman and B. de Boer, "Electrical conduction through single molecules and self-assembled monolayers," *Journal of Physics: Condensed Matter*, vol. 20, no. 1, p. 013001, 2008.

[94] A. Salomon, D. Cahen, S. Lindsay, J. Tomfohr, V. B. Engelkes, and C. D. Frisbie, "Comparison of electronic transport measurements on organic molecules," *Advanced Materials*, vol. 15, no. 22, pp. 1881–1890, 2003.

[95] W. B. Davis, W. A. Svec, M. A. Ratner, and M. R. Wasielewski, "Molecular-wire behaviour in p-phenylenevinylene oligomers," *Nature*, vol. 396, no. 6706, pp. 60–63, 1998.

[96] M. D. Curtis, J. Cao, and J. W. Kampf, "Solid-state packing of conjugated oligomers: from pi-stacks to the herringbone structure," *Journal of the American Chemical Society*, vol. 126, no. 13, pp. 4318–4328, 2004.

[97] G. Horowitz, B. Bachet, A. Yassar, P. Lang, F. Demanze, J. L. Fave, and F. Garnier, "Growth and characterization of sexithiophene single-crystals," *Chemistry of Materials*, vol. 7, no. 7, pp. 1337–1341, 1995.

[98] T. Siegrist, R. M. Fleming, R. C. Haddon, R. A. Laudise, A. J. Lovinger, H. E. Katz, P. Bridenbaugh, and D. D. Davis, "The crystal-structure of the high-temperature polymorph of alpha-hexathienyl (alpha-u-6t/ht)," *Journal of Materials Research*, vol. 10, no. 9, pp. 2170–2173, 1995.

[99] P. Leclre, M. Surin, P. Viville, R. Lazzaroni, A. F. M. Kilbinger, O. Henze, W. J. Feast, M. Cavallini, F. Biscarini, A. P. H. J. Schenning, and E. W. Meijer, "About oligothiophene self-assembly: from aggregation in solution to solid-state nanostructures," *Chemistry of Materials*, vol. 16, no. 23, pp. 4452–4466, 2004.

[100] S. Ellinger, A. Kreyes, U. Ziener, C. Hoffmann-Richter, K. Landfester, and M. Moller, "Aggregation phenomena of long alpha- and alpha,omega-substituted oligothiophenes - the effect of branched vs. linear end-groups," *European Journal of Organic Chemistry*, no. 34, pp. 5686–5702, 2007.

[101] S. Ellinger, U. Ziener, U. Thewalt, K. Landfester, and M. Moller, "Synthesis and self-organization of alpha,omega-substituted oligothiophenes with long, branched alkyl substituents," *Chemistry of Materials*, vol. 19, no. 5, pp. 1070–1075, 2007.

[102] A. B. Nepomnyashchii, R. J. Ono, D. M. Lyons, J. L. Sessler, C. W. Bielawski, and A. J. Bard, "Oligothiophene nanoparticies: Photophysical and electrogenerated chemiluminescence studies," *Journal of Physical Chemistry Letters*, vol. 3, no. 15, pp. 2035–2038, 2012.

[103] C. R. Arroyo, E. Leary, A. Castellanos-Gomez, G. Rubio-Bollinger, M. T. Gonzalez, and N. Agrait, "Influence of binding groups on molecular junction formation," *Journal of the American Chemical Society*, vol. 133, no. 36, pp. 14313–14319, 2011.

[104] H. Vázquez, R. Skouta, S. Schneebeli, M. Kamenetska, R. Breslow, L. Venkataraman, and M. Hybertsen, "Probing the conductance superposition law in single-molecule circuits with parallel paths," *Nature Nanotechnology*, vol. 7, no. 10, pp. 663–667, 2012.

[105] K. Yoshizawa, T. Tada, and A. Staykov, "Orbital views of the electron transport in molecular devices," *Journal of the American Chemical Society*, vol. 130, no. 29, pp. 9406–9413, 2008.

[106] R. Parameswaran, J. R. Widawsky, H. Vazquez, Y. S. Park, B. M. Boardman, C. Nuckolls, M. L. Steigerwald, M. S. Hybertsen, and L. Venkataraman, "Reliable formation of single molecule junctions with air-stable diphenylphosphine linkers," *The Journal of Physical Chemistry Letters*, vol. 1, no. 14, pp. 2114–2119, 2010.

[107] A. J. Heeger, "Semiconducting and metallic polymers: the fourth generation of polymeric materials (nobel lecture)," *Angew. Chem. Int. Ed.*, vol. 40, pp. 2591–2611, 2001.

[108] O. Bubnova, "Semi-metallic polymers," *Nature Mater.*, vol. 13, pp. 190–194, 2014.

[109] G. Schwartz, B. C. K. Tee, J. Mei, A. L. Appleton, D. H. Kim, H. Wang, and Z. Bao, "Flexible polymer transistors with high pressure sensitivity for application in electronic skin and health monitoring," *Nat Commun*, vol. 4, p. 1859, 2013.

[110] J. You, L. Dou, K. Yoshimura, T. Kato, K. Ohya, T. Moriarty, K. Emery, C.-C. Chen, J. Gao, G. Li, and Y. Yang, "A polymer tandem solar cell with 10.6power conversion efficiency," *Nat Commun*, vol. 4, p. 1446, 2013.

[111] G. Gustafsson, Y. Cao, G. M. Treacy, F. Klavetter, N. Colaneri, and A. J. Heeger, "Flexible light-emitting diodes made from soluble conducting polymers," *Nature*, vol. 357, no. 6378, pp. 477–479, 1992.

[112] E. J. Meijer, D. M. de Leeuw, S. Setayesh, E. van Veenendaal, B. H. Huisman, P. W. M. Blom, J. C. Hummelen, U. Scherf, and T. M. Klapwijk, "Solution-processed ambipolar organic field-effect transistors and inverters," *Nat Mater*, vol. 2, no. 10, pp. 678–682, 2003.

[113] A. Facchetti, M. Mushrush, H. E. Katz, and T. J. Marks, "n-type building blocks for organic electronics: a homologous family of fluorocarbon-substituted thiophene oligomers with high carrier mobility," *Adv. Mater.*, vol. 15, pp. 33–38, 2003.

[114] H. E. Katz, A. J. Lovinger, J. Johnson, C. Kloc, T. Siegrist, W. Li, Y. Y. Lin, and A. Dodabalapur, "A soluble and air-stable organic semiconductor with high electron mobility," *Nature*, vol. 404, no. 6777, pp. 478–481, 2000.

[115] J. E. Anthony, A. Facchetti, M. Heeney, S. R. Marder, and X. W. Zhan, "n-type organic semiconductors in organic electronics," *Adv. Mater.*, vol. 22, pp. 3876–3892, 2010.

[116] W. Chen, H. Li, J. R. Widawsky, C. Appayee, L. Venkataraman, and R. Breslow, "Aromaticity decreases single-molecule junction conductance.," *Journal of the American Chemical Society*, vol. 136, no. 3, pp. 918–920, 2014.

[117] G. Barbarella, O. Pudova, C. Arbizzani, M. Mastragostino, and A. Bongini, "Oligothiophene-s,s-dioxides: a new class of thiophene-based materials," *The Journal of Organic Chemistry*, vol. 63, no. 5, pp. 1742–1745, 1998.

[118] N. Camaioni, G. Ridolfi, V. Fattori, L. Favaretto, and G. Barbarella, "Oligothiophene-s,s-dioxides as a class of electron-acceptor materials for organic photovoltaics," *Appl. Phys. Lett.*, vol. 84, pp. 1901–1903, 2004.

[119] S. Wei, J. Xia, E. J. Dell, Y. Jiang, R. Song, H. Lee, P. Rodenbough, A. L. Briseno, and L. M. Campos, "Bandgap engineering through controlled oxidation of polythiophenes," *Angewandte Chemie International Edition*, vol. 53, no. 7, pp. 1832–1836, 2014.

[120] S. Potash and S. Rozen, "New conjugated oligothiophenes containing the unique arrangement of internal adjacent [all]-s,s-oxygenated thiophene fragments," *Chem. Eur. J.*, vol. 19, pp. 5289–5296, 2013.

[121] E. J. Dell and L. M. Campos, "The preparation of thiophene-s,s-dioxides and their role in organic electronics," *Journal of Materials Chemistry*, vol. 22, no. 26, pp. 12945–12952, 2012.

[122] J. A. Malen, P. Doak, K. Baheti, T. D. Tilley, R. A. Segalman, and A. Majumdar, "Identifying the length dependence of orbital alignment and contact coupling in molecular heterojunctions," *Nano Letters*, vol. 9, no. 3, pp. 1164–1169, 2009.

[123] G. Yu, J. Gao, J. C. Hummelen, F. Wudl, and A. J. Heeger, "Polymer photovoltaic cellsenhanced efficiencies via a network of internal donoracceptor heterojunctions," *Science*, vol. 270, pp. 1789–1791, 1995.

[124] E. Amir, K. Sivanandan, J. E. Cochran, J. J. Cowart, S.-Y. Ku, J. H. Seo, M. L. Chabinyc, and C. J. Hawker, "Synthesis and characterization of soluble low-bandgap oligothiophene-[all]-s,s-dioxides-based conjugated oligomers and polymers," *Journal of Polymer Science Part A: Polymer Chemistry*, vol. 49, no. 9, pp. 1933–1941, 2011.

[125] P. Sonar, E. L. Williams, S. P. Singh, and A. Dodabalapur, "Thiophenebenzothiadiazolethiophene (d-a-d) based polymers: effect of donor/acceptor moieties adjacent to d-a-d segment on photophysical and photovoltaic properties," *J. Mater. Chem.*, vol. 21, pp. 10532–10541, 2011.

[126] L. E. Bolivar-Marinez, M. C. dos Santos, and D. S. Galvao, "Electronic structure of pushpull molecules based on thiophene oligomers," *J. Phys. Chem.*, vol. 100, pp. 11029–11032, 1996.

[127] J. L. Brédas, R. Silbey, D. S. Boudreaux, and R. R. Chance, "Chain-length dependence of electronic and electrochemical properties of conjugated systems: polyacetylene, polyphenylene, polythiophene, and polypyrrole," *J. Am. Chem. Soc.*, vol. 105, pp. 6555–6559, 1983.

[128] B. Capozzi, E. J. Dell, T. C. Berkelbach, D. R. Reichman, L. Venkataraman, and L. M. Campos, "Length-dependent conductance of oligothiophenes," *Journal of the American Chemical Society*, vol. 136, no. 29, pp. 10486–10492, 2014.

[129] S. K. Yee, J. A. Malen, A. Majumdar, and R. A. Segalman, "Thermoelectricity in fullerene-metal heterojunctions," *Nano Lett.*, vol. 11, pp. 4089–4094, 2011.

[130] J. L. Brédas, "Mind the gap!," *Mater. Horiz.*, vol. 1, pp. 17–19, 2014.

[131] I. Visoly-Fisher, K. Daie, Y. Terazono, C. Herrero, F. Fungo, L. Otero, E. Durantini, J. J. Silber, L. Sereno, D. Gust, T. A. Moore, A. L. Moore, and S. M. Lindsay, "Conductance of a biomolecular wire," *Proceedings of the National Academy of Sciences*, vol. 103, no. 23, pp. 8686–8690, 2006.

[132] J. R. Widawsky, W. Chen, H. Vázquez, T. Kim, R. Breslow, M. S. Hybertsen, and L. Venkataraman, "Length-dependent thermopower of highly conducting auc bonded single molecule junctions," *Nano Letters*, vol. 13, no. 6, pp. 2889–2894, 2013.

[133] C. Evangeli, K. Gillemot, E. Leary, M. T. González, G. Rubio-Bollinger, C. J. Lambert, and N. Agrat, "Engineering the thermopower of c60 molecular junctions," *Nano Letters*, vol. 13, no. 5, pp. 2141–2145, 2013.

[134] E. J. Dell, B. Capozzi, J. Xia, L. Venkataraman, and L. M. Campos, "Molecular length dictates the nature of charge carriers in single-molecule junctions of oxidized oligothiophenes," *Nat Chem*, vol. advance online publication, 2015.

[135] V. D. Parker, "Problem of assigning values to energy changes of electrode reactions," *Journal of the American Chemical Society*, vol. 96, no. 17, pp. 5656–5659, 1974.

[136] T. Kim, P. Darancet, J. R. Widawsky, M. Kotiuga, S. Y. Quek, J. B. Neaton, and L. Venkataraman, "Determination of energy level alignment and coupling strength in 4,4-bipyridine single-molecule junctions," *Nano Letters*, vol. 14, no. 2, pp. 794–798, 2014.

[137] J. R. Widawsky, M. Kamenetska, J. Klare, C. Nuckolls, M. L. Steigerwald, M. S. Hybertsen, and L. Venkataraman, "Measurement of voltage-dependent electronic transport across amine-linked single-molecular-wire junctions," *Nanotechnology*, vol. 20, no. 43, p. 434009, 2009.

[138] A. Mishchenko, D. Vonlanthen, V. Meded, M. Burkle, C. Li, I. V. Pobelov, A. Bagrets, J. K. Viljas, F. Pauly, F. Evers, M. Mayor, and T. Wandlowski, "Influence of conformation on conductance of biphenyl-dithiol single-molecule contacts," *Nano Letters*, vol. 10, no. 1, pp. 156–163, 2010.

[139] W. Haiss, C. Wang, I. Grace, A. S. Batsanov, D. J. Schiffrin, S. J. Higgins, M. R. Bryce, C. J. Lambert, and R. J. Nichols, "Precision control of single-molecule electrical junctions," *Nat Mater*, vol. 5, no. 12, pp. 995–1002, 2006.

[140] E. D. Minot, A. M. Janssens, I. Heller, H. A. Heering, C. Dekker, and S. G. Lemay, "Carbon nanotube biosensors: The critical role of the reference electrode," *Applied Physics Letters*, vol. 91, no. 9, pp. 093507–3, 2007.

[141] I. Heller, S. Chatoor, J. Mnnik, M. A. G. Zevenbergen, C. Dekker, and S. G. Lemay, "Influence of electrolyte composition on liquid-gated carbon nanotube and graphene transistors," *Journal of the American Chemical Society*, vol. 132, no. 48, pp. 17149–17156, 2010.

[142] J. H. Cho, J. Lee, Y. Xia, B. Kim, Y. He, M. J. Renn, T. P. Lodge, and C. Daniel Frisbie, "Printable ion-gel gate dielectrics for low-voltage polymer thin-film transistors on plastic," *Nat Mater*, vol. 7, no. 11, pp. 900–906, 2008.

[143] R. Misra, M. McCarthy, and A. F. Hebard, "Electric field gating with ionic liquids," *Applied Physics Letters*, vol. 90, no. 5, pp. 052905–3, 2007.

[144] S. Ono, K. Miwa, S. Seki, and J. Takeya, "A comparative study of organic single-crystal transistors gated with various ionic-liquid electrolytes," *Applied Physics Letters*, vol. 94, no. 6, pp. –, 2009.

[145] I. Díez-Pérez, Z. Li, S. Guo, C. Madden, H. Huang, Y. Che, X. Yang, L. Zang, and N. Tao, "Ambipolar transport in an electrochemically gated single-molecule field-effect transistor," *ACS Nano*, vol. 6, no. 8, pp. 7044–7052, 2012.

[146] X. Li, B. Xu, X. Xiao, X. Yang, L. Zang, and N. Tao, "Controlling charge transport in single molecules using electrochemical gate," *Faraday Discussions*, vol. 131, no. 0, pp. 111–120, 2006.

[147] J. He, Q. Fu, S. Lindsay, J. W. Ciszek, and J. M. Tour, "Electrochemical origin of voltage-controlled molecular conductance switching," *Journal of the American Chemical Society*, vol. 128, no. 46, pp. 14828–14835, 2006.

[148] W. Haiss, T. Albrecht, H. van Zalinge, S. J. Higgins, D. Bethell, H. Hbenreich, D. J. Schiffrin, R. J. Nichols, A. M. Kuznetsov, J. Zhang, Q. Chi, and J. Ulstrup, "Single-molecule conductance of redox molecules in electrochemical scanning tunneling microscopy," *The Journal of Physical Chemistry B*, vol. 111, no. 24, pp. 6703–6712, 2007.

[149] N. Darwish, I. Díez-Pérez, P. DaSilva, N. Tao, J. J. Gooding, and M. N. Paddon-Row, "Observation of electrochemically controlled quantum interference in a single anthraquinone-based norbornylogous bridge molecule," *Angewandte Chemie International Edition*, vol. 51, no. 13, pp. 3203–3206, 2012.

[150] M. Kamenetska, S. Y. Quek, A. C. Whalley, M. L. Steigerwald, H. J. Choi, S. G. Louie, C. Nuckolls, M. S. Hybertsen, J. B. Neaton, and L. Venkataraman, "Conductance and geometry of pyridine-linked single-molecule junctions," *Journal of the American Chemical Society*, vol. 132, no. 19, pp. 6817–6821, 2010.

[151] Y. S. Park, J. R. Widawsky, M. Kamenetska, M. L. Steigerwald, M. S. Hybertsen, C. Nuckolls, and L. Venkataraman, "Frustrated rotations in single-molecule junctions," *Journal of the American Chemical Society*, vol. 131, no. 31, pp. 10820–10821, 2009.

[152] P. Ordejón, E. Artacho, and J. M. Soler, "Self-consistent order-n density-functional calculations for very large systems," *Physical Review B*, vol. 53, no. 16, pp. R10441–R10444, 1996.

[153] M. S. José, A. Emilio, D. G. Julian, G. Alberto, J. Javier, O. Pablo, and S.-P. Daniel, "The siesta method for ab initio order- n materials simulation," *Journal of Physics: Condensed Matter*, vol. 14, no. 11, p. 2745, 2002.

[154] J. P. Perdew, K. Burke, and M. Ernzerhof, "Generalized gradient approximation made simple," *Physical Review Letters*, vol. 77, no. 18, pp. 3865–3868, 1996.

[155] S. Y. Quek, L. Venkataraman, H. J. Choi, S. G. Louie, M. S. Hybertsen, and J. B. Neaton, "Aminegold linked single-molecule circuits: experiment and theory," *Nano Letters*, vol. 7, no. 11, pp. 3477–3482, 2007.

[156] H. J. Choi, M. L. Cohen, and S. G. Louie, "First-principles scattering-state approach for nonlinear electrical transport in nanostructures," *Physical Review B*, vol. 76, no. 15, p. 155420, 2007.

[157] D. Daghero, F. Paolucci, A. Sola, M. Tortello, G. A. Ummarino, M. Agosto, R. S. Gonnelli, J. R. Nair, and C. Gerbaldi, "Large conductance modulation of gold thin films by huge charge injection via electrochemical gating," *Physical Review Letters*, vol. 108, no. 6, 2012.

[158] H. Yuan, H. Shimotani, J. Ye, S. Yoon, H. Aliah, A. Tsukazaki, M. Kawasaki, and Y. Iwasa, "Electrostatic and electrochemical nature of liquid-gated electric-double-layer transistors based on oxide semiconductors," *Journal of the American Chemical Society*, vol. 132, no. 51, pp. 18402–18407, 2010.

[159] A. Nitzan and M. A. Ratner, "Electron transport in molecular wire junctions," *Science*, vol. 300, no. 5624, pp. 1384–1389, 2003.

[160] N. J. Tao, "Electron transport in molecular junctions," *Nat Nano*, vol. 1, no. 3, pp. 173–181, 2006.

[161] S. V. Aradhya and L. Venkataraman, "Single-molecule junctions beyond electronic transport," *Nat Nano*, vol. 8, no. 6, pp. 399–410, 2013.

[162] J. C. Ellenbogen and J. C. Love, "Architectures for molecular electronic computers. i. logic structures and an adder designed from molecular electronic diodes," *Proceedings of the IEEE*, vol. 88, no. 3, pp. 386–426, 2000.

[163] M. Mayor, H. B. Weber, J. Reichert, M. Elbing, C. von Hnisch, D. Beckmann, and M. Fischer, "Electric current through a molecular rodrelevance of the position of the anchor groups," *Angewandte Chemie International Edition*, vol. 42, no. 47, pp. 5834–5838, 2003.

[164] T. Kim, Z.-F. Liu, C. Lee, J. B. Neaton, and L. Venkataraman, "Charge transport and rectification in molecular junctions formed with carbon-based electrodes," *Proceedings of the National Academy of Sciences*, vol. 111, no. 30, pp. 10928–10932, 2014.

[165] K. Stokbro, J. Taylor, and M. Brandbyge, "Do aviramratner diodes rectify?," *Journal of the American Chemical Society*, vol. 125, no. 13, pp. 3674–3675, 2003.

[166] R. M. Metzger, "Unimolecular electrical rectifiers," *Chemical Reviews*, vol. 103, no. 9, pp. 3803–3834, 2003.

[167] N. Nerngchamnong, L. Yuan, D.-C. Qi, J. Li, D. Thompson, and C. A. Nijhuis, "The role of van der waals forces in the performance of molecular diodes," *Nat Nano*, vol. 8, no. 2, pp. 113–118, 2013. 10.1038/nnano.2012.238.

[168] M. Ciszkowska and Z. Stojek, "Voltammetry in solutions of low ionic strength. electrochemical and analytical aspects," *Journal of Electroanalytical Chemistry*, vol. 466, no. 2, pp. 129–143, 1999.

[169] M. Brandbyge, J.-L. Mozos, P. Ordejón, J. Taylor, and K. Stokbro, "Density-functional method for nonequilibrium electron transport," *Physical Review B*, vol. 65, no. 16, p. 165401, 2002.

[170] X. Guo, J. P. Small, J. E. Klare, Y. Wang, M. S. Purewal, I. W. Tam, B. H. Hong, R. Caldwell, L. Huang, S. O'Brien, J. Yan, R. Breslow, S. J. Wind, J. Hone, P. Kim, and C. Nuckolls, "Covalently bridging gaps in single-walled carbon nanotubes with conducting molecules," *Science*, vol. 311, no. 5759, pp. 356–359, 2006.

[171] F. Prins, A. Barreiro, J. W. Ruitenberg, J. S. Seldenthuis, N. Aliaga-Alcalde, L. M. K. Vandersypen, and H. S. J. van der Zant, "Room-temperature gating of molecular junctions using few-layer graphene nanogap electrodes," *Nano Letters*, vol. 11, no. 11, pp. 4607–4611, 2011.

[172] R. Huber, M. T. González, S. Wu, M. Langer, S. Grunder, V. Horhoiu, M. Mayor, M. R. Bryce, C. Wang, R. Jitchati, C. Schnenberger, and M. Calame, "Electrical conductance of conjugated oligomers at the single molecule level," *Journal of the American Chemical Society*, vol. 130, no. 3, pp. 1080–1084, 2007.

[173] R. L. Carroll and C. B. Gorman, "The genesis of molecular electronics," *Angewandte Chemie International Edition*, vol. 41, no. 23, pp. 4378–4400, 2002.

[174] O. Adak, R. Korytar, A. Y. Joe, F. Evers, and L. Venkataraman, "Impact of electrode density of states on transport through pyridine-linked single molecule junctions," *arXiv:1504.00242*, 2015.

[175] L. A. Zotti, T. Kirchner, J.-C. Cuevas, F. Pauly, T. Huhn, E. Scheer, and A. Erbe, "Revealing the role of anchoring groups in the electrical conduction through single-molecule junctions," *Small*, vol. 6, no. 14, pp. 1529–1535, 2010.

[176] X. Chen, A. Braunschweig, M. Wiester, S. Yeganeh, M. Ratner, and C. Mirkin, "Spectroscopic tracking of molecular transport junctions generated by using click chemistry," *Angewandte Chemie International Edition*, vol. 48, no. 28, pp. 5178–5181, 2009.

[177] Y. Dubi and M. Di Ventra, "*Colloquium* : Heat flow and thermoelectricity in atomic and molecular junctions," *Reviews of Modern Physics*, vol. 83, no. 1, pp. 131–155, 2011.

[178] P. Darancet, J. R. Widawsky, H. J. Choi, L. Venkataraman, and J. B. Neaton, "Quantitative currentvoltage characteristics in molecular junctions from first principles," *Nano Letters*, vol. 12, no. 12, pp. 6250–6254, 2012.

[179] D. Xiang, H. Jeong, D. Kim, T. Lee, Y. Cheng, Q. Wang, and D. Mayer, "Three-terminal single-molecule junctions formed by mechanically controllable break junctions with side gating," *Nano Letters*, vol. 13, no. 6, pp. 2809–2813, 2013.

[180] Z. K. Keane, J. W. Ciszek, J. M. Tour, and D. Natelson, "Three-terminal devices to examine single-molecule conductance switching," *Nano Letters*, vol. 6, no. 7, pp. 1518–1521, 2006.

[181] A. R. Champagne, A. N. Pasupathy, and D. C. Ralph, "Mechanically adjustable and electrically gated single-molecule transistors," *Nano Letters*, vol. 5, no. 2, pp. 305–308, 2005.

[182] S. V. Aradhya, J. S. Meisner, M. Krikorian, S. Ahn, R. Parameswaran, M. L. Steigerwald, C. Nuckolls, and L. Venkataraman, "Dissecting contact mechanics from quantum interference in single-molecule junctions of stilbene derivatives," *Nano Letters*, vol. 12, no. 3, pp. 1643–1647, 2012.

[183] B. Capozz, J. Xia, O. Adak, E. Dell, Z.-F. Liu, J. C. Taylor, J. B. Neaton, L. M. Campos, and L. Venkataraman, "Single-molecule diodes with high rectification ratios through environmental control," *Nature Nanotechnology*, 2015.

[184] M. G. Reuter, G. C. Solomon, T. Hansen, T. Seideman, and M. A. Ratner, "Understanding and controlling crosstalk between parallel molecular wires," *The Journal of Physical Chemistry Letters*, vol. 2, no. 14, pp. 1667–1671, 2011.

[185] S. Datta, *Quantum Transport: Atom to Transistor*. Untied Kingdom: Cambridge University Press, 2005.